AN UNCONDITIONALLY STABLE METHOD FOR NUMERICALLY SOLVING SOLAR SAIL SPACECRAFT EQUATIONS OF MOTION

By

Alex Karwas

Submitted to the graduate degree program in Aerospace Engineering and the Graduate Faculty of the University of Kansas in partial fulfillment of the requirements for the degree of Doctor of Philosophy.

_____
Chairperson Ray Taghavi, PhD

_____
Saeed Farokhi, PhD

_____
Shawn Keshmiri, PhD

_____
Zhongquan Charlie Zheng, PhD

_____
Bedru Yimer, PhD

Date Defended: March 25 2015

The Dissertation Committee for Alex Karwas

certifies that this is the approved version of the following dissertation:

AN UNCONDITIONALLY STABLE METHOD FOR NUMERICALLY SOLVING SOLAR SAIL SPACECRAFT EQUATIONS OF MOTION

_____

Chairperson Ray Taghavi, PhD

Date approved: March 25 2015

ABSTRACT

Solar sails use the endless supply of the Sun's radiation to propel spacecraft through space. The sails use the momentum transfer from the impinging solar radiation to provide thrust to the spacecraft while expending zero fuel. Recently, the first solar sail spacecraft, or sailcraft, named IKAROS completed a successful mission to Venus and proved the concept of solar sail propulsion. Sailcraft experimental data is difficult to gather due to the large expenses of space travel, therefore, a reliable and accurate computational method is needed to make the process more efficient.

Presented in this document is a new approach to simulating solar sail spacecraft trajectories. The new method provides unconditionally stable numerical solutions for trajectory propagation and includes an improved physical description over other methods. The unconditional stability of the new method means that a unique numerical solution is always determined. The improved physical description of the trajectory provides a numerical solution and time derivatives that are continuous throughout the entire trajectory. The error of the continuous numerical solution is also known for the entire trajectory. Optimal control for maximizing thrust is also provided within the framework of the new method.

Verification of the new approach is presented through a mathematical description and through numerical simulations. The mathematical description provides details of the sailcraft equations of motion, the numerical method used to solve the equations, and the formulation for implementing the equations of motion into the numerical solver. Previous work in the field is summarized to show that the new approach can act as a replacement to previous trajectory

propagation methods. A code was developed to perform the simulations and it is also described in this document. Results of the simulations are compared to the flight data from the IKAROS mission. Comparison of the two sets of data show that the new approach is capable of accurately simulating sailcraft motion.

Sailcraft and spacecraft simulations are compared to flight data and to other numerical solution techniques. The new formulation shows an increase in accuracy over a widely used trajectory propagation technique. Simulations for two-dimensional, three-dimensional, and variable attitude trajectories are presented to show the multiple capabilities of the new technique.

An element of optimal control is also part of the new technique. An additional equation is added to the sailcraft equations of motion that maximizes thrust in a specific direction. A technical description and results of an example optimization problem are presented. The spacecraft attitude dynamics equations take the simulation a step further by providing control torques using the angular rate and acceleration outputs of the numerical formulation.

ACKNOWLEDGEMENTS

I would like to thank my wife, Rachel, for being at my side during my entire undergraduate and graduate education, my parents, Fred and Kristie, for their unconditional support, and my sisters, Dana and Karla, for their motivation and inspiration. I would like to thank my graduate advisor Dr. Ray Taghavi for his instruction during my undergraduate coursework and his guidance that has led to my doctoral degree. Also, I would like to thank Dr. Karan Surana and Dr. Daniel Nunez for their help with teaching me the finite element method.

"I am putting myself to the fullest possible use, which is all I think that any conscious entity can ever hope to do."

-The HAL 9000 Computer from 2001: A Space Odyssey

TABLE OF CONTENTS

ABSTRACT ..... **III**

ACKNOWLEDGEMENTS ..... **V**

LIST OF FIGURES ..... **X**

LIST OF TABLES ..... **XIII**

LIST OF SYMBOLS ..... **XIV**

1. INTRODUCTION **1**

1.1 Overview **1**

1.1.1 Motivation 1

1.1.2 Objective 3

1.1.3 Practical Purpose 5

1.2 Sailcraft **5**

1.2.1 General Description 5

1.2.2 The IKAROS Sailcraft 8

1.3 Literature Review **11**

1.3.1 Mathematical Models of the Sailcraft Motion 12

1.3.2 Numerical Trajectory Propagation 13

1.3.3 Numerical Integration Methods 14

1.3.4 Determination of EOM Variables and Parameters 17

1.3.5 IKAROS Flight Data 17

2. THEORETICAL CONSIDERATION 19

2.1 Sailcraft Dynamics 19

2.1.1 Frames of References 19

2.1.2 Modeling Solar Radiation Pressure 20

2.1.3 One-Dimensional SRP Model 23

2.1.4 Three-Dimensional Flat Sail Model 24

2.1.5 The Sailcraft Equations of Motion 29

2.2 Optimal Control 32

2.2.1 Optimization 33

2.2.2 Rate Equations 36

2.3 The Least Squares *hpk* Finite Element Method 37

2.3.1 Mathematical Overview 37

2.3.2 Element Mesh and Time Steps 42

2.3.3 Variable Approximations 43

2.4 Implementing the Equations of Motion 48

2.4.1 One-Dimensional SRP Thrust 48

2.4.2 Two-Dimensional EOM without Planetary Gravity 50

2.4.3 Two-Dimensional EOM with Variable Lightness Vector 53

2.4.4 Two-Dimensional EOM with Variable Attitude 56

2.4.5 Two-Dimensional EOM with Planetary Gravity 60

2.4.6 3D EOM without Planetary Gravity 64

2.4.7 Three-Dimensional EOM without Thrust 66

2.5 Numerical Solution Details 69

2.5.1 Boundary Conditions 69

2.5.2 Time Domain and Step Size 70

2.5.3 Constants 70

2.5.4 Input of Known Variables 70

3. TRAJECTORY PROPAGATION PROCEDURE 73

3.1 Overview of STAR 73

3.2 Routines 74

3.2.1 Input 74

3.2.2 Planetary Ephemerides 76

3.2.3 Calculating I, K, and g 76

3.2.4 Newton's Linear Method 77

3.2.5 Post Processing 78

4. TRAJECTORY PROPAGATION RESULTS 79

4.1 IKAROS Simulation - SRP Acceleration 79

4.2 AKATSUKI Simulation – Three-Dimensional EOM 83

4.3 Convergence Study 93

4.4 Two-Dimensional Trajectory with Variable Lightness Vector 95

5. OPTIMAL CONTROL PROCEDURE 102

5.1 Objective function 103

5.2 Attitude Adjustment Torques 103

6. OPTIMAL CONTROL RESULTS 104

6.1 Thrust Optimization 104

6.2 Torque 108

7. CONCLUSION 110

7.1 Impacts and accomplishments 111

7.2 Future Research 112

8. REFERENCES 114

APPENDIX A: FINESSE INPUT FILE 1

APPENDIX B: TWO-DIMENSIONAL SIMULATION WITH PLANETARY GRAVITY 1

APPENDIX C: HORIZONS INPUT AND OUTPUT 1

LIST OF FIGURES

Figure 1.1 Effects from light impinging the sail surface [7] 6

Figure 1.2 Stages of IKAROS Sail Deployment [10] 9

Figure 1.3 Schematic of IKAROS Sail Surface [11] 10

Figure 1.4 Photo taken of a section of the IKAROS sail [11] 10

Figure 1.5 Summary of Solar Sail Research 11

Figure 2.1 Resultant force vectors from Sunlight on a sail 20

Figure 2.2 Magnitudes of accelerations experienced by IKAROS 30

Figure 2.3 Objective Functions 35

Figure 3.1 Flow Chart of STAR Code 74

Figure 4.1 Velocity from SRP after IKAROS Sail Deployment [10] 79

Figure 4.2 Comparison of LSFEM to Flight Data for SRP Acceleration Model 82

Figure 4.3 L2-norm versus Degrees of Freedom for IKAROS Simulation 83

Figure 4.4 LSFEM Results and Flight Data of AKATSUKI Trajectory 88

Figure 4.5 Top view of AKATSUKI Trajectory LSFEM Results and Flight Data 89

Figure 4.6 L2-norm versus Degrees of Freedom for AKATSUKI Simulation 90

Figure 4.7 Inset of AKATSUKI Trajectory 91

Figure 4.8 Inset of AKATSUKI Velocity 92

Figure 4.9 Convergence Studies of 1D and 3D Simulations 94

Figure 4.10 History of Lightness Vector Components 96

Figure 4.11 Projections of a H-reversal Trajectory in HIF 97

Figure 4.12 Change in Tangential Component of Lightness Vector 100

Figure 4.13 Derivative of the Change in Tangential Component of Lightness Vector 100

Figure 4.14 LSFEM Results of H-reversal Trajectory 101

Figure 5.1 Definition of Sailcraft Azimuth Angle 102

Figure 6.1 Objective Function for Thrust Maximization at 30° Azimuth 105

Figure 6.2 Azimuth Angle of Sailcraft for Thrust Maximization 106

Figure 6.3 Azimuth Angular Rate of Sailcraft for Thrust Maximization 107

Figure 6.4 Azimuth Angular Acceleration of Sailcraft for Thrust Maximization 107

Figure 6.5 Trajectory for Thrust Optimization 108

Figure 6.6 Torque for Thrust Optimization Maneuver 109

LIST OF TABLES

Table 1.1 Comparison of ODE Integration Methods [19][22][23] 16

Table 4.1 AKATSUKI Trajectory Flight Data [26] 85

Table 4.2 AKATSUKI Velocity Flight Data [26] 86

Table 4.3 Final Data Points for LSFEM Simulation 93

Table 4.4 Final Data Points for ABM Simulation 93

Table 4.5 Summary of Errors between LSFEM and ABM for AKATSUKI Trajectory 93

Table 4.6 Time History of Lightness Vector Components and Derivatives 99

LIST OF SYMBOLS

ACRONYMS

Symbol	Description
ABM	Adams-Bashforth-Moulton
AU	Astronomical Unit
BVP	Boundary Value Problem
DOF	Degrees of Freedom
EOM	Equation of Motion
FEM	Finite Element Method
GDE	Governing Differential Equation
GNC	Guidance, Navigation, and Control
HIF	Heliocentric Inertial Frame
HOF	Heliocentric Orbital Frame
IKAROS	Interplanetary Kite-craft Accelerated by Radiation of the Sun
IVP	Initial Value Problem
JAXA	Japan Aerospace Exploration Agency
JPL	Jet Propulsion Laboratory
LSFEM	Refers to Least Squares hpk Fintie Element Method
ODE	Ordinary Differential Equation
RCD	Reflectance Control Devices
RHS	Right Hand Side
SRP	Solar Radiation Pressure

STAR	Sailcraft Trajectory Analysis Routine
TSI	Total Solar Irradiance
VC	Variationally Consistent

SYMBOLS

Symbol	Description	Units
A	Sail area	m^2
A	Differential operator	~
A_f	Absorptance coefficient	~
a	Acceleration	AU/yr^2
c	Speed of light	AU/yr
E	Residual	~
E	Total enerегy	$N \cdot m$
f	Non-homogeneous term in BVP	~
G	Gravity acceleration term	AU/yr^2
g	First variation of the residual function	~
h	Direction of angular momentum vector	~
I	Residual functional	~
I	Sailcraft moment of inertia	$kg \cdot m^2$
J_0	Radiant energy per unit area per unit time	W/m^2
K	Coefficient matrix	~
L	Lightness vector	~

L_{1AU}	Length of one AU	km
L_S	Solar luminosity	$N \cdot m/s$
m	Mass	kg
N	Approximation function	~
$\vec{n}$	Direction of the sail surface normal vector	~
P	Pressure	N/m^2
p	Momentum	$kg \cdot m/s$
p	Planetary term	~
p	Polynomial degree	~
R	Distance from the Sun	AU
R	Vector location in HIF	AU
$\Re$	Reflectance coefficient	~
r	Direction vector in HIF	~
t	Time	yr
$\vec{u}$	Direction of the sailcraft location vector	~
T	Control torque	$N \cdot m$
V	Velocity vector in HIF	AU/yr
W	Radiant energy flux	$N/m \cdot s$
x	x-component of location sailcraft in HIF	AU
$\overrightarrow{x_s}$	Direction of the sailcraft x-axis in HOF	~
y	y-component of location sailcraft in HIF	AU
z	z-component of location sailcraft in HIF	AU

GREEK SYMBOLS

Symbol	Description	Units
α	Iteration parameter for Newton's method	~
α	Sailcraft azimuth Angle	deg
$\tilde{\beta}$	Angle from diffuse momentum vector to the x-axis of the sail in HOF	~
$\beta(f)$	Reflection constant	~
γ	Absorption coefficient	~
δ	Degree of freedom vector	~
ε	Surface emittance	~
η	Normal component of lightness vector	~
κ	Sail material emissivity	~
μ	Gravitational parameter	$\frac{km^3}{s^2}$
Ξ	Transformation matrix from HOF to HIF	~
ξ	Independent variable in natural coordinate space	~
ρ	Radial component of lightness vector	~
σ	Sailcraft loading	kg/m^2
τ	Tangential component of lightness vector	~
τ_{year}	Seconds in a year	s/yr
υ	Sun incidence angle	rad
φ	Differential equation variable	~
χ	surface emission/diffusion coefficient	~

Ω	Domain of integration	~
ω	Angular velocity	rad/s
$\dot{\omega}$	Angular acceleration	rad/s^2

SUBSCRIPTS

Symbol	**Description**
b	Back
cr	Critical
d	Diffuse
e	Element
f	Front
h	Approximated variable
opt	Optimum
p	Planet
p-s	Value between planet and Sun
s	Specular

1. INTRODUCTION

Presented in this section is an overview of the research topic, which includes the motivation of the research, brief details of solar sail spacecraft, and a summary of related topics.

1.1 Overview

The following subsections explain the research and the purpose for conducting the research.

1.1.1 Motivation

Solar sail spacecraft accelerate payloads through space using zero propellant. Their source of thrust is provided from an abundant and practically free source of energy, the Sun. They utilize the Sun as a constant source of thrust to push them through our solar system. The new method for solving the sailcraft EOM will help increase the success rate of solar sail missions. It will help by providing numerical solutions that are true to the physics of sailcraft trajectories and also provide a priori error analysis.

Recently, the Japan Aerospace Exploration Agency (JAXA) sent a sailcraft named Interplanetary Kite-craft Accelerated by Radiation Of the Sun (IKAROS) on a mission to demonstrate sailcraft technologies. It successfully completed its mission to Venus proving that sailcraft are a realistic option for space travel. During its mission, IKAROS returned tracking data that show clear evidence that SRP was producing thrust and providing attitude control for the sailcraft. The next solar sail spacecraft, named LightSail, produced by The Planetary

Society, will launch in May of 2015 [1]. Its initial mission is a test flight to test the sail deployment sequence. A full solar sailing demonstration mission is set to launch in 2016. The upcoming launch of LightSail and the success of IKAROS show the current interest in sailcraft as a viable option for space travel. A summary of sailcraft missions is presented below:

- IKAROS launched by JAXA on May 21, 2010. It set a world record for becoming the first solar sail spacecraft to complete an interplanetary flight. IKAROS confirmed acceleration was achieved by a solar sail. [2]

- NanoSail launched by NASA on November 19, 2010. It was deployed in low-Earth orbit to demonstrate the deorbit capabilities of solar sails. [3]

- Cosmos 1 was produced by the planetary society and launched on June 21, 2005. It failed to reached orbit due to a launch vehicle failure. [4]

- LightSail mission one will be launched by The Planetary Society in May 2015. It will perform a test flight to determine how the sail will acts in a microgravity environment. [5]

- LightSail mission two will be launched by The Planetary Society in 2016. It will demonstrate the solar sailing capabilities of the spacecraft. [7]

The above list shows how solar sails are becoming a relevant source of propulsion for spacecraft.

To date, the data from the IKAROS mission is the only thrust data recorded for a sailcraft, therefore, the amount of experimental data related to sailcraft is scarce. Gaining more flight data requires extreme expenses of both time and money. Therefore, to efficiently design

and analyze sailcraft, an accurate and reliable computational simulation is needed. The new approach presented here has the aim of filling this need by using the most up-to-date sailcraft equations of motion coupled with an advanced numerical solver.

The numerical solver is a high-accuracy finite element method called the *hpk* least squares finite element method (LSFEM). The LSFEM incorporates high order global differentiability, high order polynomial approximations, and exact determination of numerical errors into the numerical framework. These numerical advantages give the LSFEM the ability to provide solutions that are more true to the physics of sailcraft motion.

1.1.2 Objective

A new approach is presented that combines the LSFEM with the sailcraft equations of motion to achieve an accurate and reliable method for the design and analysis of sailcraft missions. The mathematical model of the sailcraft EOM includes terms for SRP, attitude changes, planetary perturbations, and solar gravity, but it has the potential to include all physical aspects of the sailcraft motion. These include sail material degradation and relativistic affects.

The solution to the sailcraft EOM needs to be solved numerically due to the non-linear nature of the ODE system. The research presented herein shows that the LSFEM has been found to be a superior method. The LSFEM is setup to time-march through the duration of the simulation, while providing simultaneous solutions of the sailcraft location, velocity, acceleration, and, if applicable, attitude angles, rates and accelerations. The data from the simulations will be compared to the flight data of the IKAROS sailcraft to verify the accuracy of the results. Simulations are also presented for non-sail spacecraft to show the additional

capabilities of the new method.

The new method separates itself from other propagation methods by the following features:

- Unconditionally stable numerical solution for non-linear EOM
- Improved physical description through the inclusion of derivatives in the DOFs
- A priori error estimation at any point in the solution domain
- Provides control input for optimizing thrust

The new trajectory propagation method is extended further with the addition of optimal control. An additional equation is added to the EOM system to maximize thrust in a specific direction. The LSFEM formulation inherently provides a minimization within the computational framework. This is utilized to minimize an objective function that is created to maximize thrust. Outputs of the optimal control solution are the sailcraft location, velocity, acceleration, attitude angle, angular rate, and angular acceleration. The angular outputs are placed into the spacecraft attitude dynamics equations to determine the torque required to maneuver the sailcraft to the maximum thrust position.

Technical details of the EOM and LSFEM are presented, as well as the process of implementing the EOM into the LSFEM. The procedure for running the simulations and optimization are also presented, along with results for each simulation.

1.1.3 Practical Purpose

A key step in the design and analysis process for spacecraft involves propagating the trajectory. Trajectory propagation is the process of solving the EOM through a specified span of time. This is done for a number of reasons including simulating the flight path and validating design parameters. The approach to solving EOMs presented in this research acts as a replacement or a supplement to the current sailcraft trajectory propagation techniques.

1.2 Sailcraft

1.2.1 General Description

Solar sail spacecraft, or sailcraft, use light as their source of propulsion. The force resulting from the impinging light on the sail will continue as long as light is allowed to irradiate the surface of the sail. The amount of force exerted on the sailcraft depends on the surface area and surface material of the sail. The distance of the sail from the Sun also affects the amount of thrust produced by the sail. Thrust is approximately proportionate to the inverse square of the distance between the Sun and the sail. For a sail the size of IKAROS, at 1 AU, the thrust is on the order of 1 mN. Compared to the 91 mN [6] produced by the ion thrusters of the Dawn spacecraft, the sailcraft thrust is small. However, IKAROS is considered a small sailcraft based on its sail area of 196 m^2. Current sailcraft concepts increase thrust using larger sails and flight paths with close proximity to the Sun.

Force on the spacecraft is the result of momentum transported to the surface of the sail by electromagnetic radiation from the Sun. In the quantum description, light photons irradiate the

sail surface causing a momentum transfer. Using the electromagnetic description, the momentum transfer is the result of the sail interacting with radiation from electromagnetic waves. Mathematically speaking, both descriptions provide equivalent values for solar radiation. Once the radiation impinges on the surface of the sail it does one of four things: reflects spectrally, reflects diffusively, absorbs into the sail, or transmits through the sail. Figure 1.1 displays these interactions.

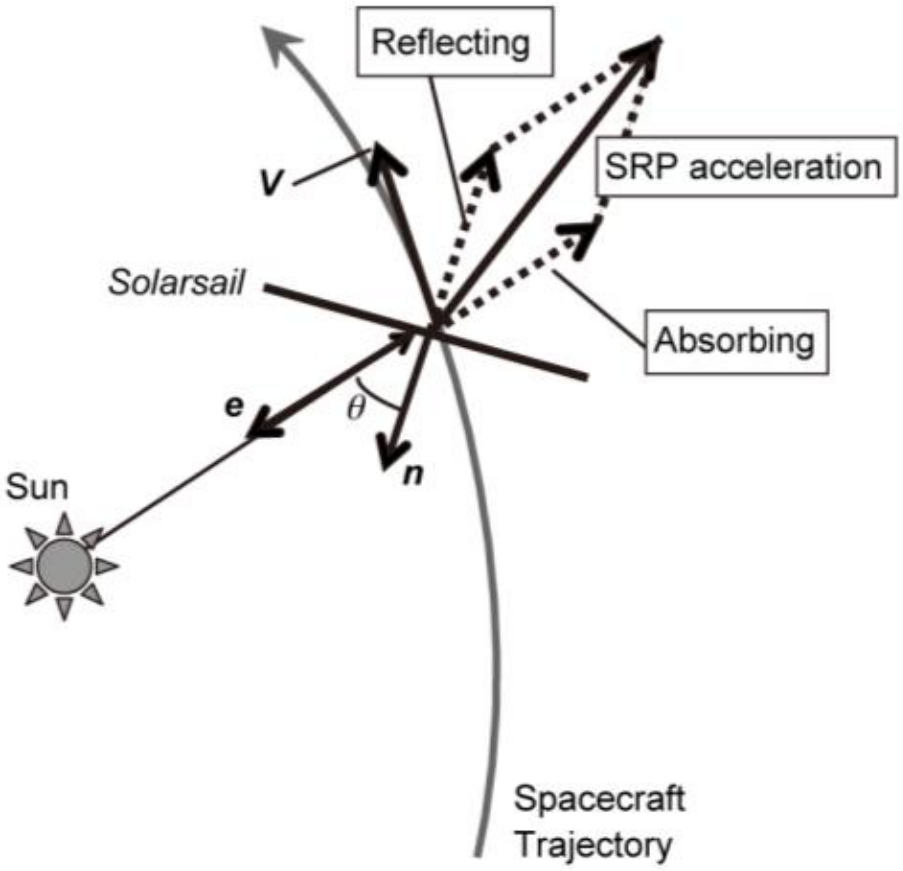

Figure 1.1 Effects from light impinging the sail surface [7]

The appearance of a sailcraft, which is based on maximizing thrust, generally takes the form of a large, flat square or circle with a relatively small, centralized payload. The large surface area is made up almost entirely by the sail, which is made of a lightweight, highly

reflective material. When Sunlight irradiates a surface it generates solar radiation pressure (SRP), thus thrust is the result of SRP acting on the sail. Keeping the sailcraft mass low results in a greater amount of acceleration for a given amount of thrust, which makes sail material and thickness key design variables. Attitude control can come from changing the orientation of certain parts of the sail, or in the case of IKAROS, by using variable reflectance panels positioned on the surface of the sail. The amount of SRP increases exponentially as the distance between the sailcraft and the Sun decreases.

Equations for the momentum transfer caused by solar radiation are briefly described below and will also be described in detail in subsequent sections. Equation (1.1) from [8] is one of the first presentations of quantifying SRP on spacecraft and it shows the relation between acceleration from SRP and distance from the sun.

$$a_{SRP} = \frac{k}{r_{Sun}^2} \tag{1.1}$$

where:

a_{SRP} is the acceleration from SRP

r_{Sun} is the distance from the Sun

k is a constant representing Sunlight properties, spacecraft mass, spacecraft surface area,and spacecraft optical properties

Despite its simplicity, Equation (1.1) shows how the position of the spacecraft and the

spacecraft physical properties affect the amount of SRP acceleration.

The sailcraft equation of motion from [9] in vector form is presented below in Equation (1.2).

$$\ddot{R} = G_{Sun} + A + \sum_{p=1} G_p \tag{1.2}$$

where:

$\ddot{R}$ is the sailcraft acceleration

G_{Sun} is the acceleration due to gravity from the Sun

A is the acceleration from the SRP

$\sum_{p=1} G_p$ is the sum of accelerations from planetary gravity

This equation states that as the sailcraft travels through the solar system it experiences forces from the Sun's gravity, nearby planetary gravity, and SRP acting on the sail.

1.2.2 The IKAROS Sailcraft

The IKAROS sailcraft was produced and launched by JAXA with the purpose of demonstrating technologies of the sailcraft concept for future missions. The main concepts demonstrated during the mission were in-space sail deployment, power generation using solar

cells on the sail, thrust from SRP, and guidance and navigation capabilities of a sailcraft. Its launch took place on May 21, 2010 at the Tanegashima space center aboard the H-IIA rocket as a piggy-back payload of the AKATSUKI Venus climate orbiter [10]. Once IKAROS was injected into the Venus transfer trajectory, it separated from the rest of the payload and began its 180 day trip to Venus. Shortly after separation, the 20 m-span sail was deployed. To deploy the sail, the sailcraft spun about its central axis while releasing tip masses at the four corners of the square sail, the centrifugal force slowly drew the sail outward until it was fully deployed. Figure 1.2 provides a visualization of each step of the sail deployment.

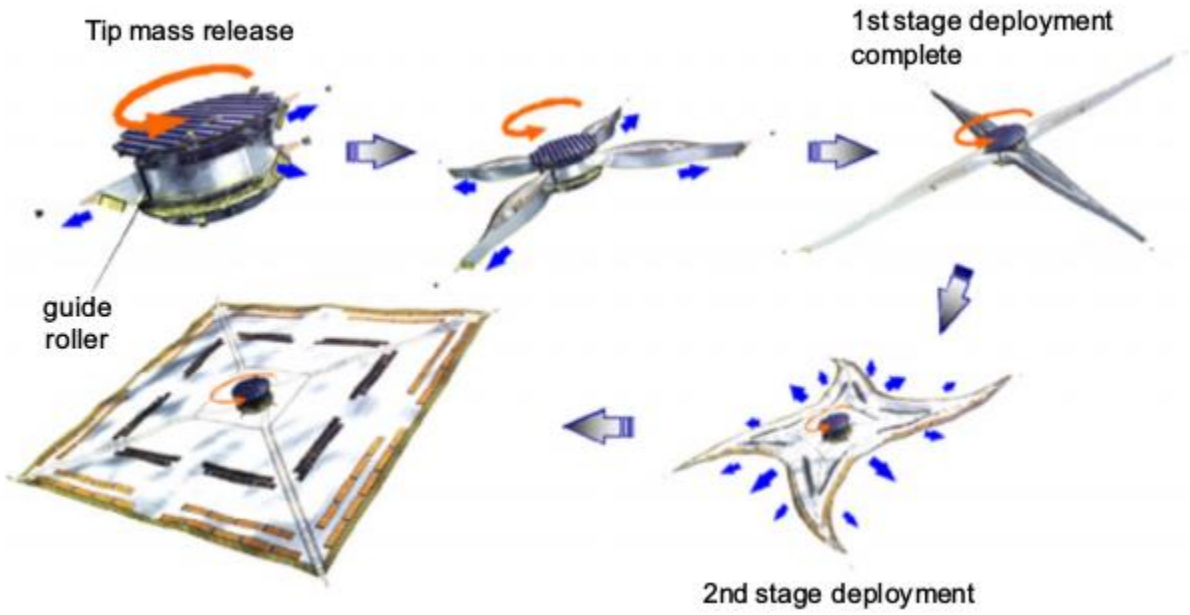

Figure 1.2 Stages of IKAROS Sail Deployment [10]

The sail of IKAROS has a mass of 16 kg, an area of 196 m^2 and a minimum thickness of 7.5 μm The total mass of the spacecraft is 307 kg. The sail weight is kept low as a result of using the centrifugal force of the tip masses to keep the sail extended instead of using support structure. Located on the sail surface are solar panels for power generation and reflectance control devices (RCD) for attitude control. The location of these devices is shown in the

schematic in Figure 1.3 and the photograph of the sail in Figure 1.4.

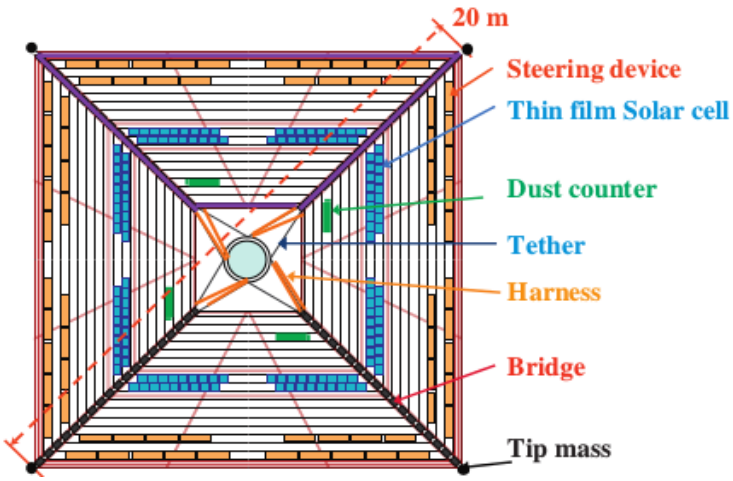

Figure 1.3 Schematic of IKAROS Sail Surface [11]

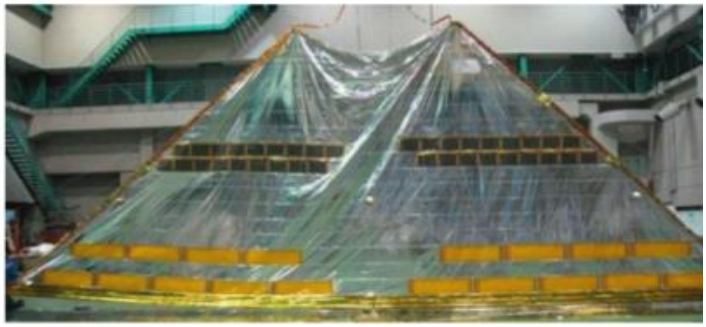

Figure 1.4 Photo taken of a section of the IKAROS sail [11]

The RCDs are flexible sheets made of encapsulated liquid crystal. When electrical voltage is applied to the sheets, the optical reflectance changes between specular and diffuse. When these changes of reflectance are synchronized with the spinning phase of the sailcraft, they change the spin axis of the sailcraft without using any propellant.

To prove the concept of using SRP for thrust, Doppler measurements were used to record the sailcraft trajectory and provide data for the amount of SRP thrust that the sail was providing. An accumulated velocity of over 100 m/s was recorded after the six month cruise to Venus.

After deployment, a thrust force of 1.12 mN was measured. Also recorded was the velocity of the sailcraft immediately following the deployment of the sail, which will be used for verifying the simulation later in this document. IKAROS successfully completed its Venus flyby mission on December 8, 2010.

1.3 Literature Review

Similar research has been reviewed to help expand the capabilities of the new method and to present comparison between methods currently in use. The flow chart shown in Figure 1.5 summarizes the history of sailcraft research.

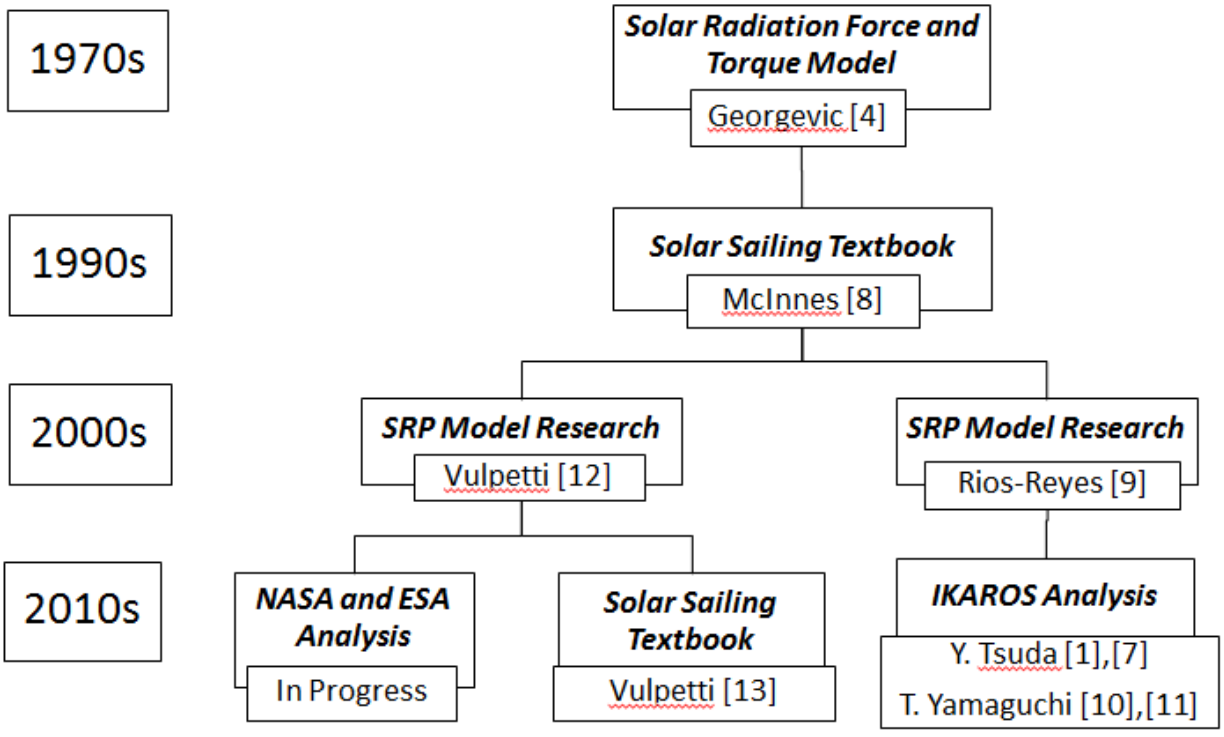

Figure 1.5 Summary of Solar Sail Research

1.3.1 Mathematical Models of the Sailcraft Motion

The work of F[8] presents a solar radiation pressure mathematical model. Its purpose is to provide an accurate model to calculate the spacecraft forces and torques for high-precision attitude control. The model takes into account spacecraft mass, irradiated surface area, incident and reflected light, absorbed light, and distance from the Sun. The outcome is an equation for SRP that is a function of the spacecraft's distance from the Sun and the spacecraft's physical properties. Compared to Sun-centered EOMs, this model is relatively simple because it uses the spacecraft reference frame and only accounts for SRP force. Despite its simple nature, it is the foundation for the more advanced models.

The work presented in [8] is expanded in [12] to become a three-dimensional, sailcraft-specific SRP thrust model. SRP is calculated similar to the model in [8], however, the terms for the material constants are more detailed and the attitude of the sailcraft with respect to the Sun is considered. The inclusion of solar gravity results in a more complicated EOM due to the coordinate transformation required between the Sun-centered and sailcraft-centered reference frames. The outcome of the model is a sailcraft EOM based on accelerations from SRP, solar gravity, and planetary gravity. The final form of the EOM is a non-linear, second order ODE. Also in [12] is a description of how sailcraft in close proximity to the Sun (within 10 solar radii of the Sun, or 0.047 AU,) will experience a decrease in SRP due to the non-parallel incidence angles of the photons. Temperature of the sail is also addressed.

A generalized sail model is developed in [13]. It uses the SRP equation from [12] to determine the forces on an arbitrary, fixed sail geometry. The model requires knowledge of the normal direction of the entire sail surface with respect to the sail-fixed reference frame, which

accounts for the changes in force vector caused by surface geometry. The normal directions of the sail surface come from splitting the sail into smaller flat surfaces. Force on the sail is calculated using radiation pressure, optical properties, sail surface normal vectors, and the solar incidence vector. The model is simplified using constants for geometric and optical properties, however, it becomes more complex when sailcraft attitude is considered.

Most recently [9] has provided the most detailed EOM for sailcraft thus far. Like the previous EOMs, this version is three-dimensional, includes sail material properties, uses a coordinate transformation from the Heliocentric Orbital Frame (HOF) to the Heliocentric Inertial Frame (HIF), and includes acceleration terms for SRP, solar gravity, and planetary gravity. It can also be formulated to consider non-flat sail geometry similar to the model in [13] and degradation of sail optical properties. Details of sail material properties include surface roughness, reflection and transmission profiles, and mean surface behavior. These characteristics are quantified for use in thrust calculations. Introduced in the text is the *lightness* vector, which acts as a scaling factor in the sailcraft EOM for the flat-sail model by scaling the SRP acceleration to the gravitational acceleration of the Sun, or central body. Also presented are approaches for trajectory optimization and the theory of *fast solar sailing*.

1.3.2 Numerical Trajectory Propagation

In the sailcraft software presented in [14] trajectory propagation is calculated using three numerical integration techniques: Adams-Bashforth-Moulton, Bulirsch-Stoer, and Runge-Kutta-Shank. The Runge-Kutta-Shanks method is a higher order version of the traditional Runge-Kutta method based on the Taylor series. Adams-Bashforth-Moulton is a mutli-step method that uses a predictor corrector technique. Details of these techniques are presented in the following

subsection.

Presented in [15] is a software toolkit developed specifically for sailcraft mission design and GNC analysis. It contains five primary modules that are each capable of calculating separate details of the simulation that combine to provide details of a sailcraft mission simulation. Of particular interest are the sections outlining the details of the SRP module and the orbit determination module, which is referred to as DET. The SRP module uses the models presented in [12] and [13] to provide thrust and torque data. The sailcraft equations of motion are handled by the DET module, which calculates the trajectory evolution by integrating the EOM.

Reference [16] presents a sailcraft simulation toolbox designed to act as a single piece of software that handles all aspects of sailcraft design and analysis. The simulation toolbox uses a MATLAB based ODE solver named 'ode113' to propagate the trajectories. [17] states that this integration sub-routine is based on the Adams-Bashforth-Moulton method.

1.3.3 Numerical Integration Methods

Sailcraft equations of motion, like most spacecraft equations of motion, take the form of a system of non-linear, second order differential equations. Equations of this nature generally have no analytical solution, however, the use of numerical integration techniques provides reasonable approximations of such equations. All of the available techniques, in some way, convert the ODE into a system of algebraic equations, and the solution of the system provides an approximate solution to the ODE. The steps used to arrive at the algebraic system are what make each technique unique.

In astrodynamics, numerical integration techniques are used to propagate spacecraft trajectories, in other words, they provide numerical solutions to spacecraft EOMs. Based on [14] and [16], common techniques are Runge-Kutta-Shanks , Bulirisch-Stoer, and Adams-Bashforth-Moulton. In all cases, the techniques can only solve a system of first order ODEs. Handling high order ODEs requires a rework of the EOMs or multiple integrations per step. This introduces an increased amount of error at each step. Also, due to the nature of the numerical techniques, there is no calculation of the exact error of the entire trajectory. At best, there errors are only known at each time step. Each technique uses either a single-step or multi-step methodology. Single-step are simple yet relatively inaccurate. Multi-step methods have high accuracy compared to single-step methods of the same order and are recommended for long-duration simulations. Also, multi-step methods usually require data from a set of previous step, single-step methods are often used to initialize this data set. Order of accuracy for each method depends on the order of the Taylor series expansion used to formulate the algebraic system.

Below is a brief review of the techniques found in sailcraft literature and techniques commonly used in astrodynamic problems. The Runge-Kutta-Shanks method from [18] is an improvement on the Runge-Kutta method by means of allowing high order approximations up to the eighth order. The method is self-starting, therefore it requires only one set of initial conditions. Like similar methods, a second order ODE must be split into a system of first order ODEs.

Reference [19] reveals that the Burlisch-Stoer reduces computer time but it has reliability issues. The Adams-Baschforth-Moulton technique uses a predictor-correcter, or mulit-step, method. It requires a series of initial conditions and, therefore, is not self-starting. To obtain the

set of initial conditions, a Runge-Kutta method with matching order is generally used. Similar to the Runge-Kutta-Shanks method mentioned above, higher order ODEs need to be integrated twice or separated into a system of equations.

In the simulation toolkit presented in [16], the MATLAB subroutine 'ode113' was used to integrate the EOM. [17] states that this subroutine implements the Adams-Bashforth-Moulton technique described above.

Presented in [20] and [21] is an advanced version of the finite element method, which is the numerical technique used for solving the sailcraft EOM for this research. This implicit form of the FEM uses high order polynomials to approximate the equation variables. Higher order global differentiability is implemented into the polynomial approximations, which provides solutions for the variables and their derivatives simultaneously. ODEs of any order can be solved as long as the appropriate initial conditions are provided. The required initial conditions are the same for solving any ODE analytically and are based on order of the equation and number of variables. A detailed description of the method is provided in Section 2.3.

Table 1.1 compares different common ODE integration methods to the LSFEM.

Table 1.1 Comparison of ODE Integration Methods [19][22][23]

Method	Unconditionally Stable	Self Starting	A Priori Error Estimation	Continuous Solution	High Order Systems
LSFEM	Yes	yes	yes	yes	yes
Runge-Kutta	Yes	yes	no	no	no
Adams-Bashforth-Moulton	No	no	no	no	no
Burlisch-Stoer	No	no	no	no	no

The numerical solution of the LSFEM can be trusted because it is variationally consistent and the

error between the numerical solution and the theoretical solution is known. For other methods to be trustworthy, there must be knowledge of the equilibrium points, the nature of the solution, and the stability properties [23].

1.3.4 Determination of EOM Variables and Parameters

Estimating the sail optical parameters is a required step in computing the EOM. [24] presents numeric computations of the specular reflectance, diffusive reflectance, and absorptive parameters of aluminum. Data for aluminum is relevant because most sailcraft designs use an aluminum coated membrane for their sail material. Computations in [24] are based on experimental data of an aluminum film similar to the type used on sailcraft. The results show values for the three parameters as functions of photon incidence angle for varying thicknesses of aluminum.

1.3.5 IKAROS Flight Data

Presented in [25] is a description of the IKAROS sailcraft and its purpose, which is to demonstrate the capabilities of a solar sail spacecraft. Provided in the literature are important details regarding physical aspects of the sail size and material. The demonstration mission of IKAROS precedes a potential sailcraft mission to Jupiter.

The flight of IKAROS is documented in [10] and [11]. It was launched in 2010 and deployed its 20 m sail to help propel it to its destination, Venus. Presented in [10] are details of the mission, the designed trajectory, and most relevant to this research, velocity measurements taken during and after sail deployment. Velocity data was collected using real time Doppler

observation minus calculation measurement during a three hour span, which captured the acceleration from the SRP. Details of IKAROS attitude, spin rate and attitude control are also provided in [10].

The content in [11] is similar to that in [10] except the data from IKAROS entire flight is presented. A key feature of [11] is flight data for the velocity due to SRP during the entire trip to Venus. The data shows a slight increase in acceleration as the sailcraft nears Venus, which is likely due to higher levels of SRP from the sailcraft nearing the Sun. Included in [11] are the time-lines of IKAROS trajectory and attitude during the flight.

2. THEORETICAL CONSIDERATION

The following sections describe the physical and mathematical details of the new trajectory propagation method. Included are details of calculating SRP, construction of the EOM, the mathematics of the FEM, and implementation of the EOM into the FEM.

2.1 Sailcraft Dynamics

2.1.1 Frames of References

The frames of reference are described in this section to clarify the different coordinate systems that are utilized in sailcraft dynamics. The two frames of reference used in the model are the HOF and HIF.

At the origin of the HOF is the barycenter of the sailcraft. Its axes are based on Cartesian coordinates and orient themselves with respect to the sailcraft and the Sun. The HOF x-axis extends from the sailcraft to the barycenter of the Sun. The z-axis is given by the direction of the sailcraft angular momentum vector. Using HOF, sailcraft attitude and elevation angles are measured from the x-axis using the sailcraft rotation about the z-axis and y-axis, respectively. During FEM implementation, it is straightforward to handle attitude and elevation in the HOF frame as opposed to calculating them in HIF.

HIF share's its origin with the Sun's barycenter. The reference plane, or the x-y plane, uses the mean ecliptic at J2000 and the x-axis is directed along the equinox at J2000. Simulations presented herein are based in HIF with attitude variables presented in HOF.

2.1.2 Modeling Solar Radiation Pressure

SRP is the result of Sunlight impinging on a surface, which causes a momentum transfer from the light photons to the surface. When incident light shines on a surface, the light does one of four things, it can reflect spectrally, reflect diffusively, absorb into the surface, or transmit through the surface. Spectral reflection provides the greatest amount of pressure, followed by diffuse reflection, then by absorption. When light transmits through a surface, no pressure is exerted. Pressure from reflected light produces a resultant force normal to the surface. When light is absorbed, the resultant force is parallel to the incident light. Figure 2.1 shows the force vectors resulting from Sunlight impinging on the surface of a sailcraft.

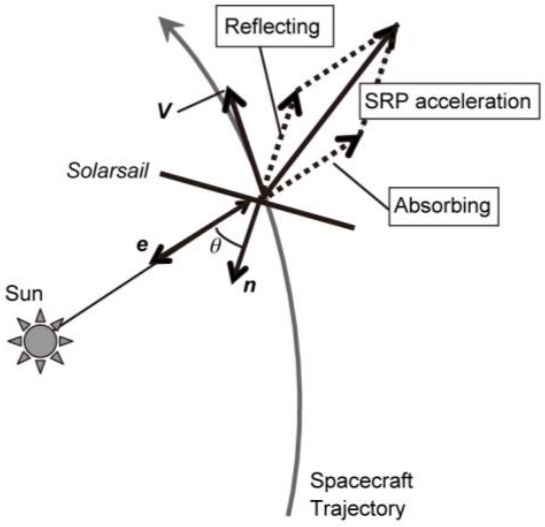

Figure 2.1 Resultant force vectors from Sunlight on a sail

Momentum is transferred to the sail from SRP when solar photons impinge on the sail surface. The effect of the photon interaction is described using the mass energy equivalence of a moving body from special relativity.

$$E^2 = m_0^2 c^4 + p^2 c^2 \tag{2.1}$$

where:

E is total energy

m_0 is mass

c is the speed of light

p is the momentum

The total energy of the moving body is made from two parts, the energy of the body at rest and the energy due to the motion of the body. For photons, which have zero mass, the first term disappears, resulting in:

$$E = pc \tag{2.2}$$

To calculate pressure generated by photons in motion, the momentum transported by a flux of photons is related to the total energy.

$$\Delta E = WA\Delta t \tag{2.3}$$

where:

W is the radiant energy flux or radiant energy per unit area per unit time

A is the area normal to the incident radiation

t is time

Combining these two equations provides:

$$\Delta p = \frac{WA\Delta t}{c} \tag{2.4}$$

The definition of pressure, P, related to momentum transport is:

$$P = \frac{1}{A}\left(\frac{\Delta p}{\Delta t}\right) \tag{2.5}$$

Defining P as SRP and combining the previous two equations together gives:

$$SRP = \frac{W}{c} \tag{2.6}$$

The resulting equation states that SRP is the radiant energy flux divided by the speed of light.

Flux of solar radiation can be scaled based on distance from the Sun using the following relationships.

$$W = W_E \left(\frac{R_E}{r}\right)^2 \tag{2.7}$$

$$W_E = \frac{L_S}{4\pi R_E^2} \tag{2.8}$$

where:

L_S is the solar luminosity

R_E is one astronomical unit

R is distance from the Sun

The above relationship is used as part of the formulation for defining SRP as a function of sailcraft location. To solve the SRP equations, which will be done as part of the sailcraft EOM, they must be arranged to single out acceleration. When implemented into the LSFEM, the evolution of the sailcraft location and time derivatives of location will be the solution variables for a given span of time.

2.1.3 One-Dimensional SRP Model

An early one-dimensional model of SRP derived in [1] is presented below. Equation (2.11) calculates the acceleration created by SRP on a flat surface normal to the source of solar radiation and is a function of distance from the Sun.

$$a_{SRP} = \frac{k}{r_{Sun}^2} \tag{2.9}$$

$$k = \frac{W_E}{c}\frac{S}{m}\left(1 + \gamma B(f)\right) \tag{2.10}$$

where:

a_{SRP} is the acceleration from SRP

r_{sun} is the distance between the spacecraft and the Sun

W_E is the radiant energy per unit area per unit of time at 1 AU

c is the speed of light in a vacuum

S is the surface area of the sail

m is the mass of the entire sailcraft

B(f) is the reflection constant

γ is the absorption coefficient

The acceleration equation clearly shows the inverse square law that governs the relationship between SRP acceleration and distance from the Sun. When this model is implemented in the LSFEM, it takes the following form:

$$\frac{d^2R}{dt^2} = \frac{1}{R^2}\frac{W_E}{c}\frac{S}{m}\frac{t_{yr}^2}{L_{1AU}}\left(1 + \gamma B(f)\right) \tag{2.11}$$

R is the distance from the Sun and is the only variable.

2.1.4 Three-Dimensional Flat Sail Model

A common method for calculating SRP induced acceleration on a sailcraft is performed by scaling down the solar gravity at the sailcraft location. The scale factor presented in [9],

which is also used for the FEM model presented in this research, is called the *lightness vector*. Calculating the magnitude of the solar gravity on the sailcraft is achieved by dividing the solar gravitational constant by the squared distance from the Sun. To get SRP acceleration, one simply multiplies the lightness vector by the solar gravity acceleration. Equation (2.12) shows the formulation.

$$a_{SRP} = L\frac{\mu_{Sun}}{\|R^2\|} \tag{2.12}$$

where:

L is the lightness vector

μ_{Sun} is the Solar gravitational constant

R is the position vector of the sailcraft.

L is calculated in HOF, therefore, to determine the SRP acceleration in HIF, L needs to be transformed from HOF to HIF. The SRP acceleration in HIF is presented below in Equation (2.13) and Equation (2.14).

$$a_{SRP} = \Xi L\frac{\mu_{Sun}}{\|R\|^2} \tag{2.13}$$

$$\Xi = (r\ h \times r\ h) \tag{2.14}$$

where:

Ξ is the transformation matrix from HOF to HIF

r is the direction of the sailcraft position vector in HIF

h is the direction of sailcraft angular momentum vector h

L accounts for all aspects related to SRP acceleration, which includes sailcraft area, mass, optical properties, and attitude angles. It is often reasonable to assume constant sailcraft properties, however, considerations for attitude adjustments and sail material degradation can make L a function of time. The definition of L is presented below in Equation (2.15).

$$\vec{L} = \frac{1}{2}\frac{\sigma_{cr}}{\sigma} cos(\upsilon_{Sun})\Big[\big(2\Re_s cos(\upsilon_{Sun}) + \chi_f \Re_d sin(\beta) + A_f \kappa_{sail}\big)\vec{n} + \big(A_f + \Re_d\big)\vec{u} - \Big(\chi_f \Re_d cos(\beta)\Big)\overrightarrow{x_s}\Big] \tag{2.15}$$

The part of the RHS outside of the brackets describes the total amount of SRP acceleration a sailcraft can receive and is considered the acceleration for a perfect sail. The bracketed term accounts for changes in optical properties based on sail material and the orientation of the sail with respect to the Sun. The non-bracketed term is defined below.

υ_{Sun} is the Sun incidence angle

σ_{cr} is the critical sail loading

σ is the sail loading

The critical sail loading is shown in Equation (2.16) and the sail loading is shown in Equation (2.17).

$$\sigma_{cr} = \frac{2TSI}{c(\mu_{Sun}AU^2)} \tag{2.16}$$

$$\sigma = m/A \tag{2.17}$$

where:

TSI is the total solar irridiance

c is the speed of light in a vacuum

μ_{Sun} is the Solar gravitational constant

AU is the distance form Earth to the Sun

m is the sailcraft mass

A is the area of the sail

The bracket term on the RHS is defined below:

$\Re_s$ is the specular reflection coefficient

$\Re_d$ is the diffuse reflection coefficient

A_f is the absorptance coefficient

$\tilde{\beta}$ is the angle between the diffuse momentum vector and the x-axis of the sail in HOF and is often defined as $\pi/2 + 0.675\alpha$ [9]

κ is the emittance parameter

$\vec{n}$ is the direction of the sail surface normal vector

$\vec{u}$ is the direction of the location vector of the sailcraft

$\overrightarrow{x_s}$ is the direction of the sailcraft x-axis in HOF

The emittance parameter is determined from Equation (2.18).

$$\kappa = \frac{\varepsilon_f \chi_f - \varepsilon_b \chi_b}{\varepsilon_f + \varepsilon_b} \tag{2.18}$$

where:

ε_f is the front sail surface emittance

ε_b is the back sail surface emittance

χ_f is the front sail surface emission/diffusion coefficient

χ_b is the back sail surface emission/diffusion coefficient

Depending on the sailcraft mission, some of the terms in L may change over time. Most likely the sail orientation with respect to the Sun will change due to changes in sail attitude. This will affect the values of v_{Sun} and $\vec{n}$. Additionally, if material degradation occurs, the reflection, absorption and emittance parameters will change. These parameters usually change as a function of both time and location. Functions for sail degradation are found in [14]. The terms that change are considered known variables if their values are known functions of time during the simulation. Details of handling known variables are presented in Section 2.3.3.

The formula for SRP acceleration is used in the sailcraft EOM, which is described in the following section.

2.1.5 The Sailcraft Equations of Motion

An EOM for any spacecraft is simply a sum of the forces acting on the spacecraft center of mass. Generally, for a spacecraft in orbit, or a spacecraft in an interplanetary trajectory, the EOM includes terms for Solar gravity and planetary gravity. Additional terms including disturbances from molecular mean free path or the solar wind can be included. When a solar sail is in motion it, experiences an additional force from Sunlight irradiating the sail. Unlike most other spacecraft, the SRP is constant at any reasonable distance from the Sun. The result is an EOM that includes forces from Solar gravity, planetary gravity, and SRP. Figure 2.2 shows the magnitudes of different forces acting on the IKAROS sailcraft during its flight.

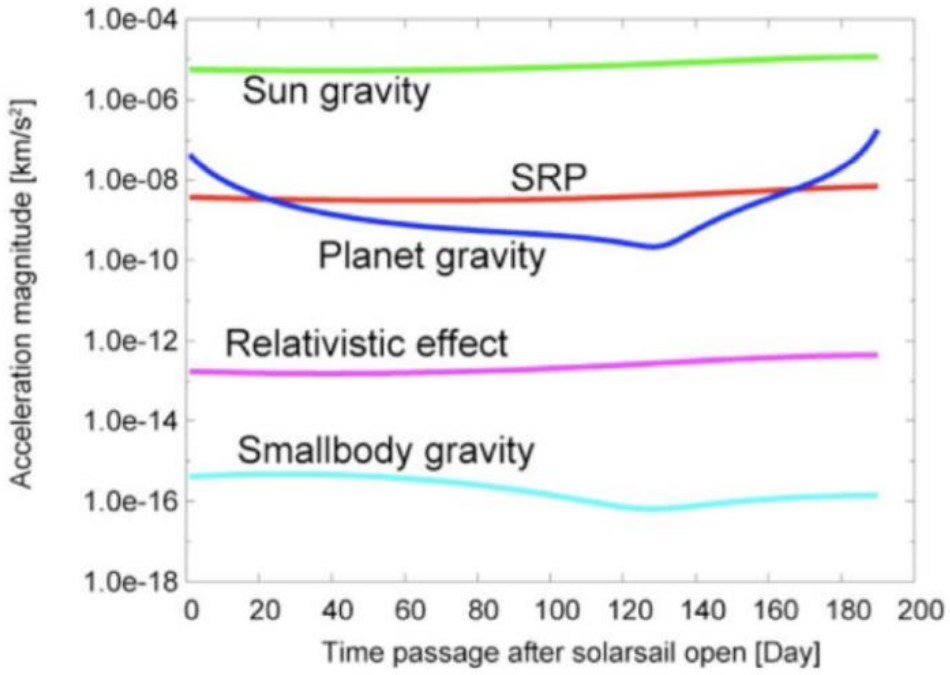

Figure 2.2 Magnitudes of accelerations experienced by IKAROS

Like the gravity terms, the SRP is constantly changing as a function of the sailcraft location, which further complicates the EOM. Mathematically speaking, the resulting sailcraft EOM is a non-linear ordinary differential equation in time. Solving such an equation requires numerical integration. This is where using the LSFEM is useful. Details of the LSFEM will be saved for Section 2.3.

The sailcraft EOM describing motion influenced by SRP, Solar gravity, and planetary gravity is shown in Equation (2.19) and Equation (2.20).

$$\dot{R} = V \tag{2.19}$$

$$\dot{V} = -\mu_{Sun}\frac{R}{\|R\|^3} + \sum_p \mu_p\left(\frac{-R_{p-s}}{\left\|R_{p-s}\right\|^3} + \frac{R_p}{\left\|R_p\right\|^3}\right) + \frac{\mu_{Sun}}{\|R\|^2}\Xi L \tag{2.20}$$

where:

$\dot{V}$ is the sailcraft acceleration vector in HIF

V is the sailcraft velocity vector in HIF

R is the sailcraft location vector in HIF

R_{p-s} is the vector describing the distance from sailcraft to planet *p*

R_p is the location vector of planet *p* in HIF

L is the lightness vector

Ξ is the transformation matrix from HOF to HIF

μ_{Sun} is the Solar gravitation constant

μ_p is the gravitation constant of planet *p*

For simplicity the velocity vector is left out to make the EOM take the form shown in Equation (2.21).

$$\ddot{R} = -\mu_{Sun}\frac{R}{\|R\|^3} + \sum_p \mu_p \left(\frac{-R_{p-s}}{\left\|R_{p-s}\right\|^3} + \frac{R_p}{\left\|R_p\right\|^3} \right) + \frac{\mu_{Sun}}{\|R\|^2} \Xi L \tag{2.21}$$

where:

$\ddot{R}$ is the sailcraft acceleration vector in HIF, as the second time derivative of location

The first RHS term quantifies the influence from solar gravity and the summed term provides the influence of planetary gravity for any number of planets. The last term represents the acceleration from SRP. A unique feature of the EOM is that despite including a thrust term, the mass of the sailcraft remains constant, therefore, the sailcraft mass can be removed from the EOM, resulting in a collection of acceleration terms.

2.2 Optimal Control

The LSFEM inherently has an optimization procedure that minimizes the squared residuals of the sailcraft EOM. This optimization procedure will be used to maximize the thrust of a sailcraft along a specific direction, which is controlled by sailcraft attitude adjustments. The ability of the LSFEM to use high order polynomials for variable approximation functions means the derivatives of the attitude angles are directly calculated within the LSFEM formulation. The advantage of obtaining the derivatives is that they can be input directly into the spacecraft angular rate equations to produce the torques required to perform the attitude changes.

An additional equation is solved alongside the equations of motion that adds the

capability of thrust optimization to the LSFEM simulation. This new equation is, in terms of optimal control theory, acts as an objective function that solves for the optimum attitude angles.

2.2.1 Optimization

An optimization routine is found within the formulation of the finite element method. Discussed in the finite element section are details of the conditions required to minimize the residual functional. In particular, existence, necessary conditions, and sufficient conditions are presented for determining a minimum of a functional [20][21]. This definition of determining the minimum matches the necessary and sufficient conditions for determining a minimum using optimal control theory [27][28][29][30]. In terms of optimal control, which include objective functions and constraints, the equations of motion are the objective functions. Additional objective functions can be included if more minimizations are desired.

The current LSFEM framework also has the ability to add optimal control to the solution of the EOM. The LSFEM, like other finite element methods, inherently uses a minimization to solve the system of differential equations. In the case of the LSFEM, the squared residual of the system of equations is minimized. When the problem is setup appropriately, the squared residual will be minimized to a value close to zero, thus producing a numerical solution. In terms of optimal control, the squared residuals of the differential equations are objective functions. Therefore, to add optimal control to the current LSFEM formulation, an additional objective function can be added to the sailcraft EOM.

Optimal control gives the engineer the task of deciding what needs to be optimized and what will drive to the optimization. A case has been formulated to maximize sailcraft thrust

along a given direction. The optimization will be controlled by the attitude of the sailcraft. The state variables will be the location and velocity of the sailcraft, and the control variables will be the sailcraft attitude angles. The optimization will determine the attitude change needed to maximize the thrust.

Maximizing thrust in a specific direction is achieved by aligning the normal vector of the sailcraft sail along the direction of maximum thrust. When this is achieved, the sail surface is normal to the Sun, which maximizes the lightness vector, resulting in maximized thrust. An objective function has been formulated to maximize thrust by changing the sailcraft attitude from the current orientation. The following equation has been developed as the objective function for performing the thrust optimization for a two-dimensional sailcraft trajectory.

$$\alpha - \alpha_f - \left(\frac{\alpha_i - \alpha_f}{1 + t^5}\right) = 0 \qquad (2.22)$$

where:

α is the sailcraft azimuth angle

α_i is the initial azimuth angle

α_f is the azimuth angle of the desired maximum thrust direction

t is time

This objective function is formulated to provide a smooth transition from the initial sailcraft orientation to the orientation that provides the maximized thrust. Figure 2.3 shows examples of the objective functions for three optimizations:

- initial azimuth angle of 60° to azimuth angle of 30°
- initial azimuth angle of 60° to azimuth angle of 0°
- initial azimuth angle of 10° to azimuth angle of 20°

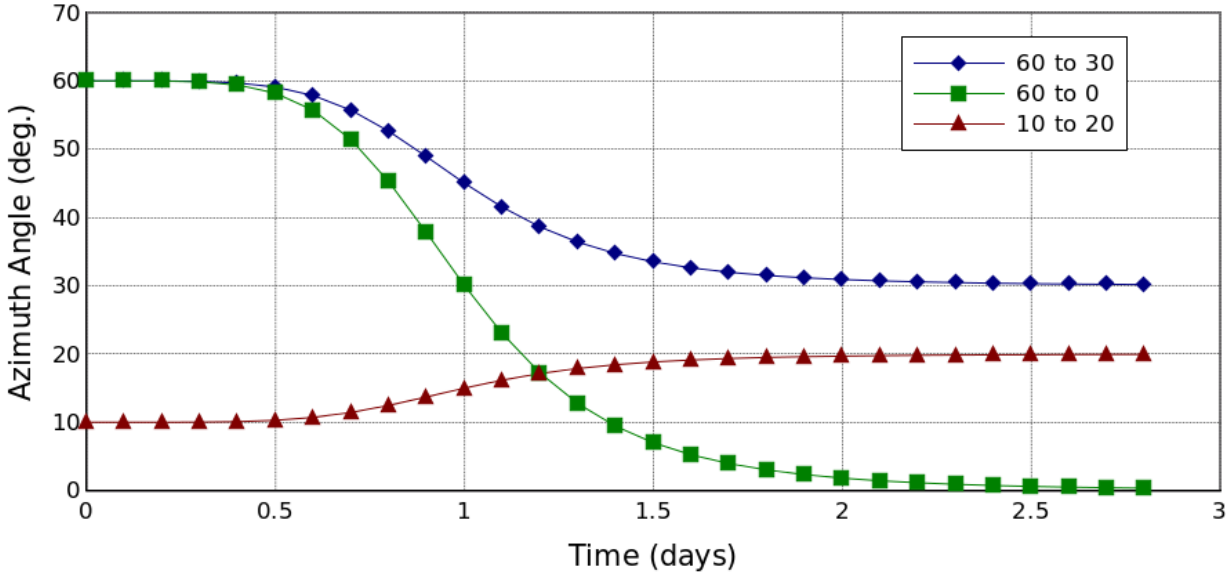

Figure 2.3 Objective Functions

The objective functions are added to the LSFEM formulation as an addition to the sailcraft EOM. The implementation into the LSFEM is performed in asimilar manner to the EOM with variable attitude angles.

2.2.2 Rate Equations

The spacecraft kinematic equations use the angular rates, angular accelerations, moments of inertia, and products of inertia to determine the torque required to change the spacecraft attitude. The optimization section shows that the attitude angles of the sailcraft can be solved using the finite element framework. High order polynomial approximations provide the first and second derivatives of the attitude angles, which fit directly into the attitude dynamics equations for determining torque.

$$I_x\dot{\omega}_x + \left(I_z - I_y\right)\omega_y\omega_z = T_x \tag{2.23}$$

$$I_y\dot{\omega}_y + (I_x - I_z)\omega_x\omega_z = T_y \tag{2.24}$$

$$I_z\dot{\omega}_z + \left(I_y - I_x\right)\omega_x\omega_y = T_z \tag{2.25}$$

where:

I is the sailcraft moment of inertia

ω is the angular velocity

$\dot{\omega}$ is the angular acceleration

T is the torque

x y z are the axes in the sailcraft HOF

Running either a variable attitude trajectory propagation or optimization, along with knowledge of the sailcraft moments of inertia, provides the information required to determine the control torques.

2.3 The Least Squares *hpk* Finite Element Method

The finite element method has made its mark in the field of structural analysis and is showing popularity in the field of fluid dynamics. The general perception of FEM is that it is used for structural mechanics and can be applied to fluid dynamics, but in reality the FEM is an ODE and PDE solver. From the point of view of the FEM, the equations of continuum mechanics used for structural and fluid analyses are simply PDEs. The independent variables can be any number or combination of physical variables. When the EOM for sailcraft is implemented in the FEM, it is seen as a one-dimensional non-linear ODE. When numerical techniques are added, which is the case for the LSFEM method presented in this document, the FEM becomes an unconditionally stable and accurate differential equation solver. Compared to currently used numerical integration techniques for spacecraft, the LSFEM proves itself superior.

The following sections provide the details of the least squares *hpk* finite element method used in this research.

2.3.1 Mathematical Overview

The finite element method takes differential equations and approximates their solutions using three steps:

1. constructing a variation of a functional from the BVP or IVP

2. substituting polynomial approximations for the dependent variables

3. solving the resulting system of equations

The least squares process (LSP) is a method for creating the variation of a functional using the differential equations. The least squares process for the FEM involves minimizing the residuals of a functional based on the governing differential equation (GDE) being solved. To understand the LSFEM consider the GDE to be a BVP in the form of Equation (2.26).

$$A\varphi - f = 0 \tag{2.26}$$

where:

A is the differential operator

φ is the dependent variable

f is the non-homogeneous term

The first step, as with all FEM, is replacing the dependent variable, φ, with an approximation of the dependent variable, φ_n. Using the BVP, let a residual E be defined as Equation (2.27) and, applying the least squares process, a residual functional $I(\varphi_n)$ is defined by Equation (2.28).

$$A\varphi_{\mathrm{n}} - f = E \tag{2.27}$$

$$I(\varphi_{\mathrm{n}}) = (E, E) = (A\varphi_{\mathrm{n}} - f, A\varphi_{\mathrm{n}} - f) \tag{2.28}$$

The meaning of the parenthesis in Equation (2.28) is defined in Equation (2.29) where Ω is defined as the domain.

$$(x, y) = \int_{\Omega} xyd\,\Omega \tag{2.29}$$

If $I(\varphi_n)$ is differentiable by φ_{n} then the necessary condition for the extremum of $I(\varphi_n)$ is that the variation of $I(\varphi_n)$ must be zero or $\delta I(\varphi_n) = 0$. Equation (2.30) shows the variational statement and how it affects the residuals.

$$\delta I(\varphi_{\mathrm{n}}) = (\delta E, E) + (E, \delta E) = 2(E, \delta E) = 0 \tag{2.30}$$

A unique extremum principle means the formulation is variationally consistent (VC), which leads to a mathematically and computationally sound formation. It also leads to a minimization of $I(\varphi_n)$ resulting in minimizing the residual of the GDE. The advantage of minimizing the residual is obvious since the residual is the error resulting from substituting the approximation functions into the GDE. When the algebraic system is formulated, the resulting coefficient matrix will be symmetric and positive definite. For a unique extremum principle the following formula in Equation (2.31) must hold true for the second variation of the residual.

$$\delta^2 I(\varphi_{\mathrm{n}}) = 2(\delta E, \delta E) + 2(E, \delta^2 E) \begin{Bmatrix} > 0 \\ = 0 \\ < 0 \end{Bmatrix} \forall v \in V_n \tag{2.31}$$

Reference [20] provides the mathematical framework for proving variational consistency of linear operators. The result of the proof eliminates the second term of the residual's second variation and shows the result is always positive. This is shown in Equation (2.32).

$$\delta^2 I(\varphi_{\mathrm{n}}) = 2(\delta E, \delta E) > 0 \tag{2.32}$$

For non-linear operators the above equation is used as a starting approximation. The first variation of a BVP with a non-linear differential operator is treated as follows in Equation (2.33).

$$\delta E = \delta(A\varphi - f) = \delta A(\varphi_n) + A(\delta\varphi_n) = \delta A(\varphi_n) + Av = 0 \tag{2.33}$$

Making the approximation from Equation (2.32) guarantees the variation of the residual to have a unique extremum principle and results in variational consistency of the integral and a unique solution. When the Newton's linear method is used along with the approximation from Equation (2.32) the solution for φ_{n} is found iteratively and still maintains uniqueness. [20] provides the mathematical proofs for the previous statements.

Newton's linear method, sometimes referred to as the Newton-Raphson method , provides the necessary means for solving non-linear PDEs and ODEs using LSFEM while maintaining

variational consistency. Iterations are carried out based on the following formulation in Equation (2.34) and Equation (2.35).

$$\varphi_n = \varphi_n^0 + \alpha \Delta \varphi_n \tag{2.34}$$

$$\Delta \varphi_n = -\frac{1}{2}[\delta^2 I]^{-1}_{\varphi_n^0} g(\varphi_n^0) \tag{2.35}$$

where:

φ_n^0 is the initial or guessed solution

α is an iteration parameter

$g(\varphi_i)$ is described in Equation (2.36)

$$g(\varphi_n) = \frac{1}{2} I(\varphi_n) \tag{2.36}$$

The parameter α is determined using the inequality in Equation (2.37).

$$I(\varphi_i) \leq I(\varphi_i^0) \tag{2.37}$$

where:

i is the number of the current iteration

Iterations are repeated using the final values of the previous solution for the initial or guessed solution of the current iteration. When a preset tolerance for either$I(\varphi_i)$ or $g(\varphi_i)$ is achieved, the iterations terminate and the numerical solution is determined.

Having a variationally consistent formulation provides numerous advantages. Variational consistency means the coefficient matrices in the algebraic system formulated from the first variation of the functional will always be symmetric and positive definite. These advantages mean the resulting algebraic system is solvable mathematically and unconditionally stable computationally.

Although this explanation of the LSFEM regards BVPs, the treatment of IVPs is no different. In the case of an IVP like the sailcraft EOM, the LSFEM formulation is setup to solve a one-dimensional, non-linear differential equation. The fact that the independent variable is time and not a spacial variable does not have any effect. However, an IVP has the ability to numerically solve the GDE through time by performing calculations one element at a time. The next section describes the mesh and time domain used in the computations and includes an explanation of calculating solutions element-by-element.

2.3.2 Element Mesh and Time Steps

At least one element is needed to run an FEM simulation. When dealing with a domain consisting of only time, this can be advantageous. This is from the nature of the evolution of all physical processes. Therefore, only a single element is needed to calculate the solution of a

differential equation and the solution will not differ from a simulation that uses multiple elements.

The setup for a time domain that requires multiple elements can be split into time steps that involve a single element. Initial conditions of the first element are used to calculate the solution at the element's end node, which then become the initial conditions for the next element. Computationally, there's generally less code involved in a single element formulation, but a time stepping loop is required when multiple elements are needed.

The element size must have the appropriate resolution to capture changes in the solution variables. If a time step is too large it may not capture changes in the variables that occur between the end nodes of the element. This LSFEM formulation is able to capture these changes, however, care needs to be taken to make sure the element size is still appropriate.

A distinct advantage of this formulation of the FEM is its ability to provide a unique solution for an overdetermined system of equations. In Section 2.5.4, the reward of this advantage will be described.

2.3.3 Variable Approximations

A distinct advantage of this LSFEM framework is the high order global differentiability. This is described in this section as part of the description of the variable approximations. In most finite element formulations, the approximations of the dependent variables are based on linear or quadratic shape functions that are multiplied by the element's degrees of freedom. This is the same technique for the present formulation, however, the shape functions are more complex

allowing the approximation functions to reach high-order polynomial shape functions and global differentiability.

Consider $N(t)_i$ the local approximation functions where δ_i^e is the nodal degree of freedom vector and x_h^e is the approximation of *x* over an element *e*. An approximation of x_h^e is presented in Equation (2.38):

$$x_h^e = \sum_{i=1}^{n} N\,(t)_i x_i^e = [N]\{x^e\} \tag{2.38}$$

where:

$N(t)_i$ is the vector of the local approximation functions

δ_i^e is the nodal degree of freedom vector

x_h^e is the approximation of *x* over an element *e*

Similarly, Equation (2.39) shows the formulation for y_h^e.

$$y_h^e = \sum_{i=1}^{n} N\,(t)_i y_i^e = [N]\{y^e\} \tag{2.39}$$

The vectors of the degrees of freedom, $\{x^e\}$ and $\{y^e\}$, depend of the type of approximation function $[N]$.

Before the approximation functions can be described the natural coordinate space will be introduced. The EOMs for sailcraft are ODEs with variables and derivatives with respect to time. During the simulations time can be input in days, months, or years, however, the LSFEM sees time in the *natural coordinate system*. The domain for each element in time is mapped into the natural coordinate system in a manner that shrinks or expands the element domain to [-1,1]. This is done using a linear interpolation that uses the end nodes of the one-dimensional time elements.

The interpolation for mapping points from physical coordinates to natural coordinates is defined by Equation (2.40).

$$t(\xi) = \left(\frac{1-\xi}{2}\right) t_1 + \left(\frac{1+\xi}{2}\right) t_2 \tag{2.40}$$

where:

$t(\xi)$ is definition of the mapping from physical to natural coordinate space

ξ is the independent variable in the natural coordinate space

t_1 is the value of t at element node 1

t_2 is the value of t at element node 2

Plugging in the node values of *t* into the Equation (2.40) and varying the value of ξ can demonstrate how the interpolation works. Notice how the two lines sum to unity across the

domain of the element, this is the case for all types of interpolating functions.

Like the time domain discussed previously, the dependent variables are required to be mapped to the natural coordinate space. As an example, Equation (2.41) shows the approximation of *x* over an element *e* in the natural coordinate space.

$$x^e = \left(\frac{1-\xi}{2}\right)x_1^e + \left(\frac{1+\xi}{2}\right)x_2^e \tag{2.41}$$

y follows the same formulation in Equation (2.42).

$$y^e = \left(\frac{1-\xi}{2}\right)y_1^e + \left(\frac{1+\xi}{2}\right)y_2^e \tag{2.42}$$

Equation (2.41) can be rearranged to match the formula in Equation (2.38) using the formulations below.

$$[N] = \left[\left(\frac{1-\xi}{2}\right)\left(\frac{1+\xi}{2}\right)\right] \tag{2.43}$$

$$\{\delta^e\} = [x_1^e\ x_2^e]^T \tag{2.44}$$

$$x^e = [N]\{\delta^e\} \tag{2.45}$$

Equation (2.41) and Equation (2.42) are linear interpolation functions and represent the

lowest and least accurate level that the LSFEM has to offer. Interpolation equations range from quadratic functions to high order polynomials exceeding 10^{th} order. Mathematical descriptions of these functions are left to [20]. Important to the research presented in this document is the third-order polynomial interpolation. [20] shows that beginning at the third order function, the degrees of freedom include derivatives of the solution variables. This means that for the approximation shown in Equation (2.46), the resulting degrees of freedom are in the vector shown in Equation (2.47).

$$x_h^e = [N]\{x^e\} \tag{2.46}$$

$$\{x^e\} = \begin{Bmatrix} x_1^e \\ \dfrac{\partial x_1^e}{\partial t} \\ x_2^e \\ \dfrac{\partial x_2^e}{\partial t} \end{Bmatrix} \tag{2.47}$$

The y approximation follows the same style. Jumping ahead to consider the EOM, the above formulation provides simultaneous solutions for location and velocity.

Starting at a third-order polynomial approximation, the LSFEM formulation provides global differentiability up to first order. Approximation functions extend further to provide higher orders of global differentiability. This means, in terms of the EOM, solutions for acceleration are solved alongside the location and velocity. The addition of these degrees of freedom allows for more information to be input into the EOM solver. This results in a more accurate solution with additional outputs. In terms of computations, high order global

differentiation results in higher accuracy.

Extending the degrees of freedom to include first and second order derivatives brings the solution closer to the true physical solution. The solution of the LSFEM formulation provides a continuous, numerical solution for the degrees of freedom. For sailcraft, degrees of freedom include vector of location, velocity, and acceleration, which, considering the physics of the trajectory, are all continuous functions. Derivatives describe the physics of the sailcraft trajectory, therefore, it is extremely important to achieve a solution with continuous derivatives. Often, spacecraft trajectory propagation methods only provide continuous solutions for location and velocity, which leaves acceleration to be calculated by differencing methods. Adding additional calculations introduces new and unknown error values. Differencing methods can provide adequate solutions for acceleration across most of the trajectory time domain, but they fall short at the boundaries where the data is limited.

2.4 Implementing the Equations of Motion

This section presents the LSFEM formulation for the sailcraft EOM using the details of the previous section. To clearly show how the EOM is implemented, the 2-D EOM with Solar gravity and SRP contributions will be described in detail. Additional formulations will be presented without description but will follow the same methodology.

2.4.1 One-Dimensional SRP Thrust

The one-dimensional equation, shown below, calculates the acceleration from SRP for a flat sail surface normal to the Sun.

$$\frac{d^2R}{dt^2} = \frac{1}{R^2}k \tag{2.48}$$

The constant *k* is defined below:

$$k = \frac{W_E}{c}\frac{S}{m}\frac{t_{yr}^2}{L_{1AU}}\left(1 + \gamma B(f)\right) \tag{2.49}$$

The residual is formed by rearranging the thrust equation and substituting the variable approximation:

$$E = \frac{d^2R_h^e}{dt^2} - \frac{1}{(R_h^e)^2}k \tag{2.50}$$

where:

$R_h^e = [N]\{R^e\}$ is the distance of the sailcraft from the Sun in AU

The variation of the residual is:

$$\delta E = (R_h^e)^2\frac{d^2N}{dt^2} + 2R_h^e\frac{d^2R_h^e}{dt^2}N - k \tag{2.51}$$

Depending on the order of the approximation space, the vector $\{R^e\}$ will include the distance between the sailcraft and the Sun and time derivatives of the distance. For a second order

variable approximation, the vector will include sailcraft distance, velocity, and acceleration relative to the Sun.

2.4.2 Two-Dimensional EOM without Planetary Gravity

The two-dimensional EOM is a truncated version of Equation (2.21) due to the removal of the planetary gravity term. Equation (2.52) shows the vector formulation of the EOM.

$$\ddot{R} = -\mu_{Sun}\frac{R}{\|R\|^3} + \frac{\mu_{Sun}}{\|R\|^2}\Xi L \tag{2.52}$$

The vectors represent only x and y terms. Separating the x and y terms results in Equation (2.53) and Equation (2.54).

$$R^3\ddot{x} = \mu(\rho x - \tau y - x) \tag{2.53}$$

$$R^3\ddot{y} = \mu(\rho y + \tau x - y) \tag{2.54}$$

The residual functions for the LSFEM are constructed from the above equations to form Equation (2.55) and Equation (2.56).

$$E_1 = R^3\ddot{x} - \mu(\rho x - \tau y - x) \tag{2.55}$$

$$E_2 = R^3\ddot{y} - \mu(\rho y + \tau x - y) \tag{2.56}$$

where:

$R = \sqrt{(x^2 + y^2)}$ is the distance between the sailcraft and the Sun

ρ is the x-component of the lightness vector

τ is the y-component of the lightness vector

Consider the local approximation functions, $N(t)_i$, the nodal degrees of freedom, δ_i^e, and the approximation of *x* over an element *e*, x_h^e. Applying the local approximations changes the residuals to the following form.

$$E_1^e = ((x_h^e)^2 + (y_h^e)^2)^{(3/2)} \frac{\partial x_h^e}{\partial t} - \mu(\rho x_h^e - \tau y_h^e - x_h^e) \tag{2.57}$$

$$E_2^e = ((x_h^e)^2 + (y_h^e)^2)^{(3/2)} \frac{\partial y_h^e}{\partial t} - \mu(\rho y_h^e + \tau x_h^e - y_h^e) \tag{2.58}$$

From the previous section, the local approximation functions of the sailcraft position components are Equation (2.59) and Equation (2.60).

$$x_h^e = [N]\{x^e\} \tag{2.59}$$

$$y_h^e = [N]\{y^e\} \tag{2.60}$$

For first order global differentiability, the degree of freedom vectors take the following

forms.

$$\{x^e\} = \begin{Bmatrix} x_1^e \\ \frac{\partial x_1^e}{\partial t} \\ x_2^e \\ \frac{\partial x_2^e}{\partial t} \end{Bmatrix} \tag{2.61}$$

$$\{y^e\} = \begin{Bmatrix} y_1^e \\ \frac{\partial y_1^e}{\partial t} \\ y_2^e \\ \frac{\partial y_2^e}{\partial t} \end{Bmatrix} \tag{2.62}$$

The element degrees of freedom take the following form:

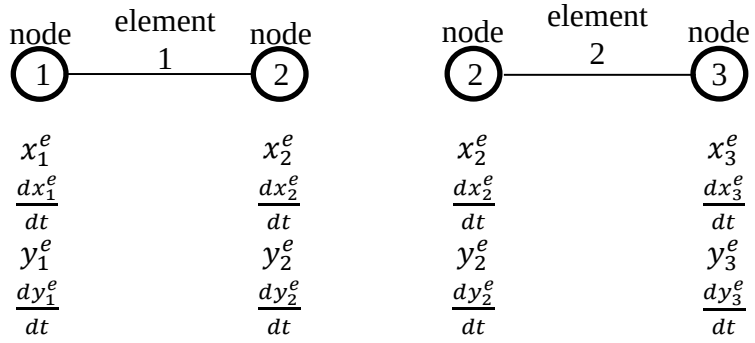

Taking the derivatives of the residuals with respect to the degree of freedom vectors provides the variations of the residuals in Equation (2.63) and Equation (2.64).

$$\{\delta E_1^e\} = \begin{Bmatrix} 3Rx\dfrac{\partial^2 x_h^e}{\partial t^2}\{N\} + R^3\left\{\dfrac{\partial^2 N}{\partial t^2}\right\} - \mu\rho\{N\} + \mu\{N\} \\ 3Ry\dfrac{\partial^2 x_h^e}{\partial t^2}\{N\} + \mu\tau\{N\} \end{Bmatrix} \tag{2.63}$$

$$\{\delta E_2^e\} = \begin{Bmatrix} 3Rx\dfrac{\partial^2 y_h^e}{\partial t^2}\{N\} - \mu\tau\{N\} \\ 3Ry\dfrac{\partial^2 y_h^e}{\partial t^2}\{N\} + R^3\left\{\dfrac{\partial^2 N}{\partial t^2}\right\} - \mu\rho\{N\} + \mu\{N\} \end{Bmatrix} \tag{2.64}$$

With the above equations the K matrix and g vector can be calculated using an initial guess for the non-linear terms.

2.4.3 Two-Dimensional EOM with Variable Lightness Vector

The vector form of the two-dimensional EOM with a variable lightness vector takes the same form as the previous EOM:

$$\ddot{R} = -\mu_{\text{Sun}}\frac{R}{\|R\|^3} + \frac{\mu_{\text{Sun}}}{\|R\|^2}\Xi\text{L} \tag{2.65}$$

where the two-dimensional vector variables are:

$$R = [x\ y]^T \tag{2.66}$$

$$L = [\rho\ \tau]^T \tag{2.67}$$

Separated out of vector form, the system of equations becomes:

$$R^3\ddot{x} - \mu(\rho x - \tau y - x) = 0 \tag{2.68}$$

$$R^3\ddot{y} - \mu(\rho x + \tau y - y) = 0 \tag{2.69}$$

At this step it is now possible to start the implementation into the LSFEM. The degrees of freedom at each node contain variables of sailcraft location, velocity, and the lightness vector components. When the lightness vector is a known variable, it can utilize first order global differentiability. If the lightness vector is an unknown variable it cannot utilize global differentiability, as this will introduce too many unknowns into the LSFEM solution. For unknown lightness vectors, the components can be solved accurately using high order polynomial approximation functions.

The residual functions for the variable lightness vector formulation are shown below:

$$E_1^e = ((x_h^e)^2 + (y_h^e)^2)^{(3/2)} \frac{\partial x_h^e}{\partial t} - \mu(\rho_h^e x_h^e - \tau_h^e y_h^e - x_h^e) \tag{2.70}$$

$$E_2^e = ((x_h^e)^2 + (y_h^e)^2)^{(3/2)} \frac{\partial y_h^e}{\partial t} - \mu(\rho_h^e y_h^e + \tau_h^e x_h^e - y_h^e) \tag{2.71}$$

The residuals are similar to the two-dimensional EOM, except that these contain approximations for the lightness vector components. Two more rows are added to the variations of the residuals due to the addition of the two lightness vector variables.

$$\{\delta E_1^e\} = \begin{Bmatrix} 3Rx \frac{\partial^2 x_h^e}{\partial t^2}\{N\} + R^3 \left\{\frac{\partial^2 N}{\partial t^2}\right\} - \mu\rho\{N\} + \mu\{N\} \\ 3Ry \frac{\partial^2 x_h^e}{\partial t^2}\{N\} + \mu\tau\{N\} \\ -\mu x_h^e\{N\} \\ \mu y_h^e\{N\} \end{Bmatrix} \tag{2.72}$$

$$\{\delta E_2^e\} = \begin{Bmatrix} 3Rx \frac{\partial^2 y_h^e}{\partial t^2}\{N\} - \mu\tau\{N\} \\ 3Ry \frac{\partial^2 y_h^e}{\partial t^2}\{N\} + R^3 \left\{\frac{\partial^2 N}{\partial t^2}\right\} - \mu\rho\{N\} + \mu\{N\} \\ -\mu y_h^e\{N\} \\ -\mu x_h^e\{N\} \end{Bmatrix} \tag{2.73}$$

The variable approximations are defined as:

$$x_h^e = [N]\{x^e\} \tag{2.74}$$

$$y_h^e = [N]\{y^e\} \tag{2.75}$$

$$\rho_h^e = [N]\{\rho^e\} \tag{2.76}$$

$$\tau_h^e = [N]\{\tau^e\} \tag{2.77}$$

Presented below are the element degrees of freedom for a variable lightness vector.

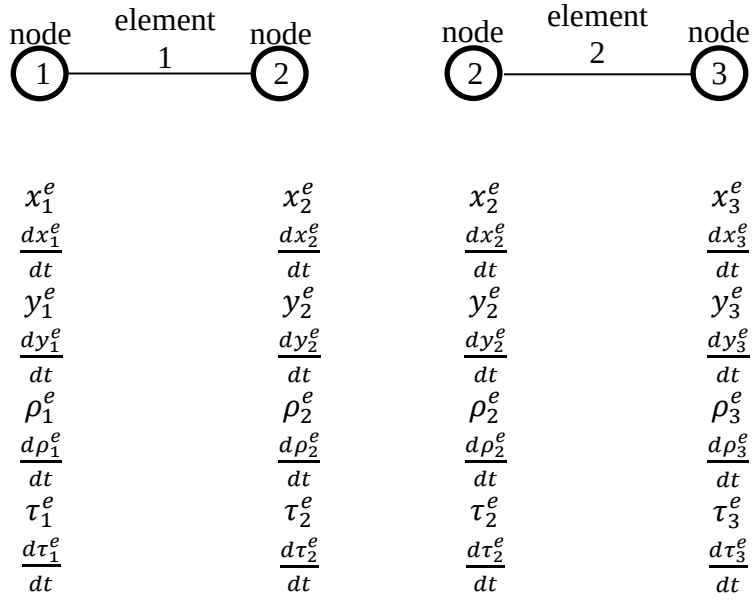

2.4.4 Two-Dimensional EOM with Variable Attitude

The EOM with variable attitude takes the same vector form as the previous two EOM formulations. The variables, however, are now location and the sailcraft azimuth angle. Starting with the two-dimensional EOM:

$$\ddot{R} = -\mu_{\text{Sun}} \frac{R}{\|R\|^3} + \frac{\mu_{\text{Sun}}}{\|R\|^2} \Xi \text{L} \tag{2.78}$$

which then takes the form:

$$R^3\ddot{x} - \mu(\rho x - \tau y - x) = 0 \tag{2.79}$$

$$R^3\ddot{y} - \mu(\rho x + \tau y - y) = 0 \tag{2.80}$$

The azimuth angle is found within the radial and tangential components of the lightness vector. For three-dimensional formulations, the azimuth and elevation angles are within all three components of the lightness vector. The lightness vector components for the two-dimensional EOM are presented below in terms of α:

$$\begin{aligned}\rho =& \frac{1}{2}\frac{\sigma_{cr}}{\sigma}\cos(\alpha)[(2\Re_s\cos(\alpha) + \chi_f\Re_d\sin(\pi/2 + 0.675\alpha) + A_f\kappa_{sail})\cos(-\alpha) \\ &+(A_f + \Re_d) - \left(\chi_f\Re_d\cos(\pi/2 + 0.675\alpha)\right)\sin(\alpha)]\end{aligned} \tag{2.81}$$

$$\begin{aligned}\tau =& \frac{1}{2}\frac{\sigma_{cr}}{\sigma}cos(\alpha)\left[\left(2\Re_s cos(\alpha) + \chi_f\Re_d sin(\pi/2 + 0.675\alpha) + A_f\kappa_{sail}\right)sin(-\alpha)\right. \\ &\left.-\left(\chi_f\Re_d cos(\pi/2 + 0.675\alpha)\right)cos(\alpha)\right]\end{aligned} \tag{2.82}$$

The residuals are presented below:

$$E_1^e = ((x_h^e)^2 + (y_h^e)^2)^{(3/2)}\frac{\partial x_h^e}{\partial t} - \mu(\rho x_h^e - \tau y_h^e - x_h^e) \tag{2.83}$$

$$E_2^e = ((x_h^e)^2 + (y_h^e)^2)^{(3/2)}\frac{\partial y_h^e}{\partial t} - \mu(\rho y_h^e + \tau x_h^e - y_h^e) \tag{2.84}$$

The variations of the residuals are presented in the following two equations:

$$\{\delta E_1^e\} = \begin{Bmatrix} 3Rx\dfrac{\partial^2 x_h^e}{\partial t^2}\{N\} + R^3\left\{\dfrac{\partial^2 N}{\partial t^2}\right\} - \mu\rho\{N\} + \mu\{N\} \\ 3Ry\dfrac{\partial^2 x_h^e}{\partial t^2}\{N\} + \mu\tau\{N\} \\ -\mu x\dfrac{\partial \rho}{\partial\{\alpha_h^e\}} + \mu y\dfrac{\partial \tau}{\partial\{\alpha_h^e\}} \end{Bmatrix} \tag{2.85}$$

$$\{\delta E_2^e\} = \begin{Bmatrix} 3Rx\dfrac{\partial^2 y_h^e}{\partial t^2}\{N\} - \mu\tau\{N\} \\ 3Ry\dfrac{\partial^2 y_h^e}{\partial t^2}\{N\} + R^3\left\{\dfrac{\partial^2 N}{\partial t^2}\right\} - \mu\rho\{N\} + \mu\{N\} \\ -\mu x\dfrac{\partial \rho}{\partial\{\alpha_h^e\}} - \mu y\dfrac{\partial \tau}{\partial\{\alpha_h^e\}} \end{Bmatrix} \tag{2.86}$$

where:

$R = \sqrt{(x^2 + y^2)}$

The derivatives of the lightness vector components with respect to the azimuth angle are presented in the following two equations:

$$\frac{\partial \rho}{\partial\{\alpha_h^e\}} = -\frac{\sigma_{cr}}{2\sigma} sin(\alpha_h^e)$$
$$\left[(2\Re_s cos(\alpha_h^e) + \chi_f \Re_d sin(\pi/2 + 0.675\alpha_h^e) + A_f \kappa_{sail}) cos(-\alpha_h^e) + \right.$$
$$\left.\left(A_f + \Re_d\right) - \left(\chi_f \Re_d cos(\pi/2 + 0.675\alpha_h^e)\right) sin(\alpha_h^e)\right] +$$
$$\frac{\sigma_{cr}}{2\sigma} cos(\alpha_h^e)$$
$$\left[-sin(-\alpha_h^e)(2\Re_s cos(\alpha_h^e) + \chi_f \Re_d sin(\pi/2 + 0.675\alpha_h^e) + A_f \kappa_{sail}) + \right] \quad (2.87)$$
$$cos(-\alpha_h^e)(-2\Re_s sin(\alpha_h^e) + 0.675\chi_f \Re_d cos(\pi/2 + 0.675\alpha_h^e)) -$$
$$cos(\alpha_h^e)(2\Re_s cos(\alpha_h^e) + \chi_f \Re_d sin(\pi/2 + 0.675\alpha_h^e) + A_f \kappa_{sail}) +$$
$$sin(\alpha_h^e)(0.675\chi_f \Re_d sin(\pi/2 + 0.675\alpha_h^e))$$

$$\frac{\partial \tau}{\partial\{\alpha_h^e\}} = -\frac{\sigma_{cr}}{2\sigma} sin(\alpha_h^e)$$
$$\left[(2\Re_s cos(\alpha_h^e) + \chi_f \Re_d sin(\pi/2 + 0.675\alpha_h^e) + A_f \kappa_{sail}) cos(-\alpha_h^e) + \right.$$
$$\left.\left(A_f + \Re_d\right) - \left(\chi_f \Re_d cos(\pi/2 + 0.675\alpha_h^e)\right) sin(\alpha_h^e)\right] +$$
$$\frac{\sigma_{cr}}{2\sigma} cos(\alpha_h^e)$$
$$\left[cos(-\alpha_h^e)(2\Re_s cos(\alpha_h^e) + \chi_f \Re_d sin(\pi/2 + 0.675\alpha_h^e) + A_f \kappa_{sail}) + \right] \quad (2.88)$$
$$sin(-\alpha_h^e)(-2\Re_s sin(\alpha_h^e) + 0.675\chi_f \Re_d cos(\pi/2 + 0.675\alpha_h^e)) +$$
$$sin(\alpha_h^e)(2\Re_s cos(\alpha_h^e) + \chi_f \Re_d sin(\pi/2 + 0.675\alpha_h^e) + A_f \kappa_{sail}) +$$
$$cos(\alpha_h^e)(0.675\chi_f \Re_d sin(\pi/2 + 0.675\alpha_h^e))$$

The variable approximations are defined as:

$$x_h^e = [N]\{x^e\} \quad (2.89)$$

$$y_h^e = [N]\{y^e\} \quad (2.90)$$

$$\alpha_h^e = [N]\{\alpha^e\} \tag{2.91}$$

The degrees of freedom for each node of an element *e* are:

$$\delta^e = [x_h^e \;\; \frac{dx_h^e}{dt} \;\; y_h^e \;\; \frac{dy_h^e}{dt} \;\; \alpha_h^e \;\; \frac{d\alpha_h^e}{dt}]^T \tag{2.92}$$

2.4.5 Two-Dimensional EOM with Planetary Gravity

The EOM is repeated below in Equation (2.93):

$$\ddot{R} = -\mu_{Sun}\frac{R}{\|R\|^3} + \sum_p \mu_p \left(\frac{-R_{p-s}}{\|R_{p-s}\|^3} + \frac{R_p}{\|R_p\|^3}\right) + \frac{\mu_{Sun}}{\|R\|^2}\Xi L \tag{2.93}$$

The component functions are shown in Equation (2.94) and Equation (2.95) with accompanying formulas in the equations below.

$$R^3\ddot{x} - (\rho x - \tau y - x) + \sum_{p=1}^{n} \mu_p D_p^3 (x - x_p) = 0 \tag{2.94}$$

$$R^3\ddot{y} - (\rho y + \tau x - y) + \sum_{p=1}^{n} \mu_p D_p^3 (y - y_p) = 0 \tag{2.95}$$

$$R = \sqrt{x^2 + y^2} \tag{2.96}$$

$$R_p = \sqrt{\left(x - x_p\right)^2 + \left(y - y_p\right)^2} \tag{2.97}$$

$$D = R/R_p \tag{2.98}$$

where:

μ_p is the gravitational constant for planet *p*

x_p is the x-component of the location of planet *p*

y_p is the y-component of the location of planet *p*

n is the total number of planets in the simulation

ρ is the x-component of the lightness vector

τ is the y-component of the lightness vector

The residuals with the variable approximations are presented in Equation (2.99) and Equation (2.100), they are found in the same manner as the previous EOM, with additional formulations in Equation (2.101) and Equation (2.102).

$$E_1^e = R^3 \frac{\partial^2 x_h^e}{\partial t^2} - \mu(\rho x_h^e - \tau y_h^e - x_h^e) + p_x \tag{2.99}$$

$$E_2^e = R^3 \frac{\partial^2 y_h^e}{\partial t^2} - \mu(\rho y_h^e + \tau x_h^e - y_h^e) + p_y \tag{2.100}$$

$$p_x = \sum_{p=1}^{n} \mu_p D_p^3 \left(x_h^e - (x_h^e)_p\right) \tag{2.101}$$

$$p_y = \sum_{p=1}^{n} \mu_p D_p^3 \left(y_h^e - (y_h^e)_p\right) \tag{2.102}$$

The variations of the residuals are presented in Equation (2.103) and Equation (2.104).

$$\{\delta E_1^e\} = \begin{Bmatrix} 3Rx \dfrac{\partial^2 x}{\partial t^2}\{N\} + R^3 \left\{\dfrac{\partial^2 N}{\partial t^2}\right\} - \mu\rho\{N\} + \mu\{N\} + \dfrac{\partial p_x}{\partial\{x\}} \\ 3Ry \dfrac{\partial^2 x}{\partial t^2}\{N\} + \mu\tau\{N\} + \dfrac{\partial p_x}{\partial\{y\}} \\ \dfrac{\partial p_x}{\partial\{x_1\}} \\ \dfrac{\partial p_x}{\partial\{y_1\}} \\ \dfrac{\partial p_x}{\partial\{x_2\}} \\ \dfrac{\partial p_x}{\partial\{y_2\}} \end{Bmatrix} \tag{2.103}$$

$$\{\delta E_2^e\} = \begin{Bmatrix} 3Rx\dfrac{\partial^2 y}{\partial t^2}\{N\} - \mu\tau\{N\} + \dfrac{\partial p_y}{\partial\{x\}} \\ 3Ry\dfrac{\partial^2 y}{\partial t^2}\{N\} + R^3\left\{\dfrac{\partial^2 N}{\partial t^2}\right\} - \mu\rho\{N\} + \mu\{N\} + \dfrac{\partial p_y}{\partial\{y\}} \\ \dfrac{\partial p_y}{\partial\{x_1\}} \\ \dfrac{\partial p_y}{\partial\{y_1\}} \\ \dfrac{\partial p_y}{\partial\{x_2\}} \\ \dfrac{\partial p_y}{\partial\{y_2\}} \end{Bmatrix} \tag{2.104}$$

The derivatives in the above equations are displayed in the following equations:

$$\frac{\partial p_x}{\partial\{x\}} = \sum_{p=1}^{n} \mu_p \left[3L_p^2\left(\frac{x}{R\cdot R_p} - \frac{R}{R_p^3}(x - x_p)\right)(x - x_p) + L_p^3\right]\{N\} \tag{2.105}$$

$$\frac{\partial p_x}{\partial\{y\}} = \sum_{p=1}^{n} \mu_p \left[3L_p^2\left(\frac{y}{R\cdot R_p} - \frac{R}{R_p^3}(y - y_p)\right)(x - x_p)\right]\{N\} \tag{2.106}$$

$$\frac{\partial p_x}{\partial\{x_p\}} = \mu_p \left[3L_p^2\frac{R}{R_p^3}(x - x_p)^2 - L_p^3\right]\{N\} \tag{2.107}$$

$$\frac{\partial p_x}{\partial\{y_p\}} = \mu_p \left[3L_p^2\frac{R}{R_p^3}(y - y_p)(x - x_p)\right]\{N\} \tag{2.108}$$

$$\frac{\partial p_y}{\partial\{x\}} = \sum_{p=1}^{n} \mu_p \left[3L_p^2 \left(\frac{x}{R \cdot R_p} - \frac{R}{R_p^3}(x - x_p) \right)(y - y_p) + L_p^3 \right] \{N\} \tag{2.109}$$

$$\frac{\partial p_y}{\partial\{y\}} = \sum_{p=1}^{n} \mu_p \left[3L_p^2 \left(\frac{y}{R \cdot R_p} - \frac{R}{R_p^3}(y - y_p) \right)(y - y_p) \right] \{N\} \tag{2.110}$$

$$\frac{\partial p_y}{\partial\{x_p\}} = \mu_p \left[3L_p^2 \frac{R}{R_p^3}(x - x_p)(y - y_p) \right] \{N\} \tag{2.111}$$

$$\frac{\partial p_y}{\partial\{y_p\}} = \mu_p \left[3L_p^2 \frac{R}{R_p^3}(y - y_p)^2 - L_p^3 \right] \{N\} \tag{2.112}$$

The degree of freedom vector follows similarly to the previous EOM with the addition of the planet variables. Equation (2.113) shows the DOF vector for this formulation.

$$\delta^e = \left[x_h^e \;\; \frac{dx_h^e}{dt} \;\; y_h^e \;\; \frac{dy_h^e}{dt} \;\; (x_h^e)_p \;\; \left(\frac{dx_h^e}{dt}\right)_p \;\; (y_h^e)_p \;\; \left(\frac{dy_h^e}{dt}\right)_p \right]^T \tag{2.113}$$

For simulations with more planets, additional degrees of freedom are included for planetary location and velocity.

2.4.6 3D EOM without Planetary Gravity

The sailcraft equation of motion with SRP and Solar gravity contributions is presented below:

$$\ddot{R} = -\mu_{Sun}\frac{R}{\|R\|^3} + \frac{\mu_{Sun}}{\|R\|^2}\Xi L \tag{2.114}$$

The following equations present the individual components of the EOM:

$$R^3 A\ddot{x} - \mu A(\rho - 1)x + \mu\tau[y(\dot{y}x - \dot{x}y) + z(\dot{z}x - \dot{x}z)] - \mu R\eta(\dot{z}y - \dot{y}z) = 0 \tag{2.115}$$

$$R^3 A\ddot{y} - \mu A(\rho - 1)y + \mu\tau[x(\dot{x}y - \dot{y}x) + z(\dot{z}y - \dot{y}z)] + \mu R\eta(\dot{z}x - \dot{x}z) = 0 \tag{2.116}$$

$$R^3 A\ddot{z} - \mu A(\rho - 1)z + \mu\tau[x(\dot{x}z - \dot{z}x) + y(\dot{y}z - \dot{z}y)] - \mu R\eta(\dot{y}x - \dot{x}y) = 0 \tag{2.117}$$

Equation (2.118) and Equation (2.119) provide the formulations used in the EOM.

$$R = \sqrt{x^2 + y^2 + z^2} \tag{2.118}$$

$$A = \sqrt{(\dot{y}x - \dot{x}y)^2 + (\dot{z}x - \dot{x}z)^2 + (\dot{z}y - \dot{y}z)^2} \tag{2.119}$$

where:

ρ is the x-component of the lightness vector

τ is the y-component of the lightness vector

η is the z-component of the lightness vector

μ is the Solar gravitational constant

2.4.7 Three-Dimensional EOM without Thrust

The EOM considering only Solar gravity is used for the AKATSUKI simulation, it is presented below:

$$\ddot{R} = -\mu_{Sun}\frac{R}{\|R\|^3} \tag{2.120}$$

The following equations show the individual components of the EOM:

$$R^3\ddot{x} + x = 0 \tag{2.121}$$

$$R^3\ddot{y} + y = 0 \tag{2.122}$$

$$R^3\ddot{z} + z = 0 \tag{2.123}$$

The formulations used in the EOM are provided below:

$$R = \sqrt{x^2 + y^2 + z^2} \tag{2.124}$$

where:

μ is the Solar gravitational constant

Consider the local approximation functions, $N(t)_i$, the nodal degrees of freedom, δ_i^e, and the approximation of *x* over an element *e*, x_h^e. Applying the local approximations changes the residuals to the following forms:

$$E_1^e = R^3 \frac{\partial^2 x_h^e}{\partial t^2} + x \tag{2.125}$$

$$E_2^e = R^3 \frac{\partial^2 y_h^e}{\partial t^2} + y \tag{2.126}$$

$$E_3^e = R^3 \frac{\partial^2 z_h^e}{\partial t^2} + \mathrm{z} \tag{2.127}$$

where:

$$\mathrm{R} = \sqrt{\left(\mathrm{x_h^e}\right)^2 + \left(\mathrm{y_h^e}\right)^2 + \left(\mathrm{z_h^e}\right)^2} \tag{2.128}$$

The variations of the residuals are:

$$E_1^e = \begin{Bmatrix} 3Rx\dfrac{\partial^2 x_h^e}{\partial t^2}\{N\} + R^3\left\{\dfrac{\partial^2 N}{\partial t^2}\right\} + \{N\} \\ 3Ry\dfrac{\partial^2 x_h^e}{\partial t^2}\{N\} \\ 3Rz\dfrac{\partial^2 x_h^e}{\partial t^2}\{N\} \end{Bmatrix} \tag{2.129}$$

$$E_2^e = \begin{Bmatrix} 3Rx\dfrac{\partial^2 y_h^e}{\partial t^2}\{N\} \\ 3Ry\dfrac{\partial^2 y_h^e}{\partial t^2}\{N\} + R^3\left\{\dfrac{\partial^2 N}{\partial t^2}\right\} + \{N\} \\ 3Rz\dfrac{\partial^2 y_h^e}{\partial t^2}\{N\} \end{Bmatrix} \tag{2.130}$$

$$E_3^e = \begin{Bmatrix} 3Rx\dfrac{\partial^2 z_h^e}{\partial t^2}\{N\} \\ 3Ry\dfrac{\partial^2 z_h^e}{\partial t^2}\{N\} \\ 3Rz\dfrac{\partial^2 z_h^e}{\partial t^2}\{N\} + R^3\left\{\dfrac{\partial^2 N}{\partial t^2}\right\} + \{N\} \end{Bmatrix} \tag{2.131}$$

The local approximation functions of the sailcraft position components are the following equations:

$$x_h^e = [N]\{x^e\} \tag{2.132}$$

$$y_h^e = [N]\{y^e\} \tag{2.133}$$

$$z_h^e = [N]\{z^e\} \tag{2.134}$$

For first order global differentiability, the degree of freedom vectors take the following forms.

$$\{x^e\} = \begin{Bmatrix} x_1^e \\ \frac{\partial x_1^e}{\partial t} \\ x_2^e \\ \frac{\partial x_2^e}{\partial t} \end{Bmatrix} \tag{2.135}$$

The $\{y^e\}$ and $\{z^e\}$ degree of freedom vectors follow same form as $\{x^e\}$.

2.5 Numerical Solution Details

This section contains the details of the parameters involved in the numerical solution of the EOM.

2.5.1 Boundary Conditions

Boundary conditions for the sailcraft EOM, mathematically speaking, follow the same guidelines shared for solving all differential equations. In the case of the two-dimensional EOM, the equations are second order with respect to both x and y meaning that two boundary conditions are needed for x and y. Luckily, problems in astrodynamics generally start with this set of conditions. They are provided in the spacecraft state vector, which is made of the spacecraft location and velocity components. Referring back to the two-dimensional EOM this means it can use x and y and the respective time derivatives to fulfill the boundary condition requirements.

2.5.2 Time Domain and Step Size

Every step is essentially a self-contained FEM simulation for a single element that spans a length of time equal to the step size. The calculated final conditions are saved and implemented into the next step's simulation. This gives a level of freedom to the size of each step. To be sure the step size is not too large a convergence study, similar to what would be used in CFD or structural analysis programs, should be performed.

2.5.3 Constants

Constants in the EOM, most of which include optical properties and sailcraft properties, are defined in the code and remain constant during each time step. As described in the previous subsection, it is possible to redefine each constant before calculation of the next step.

2.5.4 Input of Known Variables

Special treatment is needed when a situation arises where a constant in the EOM becomes a variable. The form of the LSFEM used here is able to handle, with increased physical description and high accuracy, the inclusion of known variables. The variables can be in the form of a function, in this case with respect to time, or a set of data points that correspond to the elemental nodes. Either way, the variable and its time derivative are required at each node. If the variable is in the form of a function, then the function and its time derivative must be determined at each node. The requirements for the known variables match the requirements for boundary conditions with regard to the amount required.

When expanded, the two-dimensional EOM for solar sail motion resulting from solar

gravity and SRP is a set of two equations with two unknowns. Adding terms to the EOM to handle either attitude adjustments or planetary gravitational accelerations increases the size of the EOM, however, it still is a set of two equations and two unknowns. For attitude adjustment and planetary considerations, known functions will be introduced for changes in sailcraft attitude with respect to time and changes in planet location with respect to time, respectively. For attitude adjustments, the function may resemble a step function with the step replaced by a third-degree polynomial, resulting in a piecewise differentiable function. Similarly, planetary data can be gathered as a continuous function or a set of data points for location and velocity. The nature of these functions means they can be incorporated into the FEM calculations as known variables. This provides the attitude and/or planetary accelerations as continuous functions during the entire trajectory simulation.

When solving the system of equations for the sailcraft EOM with inclusion of planetary gravitational acceleration, the solution vector contains the variables for sailcraft position and velocity and planet position and velocity. Similar to the BC requirements, the planet data must be in the form of a variable and its time derivative. In the case of the planets, location and velocity are needed. This setup is ideal for the format of the planetary data provided by the JPL from [26]. Using [26] for planetary data is ideal because it provides planet location and velocity for specified time increments in a specified time frame. For attitude variations, the value of the attitude variables and their time derivatives are needed. If the attitude changes can be described as a polynomial function of time, then this is easily obtained. All variables are needed at the beginning and end nodes of each time step. The result of this process is a numerical solution of the EOM based on third order or greater polynomial approximations of planetary data and/or attitude changes. Other methods of trajectory propagation use constant values based on values at

the start of the time step. Any known functions of time within the EOM can be solved with the LSFEM if the above requirements are met.

3. Trajectory Propagation Procedure

Described in this section is the procedure for running a sailcraft simulation using the method described in the previous sections. Also included are numerical details involved in the computational process of the sailcraft trajectory analysis routine called STAR. The two-dimensional EOM with Solar gravity and SRP contributions will be used to demonstrate the procedure for solving the sailcraft EOM system using the LSFEM. STAR, written in MATLAB [33], has the ability to handle all forms of the EOM.

3.1 Overview of STAR

Figure 3.1 is a flow chart of the STAR code:

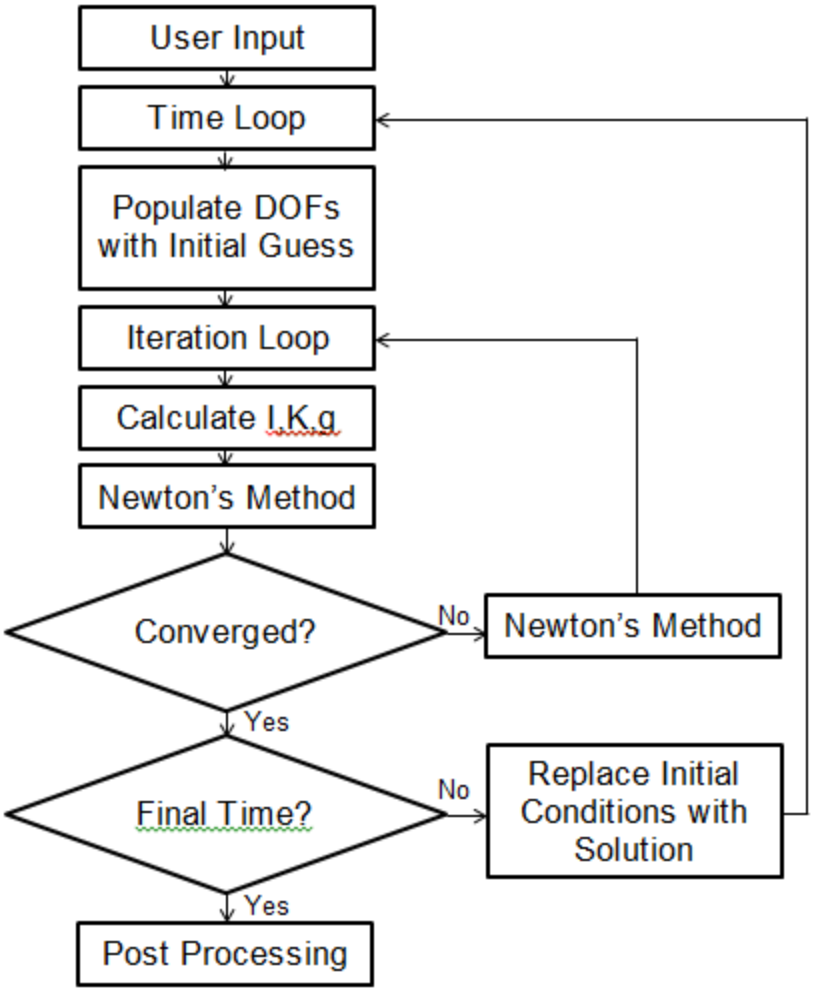

Figure 3.1 Flow Chart of STAR Code

3.2 Routines

STAR code is made of multiple routines for calculating the solution of the sailcraft EOM.

3.2.1 Input

The following list shows the inputs required for simulations including Solar and planetary gravitation, SRP acceleration, and constant sail attitude.

- Time step [yrs]

- Number of steps
- Number of data points to be plotted between nodes
- Radial value of the lightness vector
- Tangential value of the lightness vector
- Earth gravitational constant
- Venus gravitational constant
- x-component of sailcraft initial location
- x-component of sailcraft initial velocity
- y-component of sailcraft initial location
- y-component of sailcraft initial velocity

The initial conditions for the sailcraft location and velocity are also used as the initial guesses for Newton's linear method. After each iteration, the guessed values are updated but the initial conditions stay the same. When the iterative solution converges, the final solution replaces the values of the initial conditions and the routine repeats the same process until solutions are obtained for all elements in the time domain.

3.2.2 Planetary Ephemerides

The data for the planetary ephemerides is input prior to running STAR. Data values for planet location and velocity are needed for the beginning and end of each time step. This data can be obtained easily from [26]. This method is also used for simulations with variables attitude angles and lightness vector components. The requirements for such a simulation are the attitude value and its derivative with respect to time at each time increment.

3.2.3 Calculating I, K, and g

The values most important to the calculating the numerical solution are I, K, and g, which were previously described in Section 2.3. K and g share obvious importance in the solution because they are the two variables involved in the iterative procedure. g also acts as a convergence test. When g converges below a user defined value, the iterative solution achieves convergence. It is general practice when using the LSFEM to set the maximum g at 1×10^{-6}. Calculating K requires two parts:

1. multiplying the variation of the residuals

2. integrating across the element natural domain

Gauss quadrature is used for the numerical integration. [20] suggests using $2p + 1$ integration points when integrating p-ordered functions. In the case of third order approximation functions, which are described in Section 2.3.3, seven integration points are used in the Gauss quadrature routine. This routine is made more simple by the integration domain in the natural

coordinate system, which is $[-1,1]$.

The calculation of I provides the norm of the error function. This result is the purpose of the LSFEM, which is to minimize the residual functional. Values of I are calculated for each time step and can be used to identify areas in the domain that may need smaller time steps. Large I indicates large numerical solution error.

3.2.4 Newton's Linear Method

Newton's linear method is the iterative procedure for determining the solution to the non-linear system of equations. In Section 2.3 there are details of how to define α, however, if a reasonable initial guess is used α can be fixed. In the case of the simulations presented in this document a value of unity was used for α, and no convergence issues were encountered. This is the result of small time step sizes and the use of the initial conditions for the initial guessed solution instead of a zero solution.

If the solution does not converge after an iteration, the solution calculated during that iteration is used for the following iteration's initial guess. Once a converged solution is reached, the solutions values are used as the initial conditions for the next time step. If the entire time domain is covered by multiple elements in the same calculation, then the converged solution is the final solution. A solution is considered converge when the value of g shrinks below a reasonably small value.

3.2.5 Post Processing

A unique trait of the FEM is its ability to provide values of the numerical solution between element nodes. This feature comes from the continuous solution provided by the LSFEM. The user is able to choose any amount of data points to provide the solution between element nodes. The approximation functions are reused in this step to provide data between the end nodes of each element.

4. Trajectory Propagation Results

Presented in this section are the results of the LSFEM simulations for multiple EOM systems, as well as comparisons to flight data and other propagation methods.

4.1 IKAROS Simulation - SRP Acceleration

Reference [10] provides velocity data for IKAROS during the 2nd stage deployment of the sail shown in Figure 4.1.

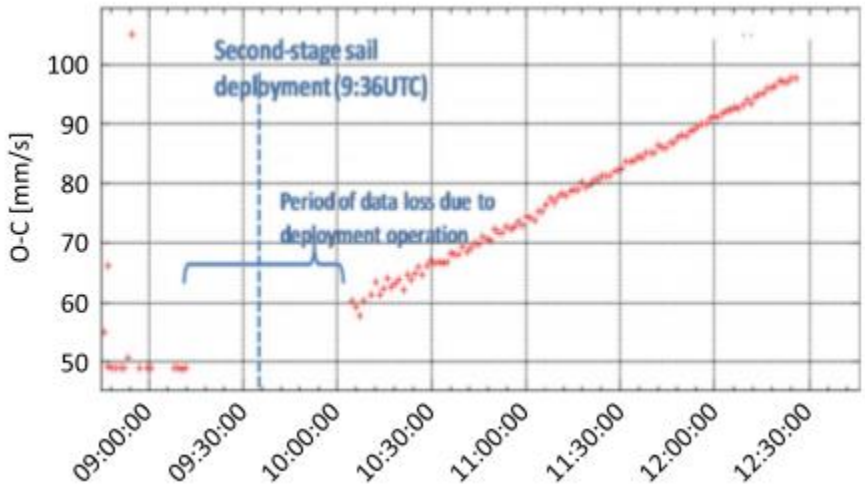

Figure 4.1 Velocity from SRP after IKAROS Sail Deployment [10]

A simulation was performed using the SRP acceleration model provided in [1]. Given the above data this model is appropriate because the data has been filtered to only show the velocity change caused by the SRP. The LSFEM was used to simulate the flight by using the data from [10] for initial conditions and sail properties. The LSFEM software package FINESSE [32] is used to calculate the SRP acceleration results. FINESSE provides the LSFEM framework to solve a set of user-input differential equations.

Equation (4.1) shows all terms in the SRP acceleration model.

$$R^2 \frac{d^2R}{dt^2} = \frac{W_E}{c}\frac{S}{m}\frac{t_{yr}^2}{L_{1AU}}\left(1 + \gamma B(f)\right) \tag{4.1}$$

where:

R is the sailcraft distance from the Sun

t is time

$W_E = 1367\ W/m^2$

$c = 299{,}792{,}500\ m/s$

$S = 173.63\ m^2$

$m = 287\ kg$

$t_{yr} = 3.1536e7\ s$

$L_{1AU} = 1.4959x10^{11}\ m$

$\gamma = 0.928$

$B(f) = 0.798$

The initial conditions are:

$t = 0$ is the initial time

$R(0) = 1\ AU$ is the initial location

$\dot{R}(0) = 0.6\ AU/yr$ is the initial velocity

$\ddot{R}(0) = 28.13\ AU/yr^2$ is the initial acceleration

The time domain matches the two and a half hour duration of the IKAROS velocity data collection. Four time steps are used to perform the propagation. Four elements and a fifth order polynomial approximation function with 2nd order global differentiability are used to carry out the simulation. The LSFEM solution provides location, velocity, and acceleration data for the entire time domain. Figure 4.2 shows the velocity results of the LSFEM simulation plotted with the flight data from Figure 4.1.

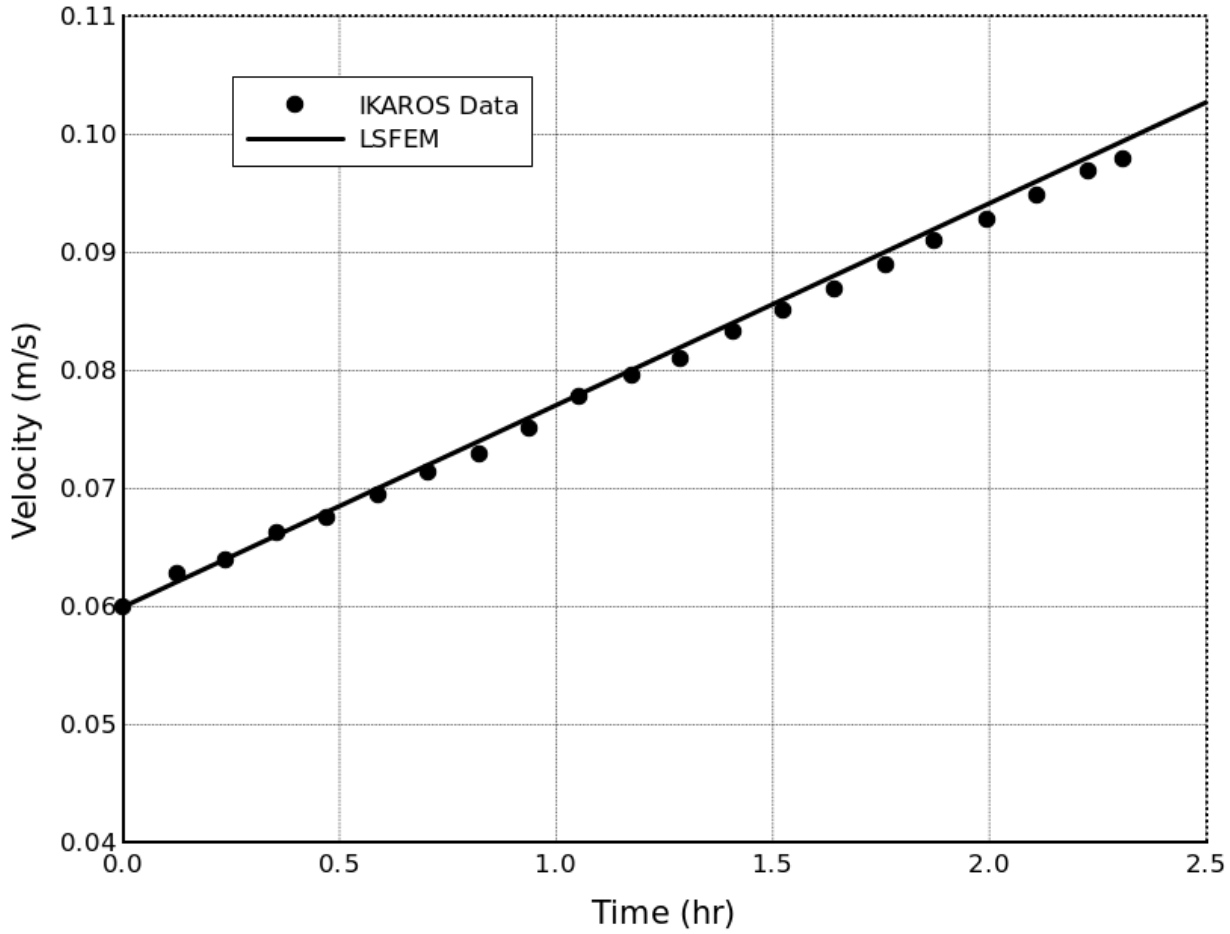

Figure 4.2 Comparison of LSFEM to Flight Data for SRP Acceleration Model

The results of the LSFEM propagation match very closely to the flight data. Computational error of the simulation is on the order of $1x10^{-16}$. Figure 4.3 shows the L2-norm plotted versus degrees of freedom that result from increasing the element amount.

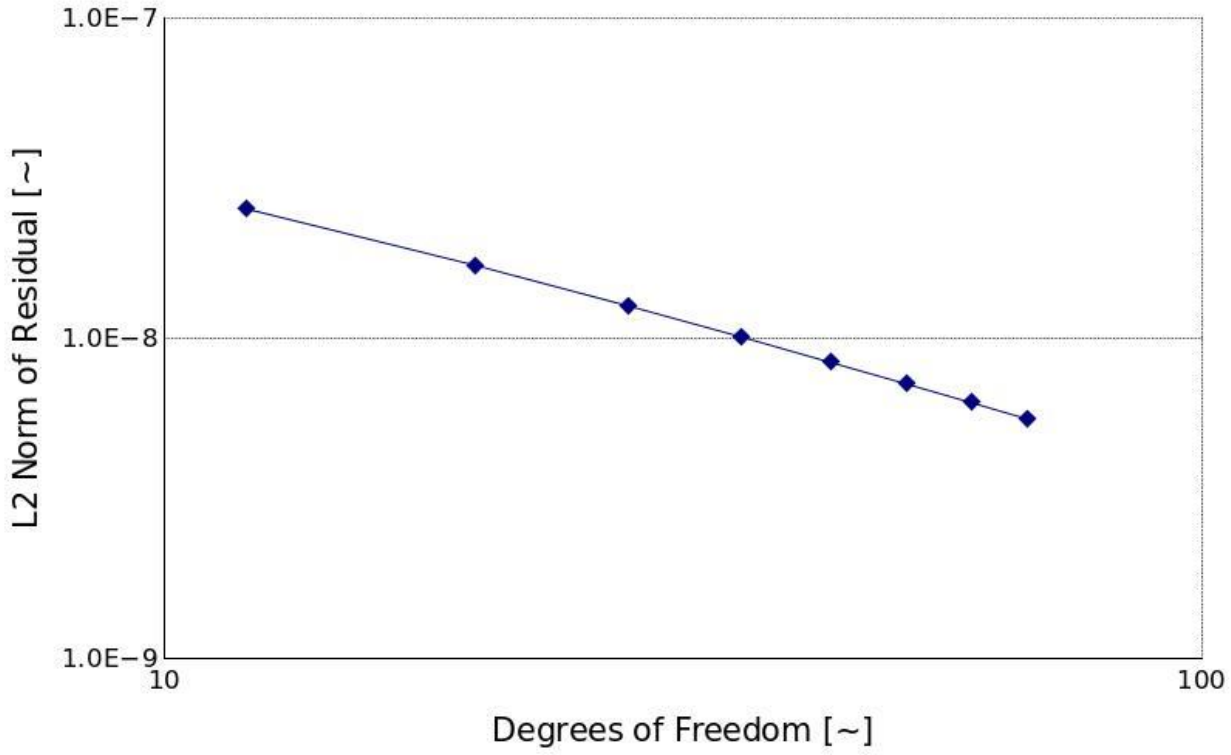

Figure 4.3 L2-norm versus Degrees of Freedom for IKAROS Simulation

The L2-norm begins to show convergence as the degrees of freedom exceed 50. The L2 norm of the residual is defined by the following equation:

$$\|E\|^2 = \sqrt{\int (E^2) dt} \tag{4.2}$$

where *E* is the sum of the residuals of all elements in the simulation.

4.2 AKATSUKI Simulation – Three-Dimensional EOM

The LSFEM model also has the ability to calculate three-dimensional trajectories. The three-dimensional sailcraft EOM was implemented into the STAR code. The trajectory of the

AKATSUKI spacecraft will be simulated to show the capabilities of the three-dimensional model. The AKATSUKI spacecraft is used for comparison because three-dimensional flight data is not available for IKAROS. Three-dimensional flight data for AKATSUKI is available from the JPL Horizons program [26]. The two satellites were launched on the same booster and traveled on almost identical flight paths during their trips from Earth to Venus. This simulation will also show that the LSFEM formulation is able to handle spacecraft and sailcraft. The trajectory flight data for the six month flight of AKATSUKI is provided in Table 4.1.

Table 4.1 AKATSUKI Trajectory Flight Data [26]

Time [days]	X [AU] (J2000EQ)	Y [AU] (J2000EQ)	Z [AU] (J2000EQ)
0	−0.150	−0.953	−0.428
5	−0.076	−0.963	−0.436
10	−0.001	−0.968	−0.440
15	0.074	−0.966	−0.442
20	0.148	−0.959	−0.441
25	0.222	−0.945	−0.438
30	0.294	−0.926	−0.431
35	0.364	−0.901	−0.422
40	0.432	−0.871	−0.411
45	0.497	−0.835	−0.397
50	0.560	−0.794	−0.380
55	0.618	−0.748	−0.361
60	0.673	−0.696	−0.339
65	0.722	−0.640	−0.316
70	0.767	−0.580	−0.289
75	0.806	−0.515	−0.261
80	0.839	−0.446	−0.231
85	0.866	−0.374	−0.199
90	0.885	−0.298	−0.165
95	0.896	−0.220	−0.130
100	0.899	−0.140	−0.094
105	0.894	−0.059	−0.057
110	0.880	0.023	−0.019
115	0.856	0.105	0.019
120	0.822	0.185	0.057
125	0.778	0.263	0.094
130	0.723	0.338	0.130
135	0.659	0.408	0.164
140	0.585	0.472	0.195
145	0.502	0.528	0.224
150	0.410	0.576	0.248

Table 4.2 shows the velocity flight data of AKATSUKI.

Table 4.2 AKATSUKI Velocity Flight Data [26]

Time [days]	V_X [AU/yr]	V_Y [A/yr]	V_Z [AU/yr]
0	0.859	−0.156	−0.100
5	0.868	−0.086	−0.068
10	0.871	−0.017	−0.037
15	0.868	0.052	−0.005
20	0.860	0.120	0.026
25	0.847	0.188	0.057
30	0.829	0.255	0.088
35	0.805	0.321	0.119
40	0.776	0.385	0.149
45	0.742	0.448	0.179
50	0.702	0.509	0.208
55	0.657	0.568	0.236
60	0.606	0.625	0.264
65	0.550	0.679	0.290
70	0.488	0.730	0.316
75	0.420	0.777	0.340
80	0.345	0.820	0.362
85	0.265	0.859	0.382
90	0.179	0.892	0.400
95	0.087	0.919	0.415
100	−0.011	0.938	0.427
105	−0.115	0.950	0.436
110	−0.223	0.952	0.441
115	−0.336	0.944	0.441
120	−0.452	0.923	0.435
125	−0.571	0.890	0.424
130	−0.689	0.843	0.407
135	−0.805	0.780	0.382
140	−0.916	0.702	0.350
145	−1.018	0.607	0.310
150	−1.109	0.497	0.263

The flight data is provided for a time span of 150 days at increments of 5 days. This same time span and time increment are used in the LSFEM simulation. The initial conditions are:

$$R = [-0.150 \ -0.953 \ -0.428]^T$$

$$\dot{R} = [0.859 \ -0.156 \ -0.100]^T$$

The LSFEM simulation is run in STAR using 1st order global differentiability and 3rd order polynomial approximations. Figure 4.4 presents the results of the LSFEM simulation and the flight data of the AKATSUKI trajectory.

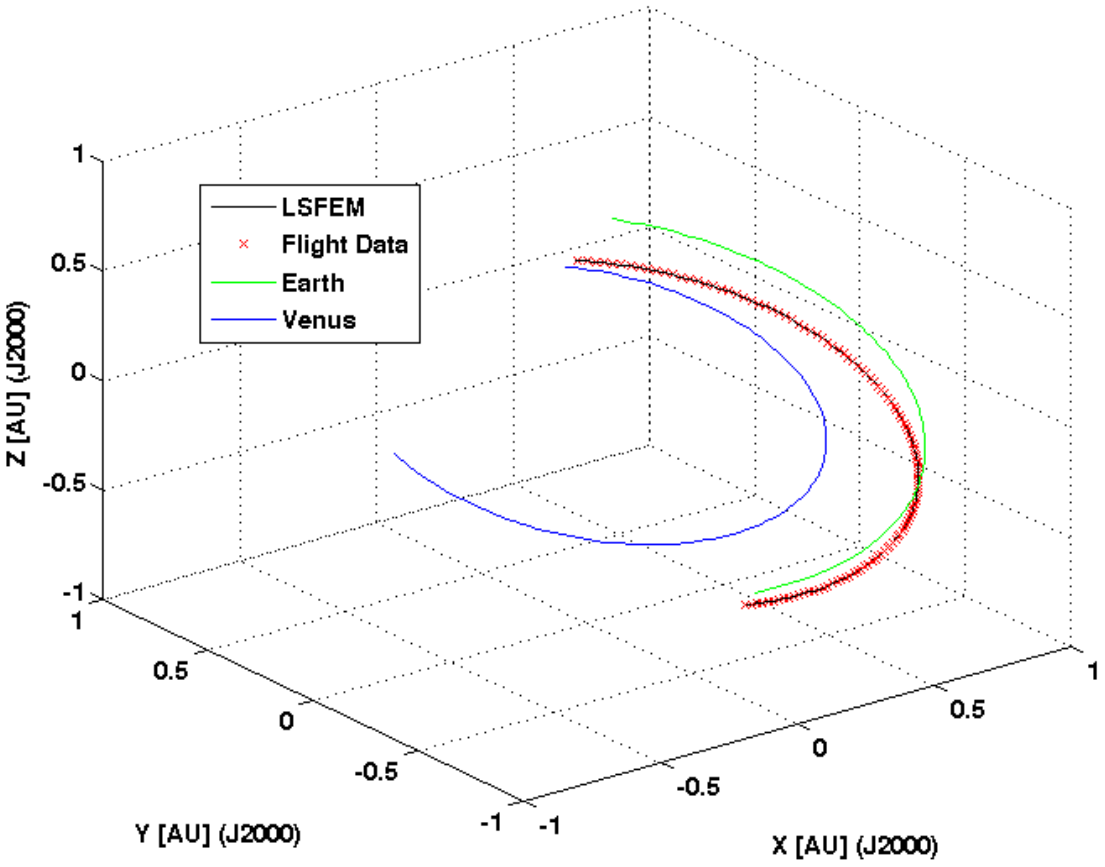

Figure 4.4 LSFEM Results and Flight Data of AKATSUKI Trajectory

The results show the three-dimensional flight path from Earth to Venus. No visible difference exists between the LSFEM results and the flight data. Figure 4.5 shows a top view of the trajectory with LSFEM results and flight data.

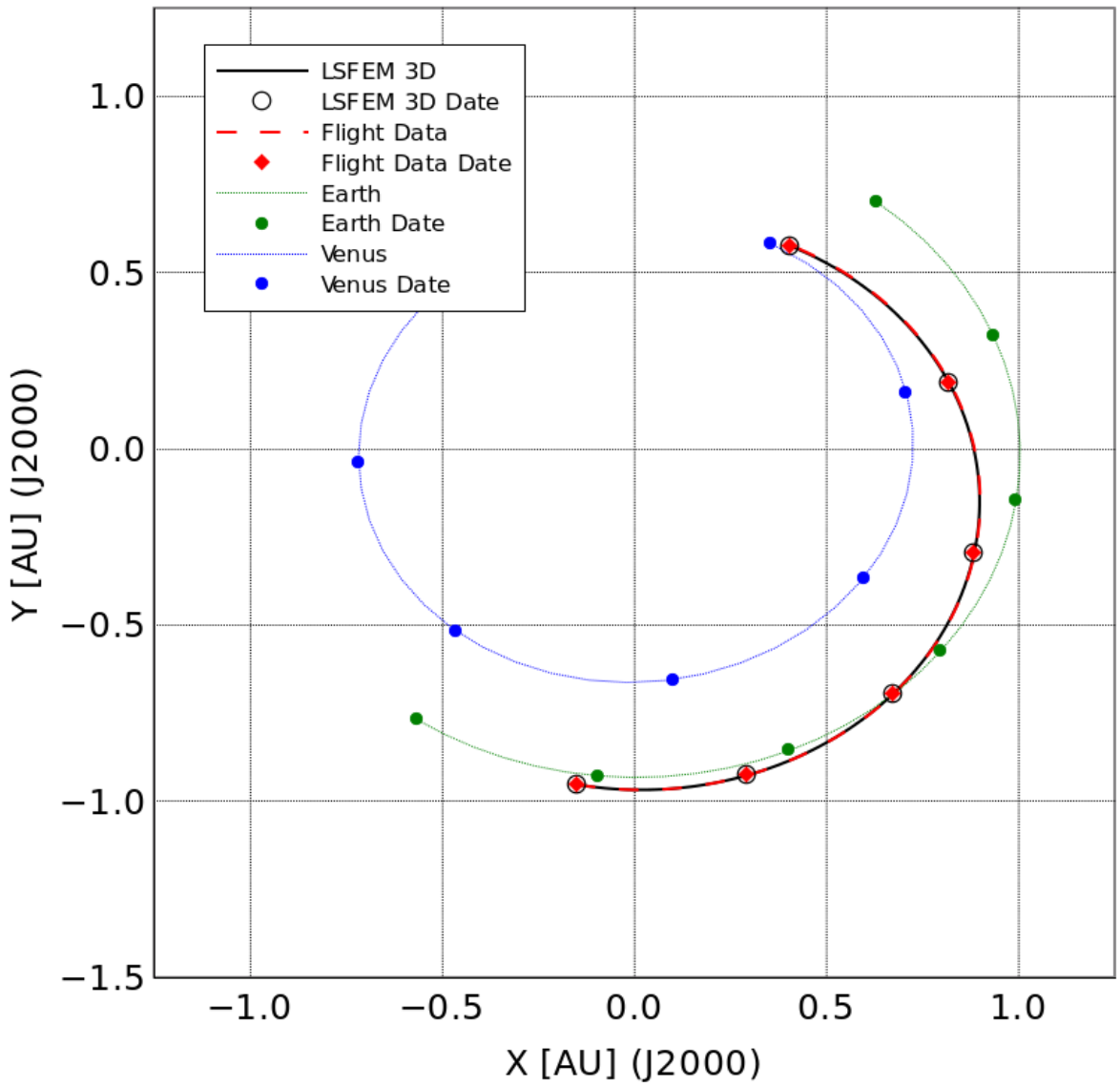

Figure 4.5 Top view of AKATSUKI Trajectory LSFEM Results and Flight Data

The top view includes results for the full trajectory and includes data points every month during the flight. The data points show that the simulation is accurate in both space and time. Figure 4.6 presents the L2-norm versus degrees of freedom.

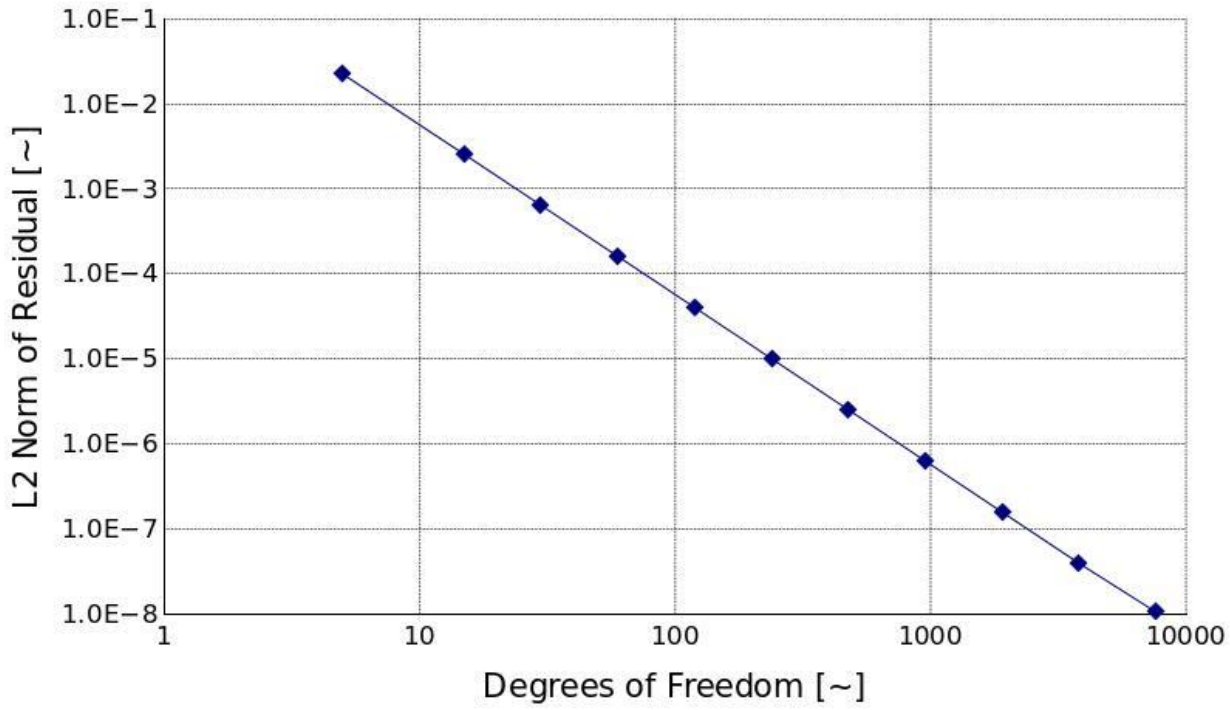

Figure 4.6 L2-norm versus Degrees of Freedom for AKATSUKI Simulation

The L2 norm is calculated using Equation (4.2).

A comparison between the LSFEM formulation and the Adams-Bashforth-Moulton method is made using the AKATSUKI trajectory. Both methods were used to simulate the five month flight path from Earth to Venus. The LSFEM setup is identical to the details mentioned above. The ABM setup uses the same initial conditions and time steps as the LSFEM formulation. Figure 4.7 and Figure 4.8 show close-up views of the AKATSUKI trajectory and velocity, respectively.

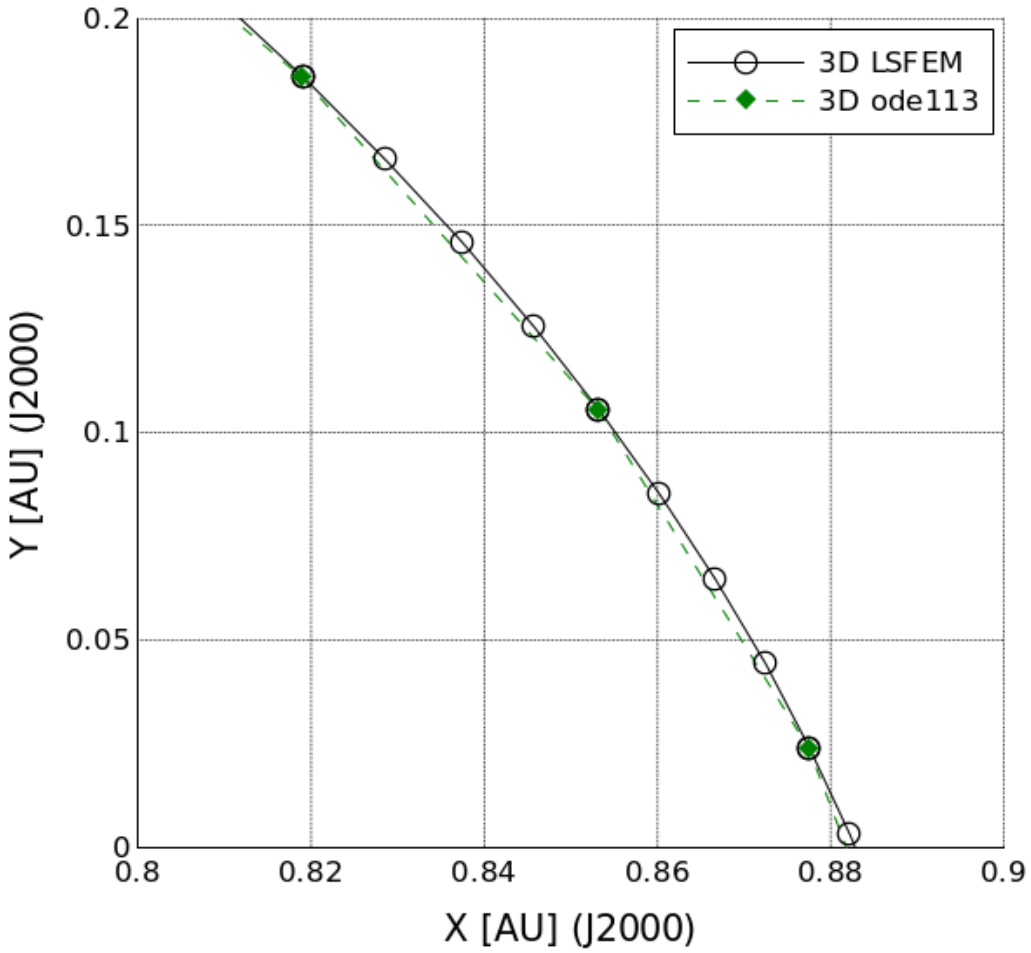

Figure 4.7 Inset of AKATSUKI Trajectory

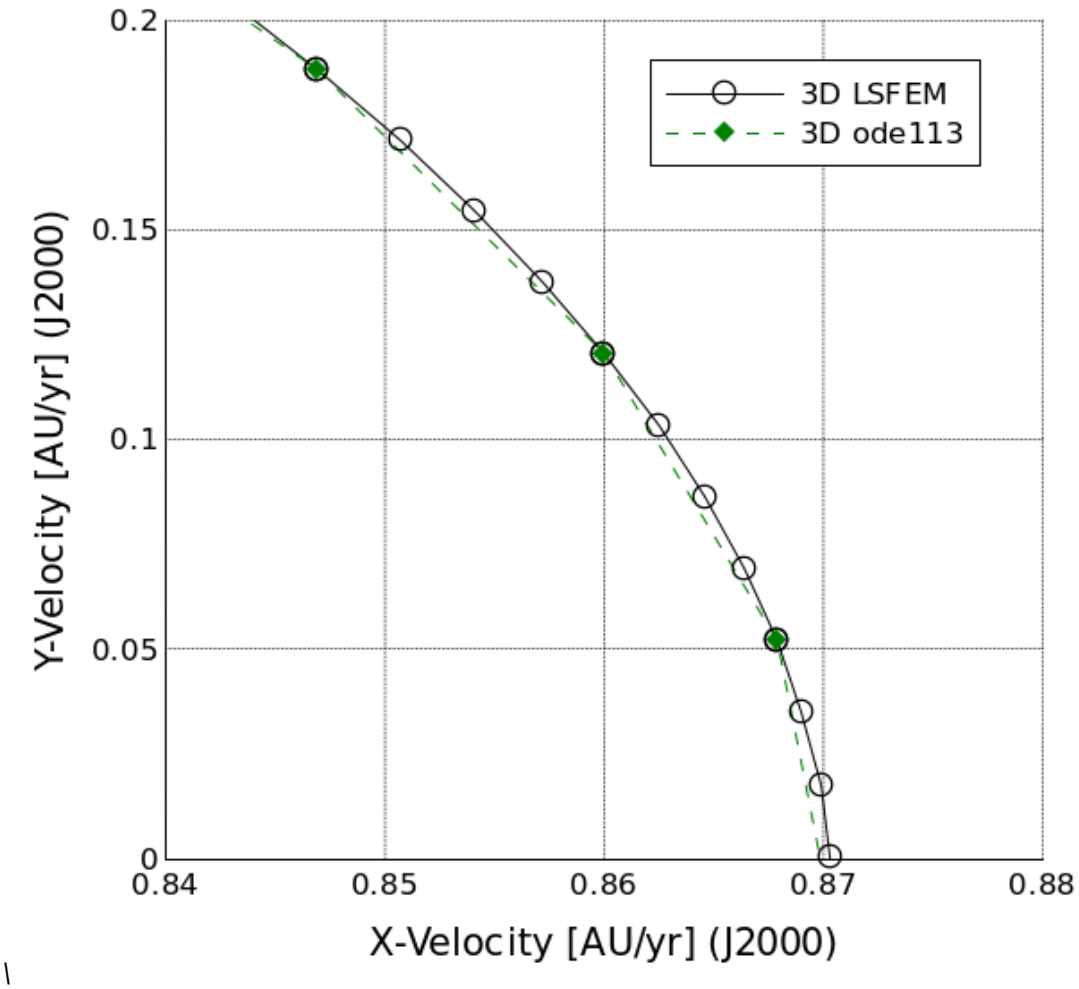

Figure 4.8 Inset of AKATSUKI Velocity

Both figures show that the LSFEM and ABM results are identical at each time step, however, the LSFEM is able to provide data between the end points of each step. For this simulation, five points per step is chosen, but any number of points can be used. This feature of the LSFEM provides more detailed results compared to the ABM.

Although no visible difference is apparent between the data in the figure, a closer examination of the data at the end of the flight path shows an increase in accuracy for the LSFEM simulation. Table 4.3 and Table 4.4 present the final conditions of each simulation, and include the final conditions from the flight data.

Table 4.3 Final Data Points for LSFEM Simulation

Parameter	X [AU]	Y [AU]	Z [AU]
Flight Data	0.4100	0.5759	0.2482
FEM	0.4047	0.5759	0.2486
Error [%]	−1.2934	−0.0004	0.1713

Table 4.4 Final Data Points for ABM Simulation

Parameter	X [AU]	Y [AU]	Z [AU]
Flight Data	0.4100	0.5759	0.2482
ABM	0.4044	0.5757	0.2486
Error [%]	−1.3628	−0.0313	0.1424

The errors are summarized in Table 4.5.

Table 4.5 Summary of Errors between LSFEM and ABM for AKATSUKI Trajectory

Location	LSFEM Error [%]	ABM Error [%]	Absolute Difference [%]
X	1.293	1.363	0.069
Y	0.000	0.031	0.031
Z	0.171	0.142	-0.029
Sum	1.464	1.537	0.072

The absolute difference between the LSFEM and the ABM is 0.072%, with LSFEM producing the smaller error. Therefore, the LSFEM final location is 0.072% more accurate than the ABM, which equates to 107710 km.

4.3 Convergence Study

Convergence studies are performed for the 1D IKAROS and 3D AKATSUKI simulations. The L2 norm of each simulation is calculated for decreasing time step size. The L2 norm of the residual is defined by the following equation:

$$\|E\|^2 = \sqrt{\int (E^2) dt} \tag{4.3}$$

where *E* is the sum of the residuals of all elements in the simulation. Comparison of the L2 norm to the time step size determines the truncation error of the numerical solution.

Figure 4.9 shows the comparison of the time step size to L2 norm for the 1D and 3D simulations.

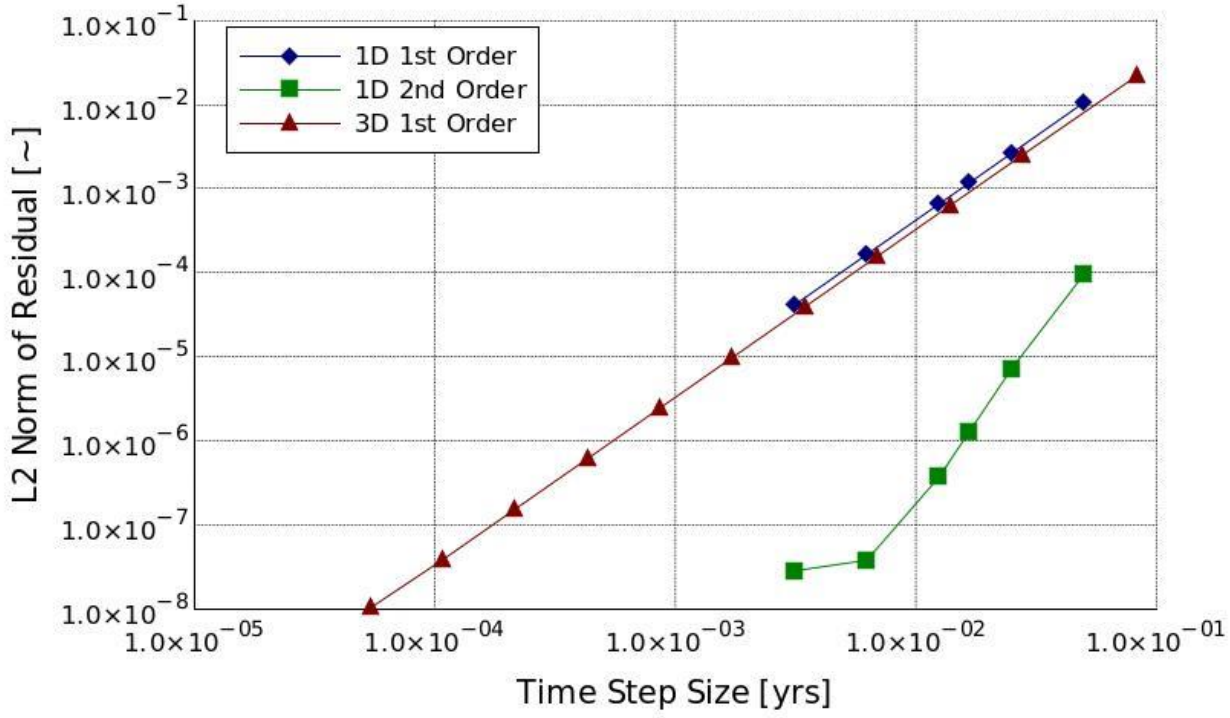

Figure 4.9 Convergence Studies of 1D and 3D Simulations

The convergence study is performed for the 1D simulation with first and second order global differentiability, which is denoted by 1D 1st order and 1D 2nd order in the legend. The 3D results are for 1st order global differentiability, which is denoted as 3D 1st order. The studies

show that first order global differentiability provides nearly second order accuracy and second order global differentiability provides almost fourth order accuracy. The 1D simulation with second order global differentiability stops at a minimum of 10^{-8}, which is due to the L2 norm taking the square root of a value on the order of 10^{-16}. The simulation is calculated on a computer with a machine epsilon of 10^{-16}.

4.4 Two-Dimensional Trajectory with Variable Lightness Vector

The LSFEM formulation will be used to propagate the trajectory of a sailcraft that changes attitude angles during flight. Modeling the attitude change is done using the lightness vector components because the lightness vector accounts for changes in sailcraft attitude.

The ability of the LSFEM formulation to run simulations with variable lightness vector values is demonstrated by simulating an H-reversal trajectory from [9]. H-reversal refers to the reversal of the direction of the spacecraft angular momentum vector. This type of trajectory has been demonstrated to have the ability of accelerating sailcraft to relatively high speeds compared to other propulsion techniques [9] [14]. Performing a H-reversal requires the sailcraft to change the tangential component of the lightness vector. Figure 4.10 presents the three-dimensional values of the lightness vector for maneuvering the sailcraft into a H-reversal trajectory.

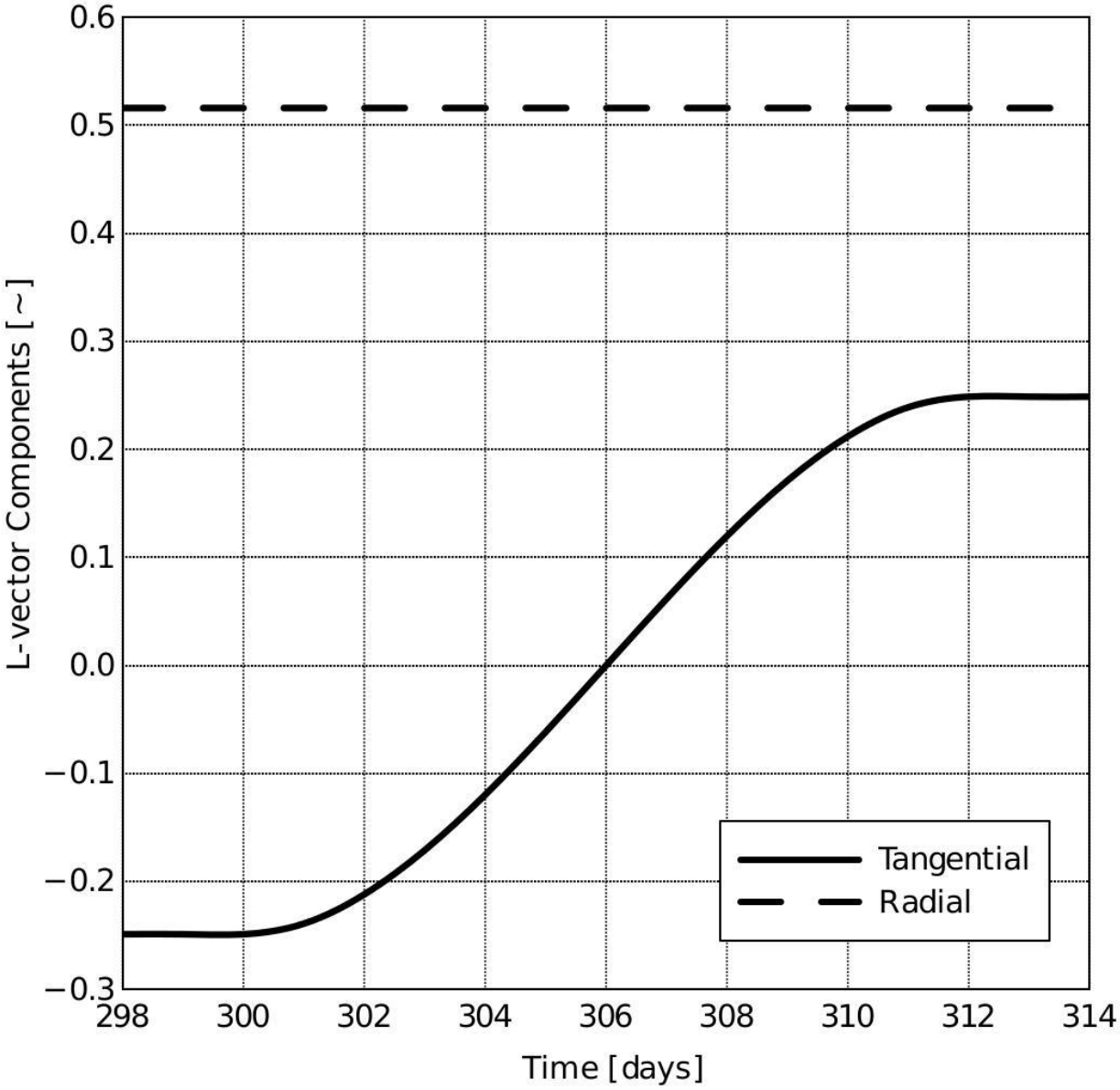

Figure 4.10 History of Lightness Vector Components

Figure 4.11 presents an example of a H-reversal trajectory in HIF.

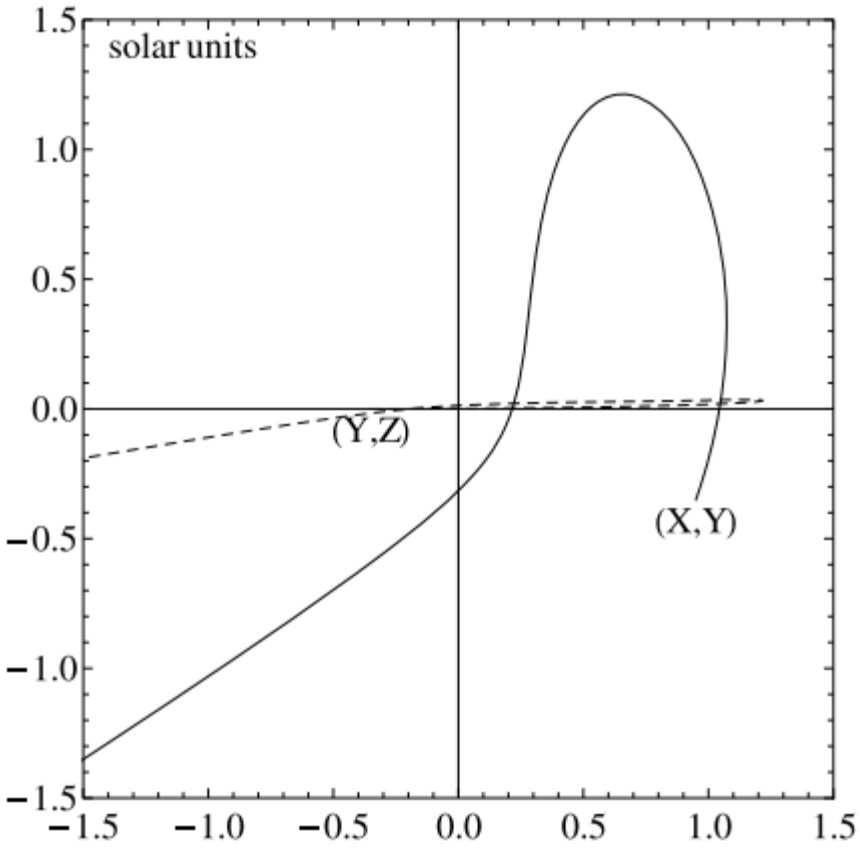

Figure 4.11 Projections of a H-reversal Trajectory in HIF

For the two-dimensional simulation, the radial lightness vector component is considered constant and the normal component is not considered. Inputting the time history of the lightness vector into the LSFEM simulation is done by the addition of the tangential component of the lightness vector and its first derivative at each element node. The time history of the tangential component is determined from Figure 4.10 and the derivative is determined using a third-order polynomial to define the change that occurs in the tangential component.

A third-order polynomial is used because it accurately defines the lightness vector variation and is a continuous function. The polynomial function is determined using the equation for a third-order polynomial and the known values of the lightness vector and its time derivative at the start and finish of the maneuver. The equation for a third-order polynomial is:

$$L_\tau = at^3 + bt^2 + ct + d \tag{4.4}$$

The derivative of the polynomial equation is:

$$\frac{\mathrm{dL_\tau}}{\mathrm{dt}} = 3\mathrm{at}^2 + 2\mathrm{bt} + \mathrm{c} \tag{4.5}$$

The known values at each end point are the tangential component of the lightness vector and its time derivative. The endpoint derivatives are both zero because, before and after the maneuver, the lightness vector is constant. The coefficients in the polynomial equation are solved using the known values at the endpoints, which results in a solvable system of four equations and four unknowns. The resulting equation for the polynomial is:

$$\mathrm{L_\tau} = (-6.64\mathrm{E}6)\mathrm{t}^3 + (4.63\mathrm{E}5)\mathrm{t}^2 + (-1.12\mathrm{E}4)\mathrm{t} + (7.32\mathrm{E}1) \tag{4.6}$$

The trajectory is simulated over a time span of 390 days using 3 day long time-steps. The initial conditions are based on a H-reversal trajectory from [9] and are presented below:

x = 0.9826 AU

$\dot{x}$ = -0.1886 AU/yr

y = 0.1898 AU

$\dot{y}$ = 0.9814 AU/yr

The values of the tangential component of the lightness vector are summarized below in Table 4.6.

Table 4.6 Time History of Lightness Vector Components and Derivatives

t [day]	L_τ	$\frac{dL_\tau}{dt}$
0 to 297	−0.2488	0.00
300	−0.2488	0.00
303	−0.1708	17.07
306	0.0000	22.76
309	0.1721	17.07
312	0.2488	0.00
315 to 390	0.2488	0.00

Figure 4.12 shows the change in lightness vector over the 12 day maneuver.

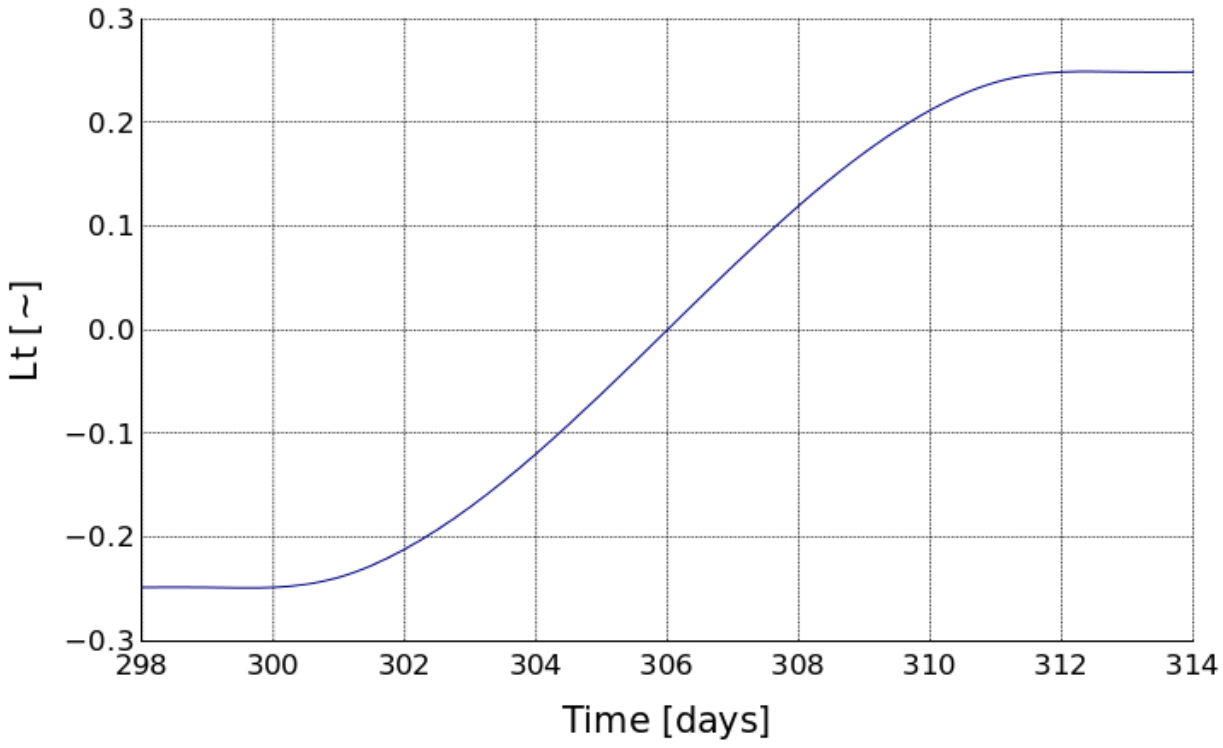

Figure 4.12 Change in Tangential Component of Lightness Vector

Figure 4.13 shows the derivative of the change in the tangential component of the lightness vector during the maneuver.

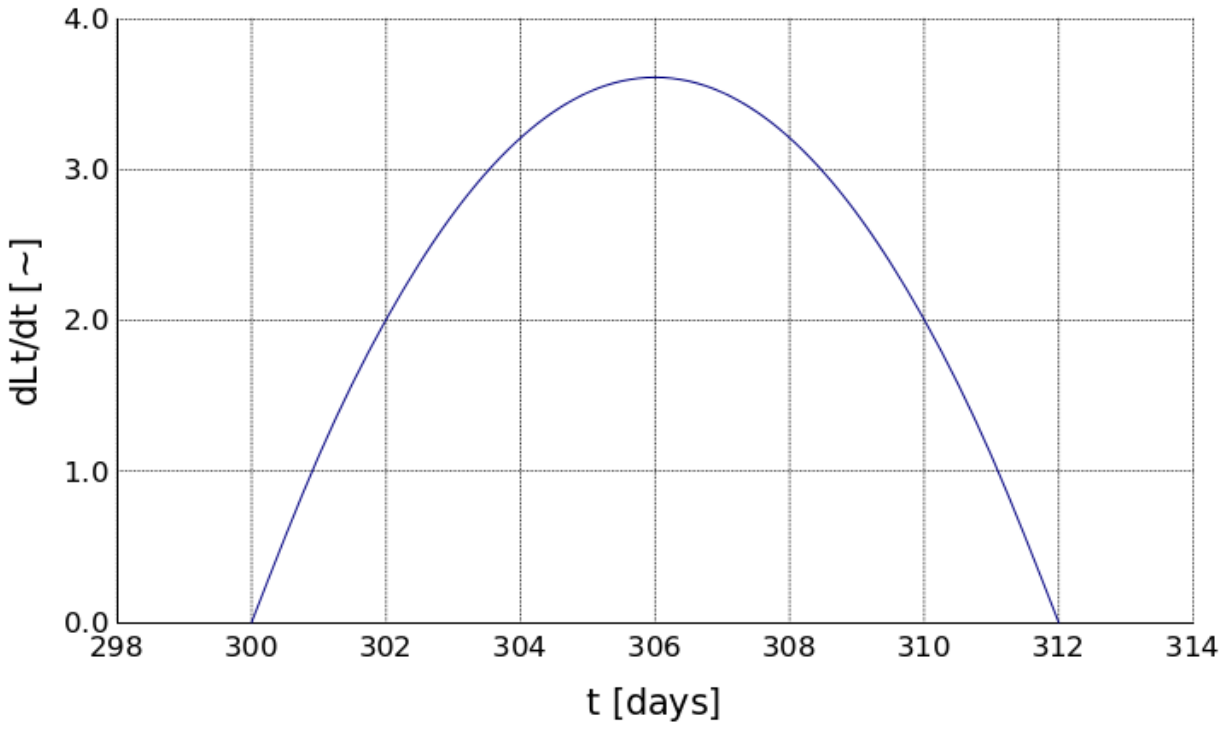

Figure 4.13 Derivative of the Change in Tangential Component of Lightness Vector

The radial component is constant during the simulation and is defined as:

L_ρ = 0.5348

$\frac{dL_\rho}{dt}$ = 0.0

Figure 4.14 shows the results of the simulation with and without variable lightness vector values.

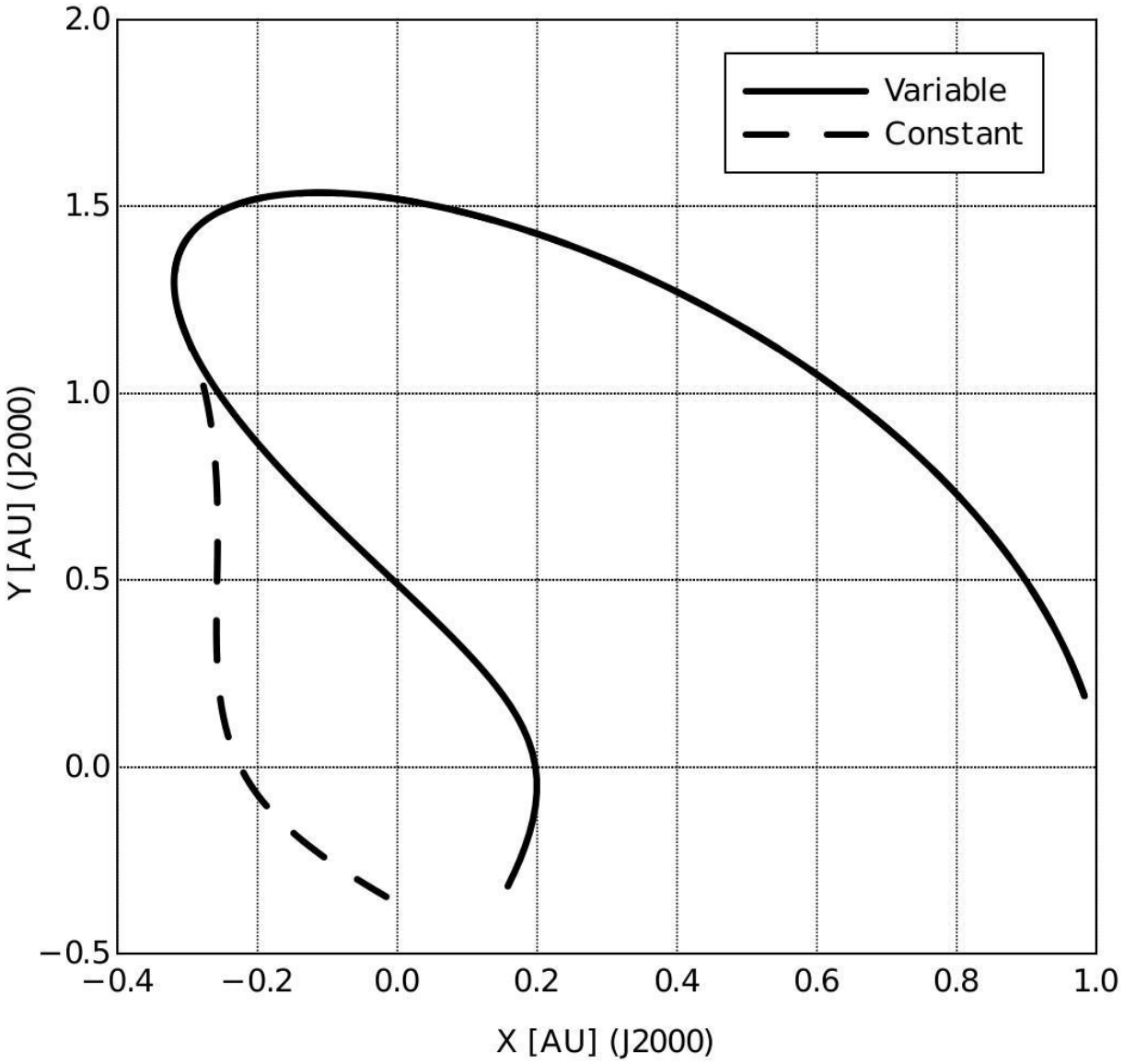

Figure 4.14 LSFEM Results of H-reversal Trajectory

The results for the variable lightness vector simulation clearly resemble a H-reversal type of trajectory.

5. Optimal Control Procedure

Optimal control is carried out by the addition of an objective function to the system of equations solved by the LSFEM. A two-dimensional optimization routine is implemented in the LSFEM to maximize sailcraft thrust in a specific direction. The control in a two-dimensional simulation is provided by the azimuth angle. This is the angle that specifies the orientation of the sail surface normal vector about the z-axis in HOF. Figure 5.1 is a top view of the xy-plane in HOF showing a schematic of sailcraft vectors and the azimuth angle.

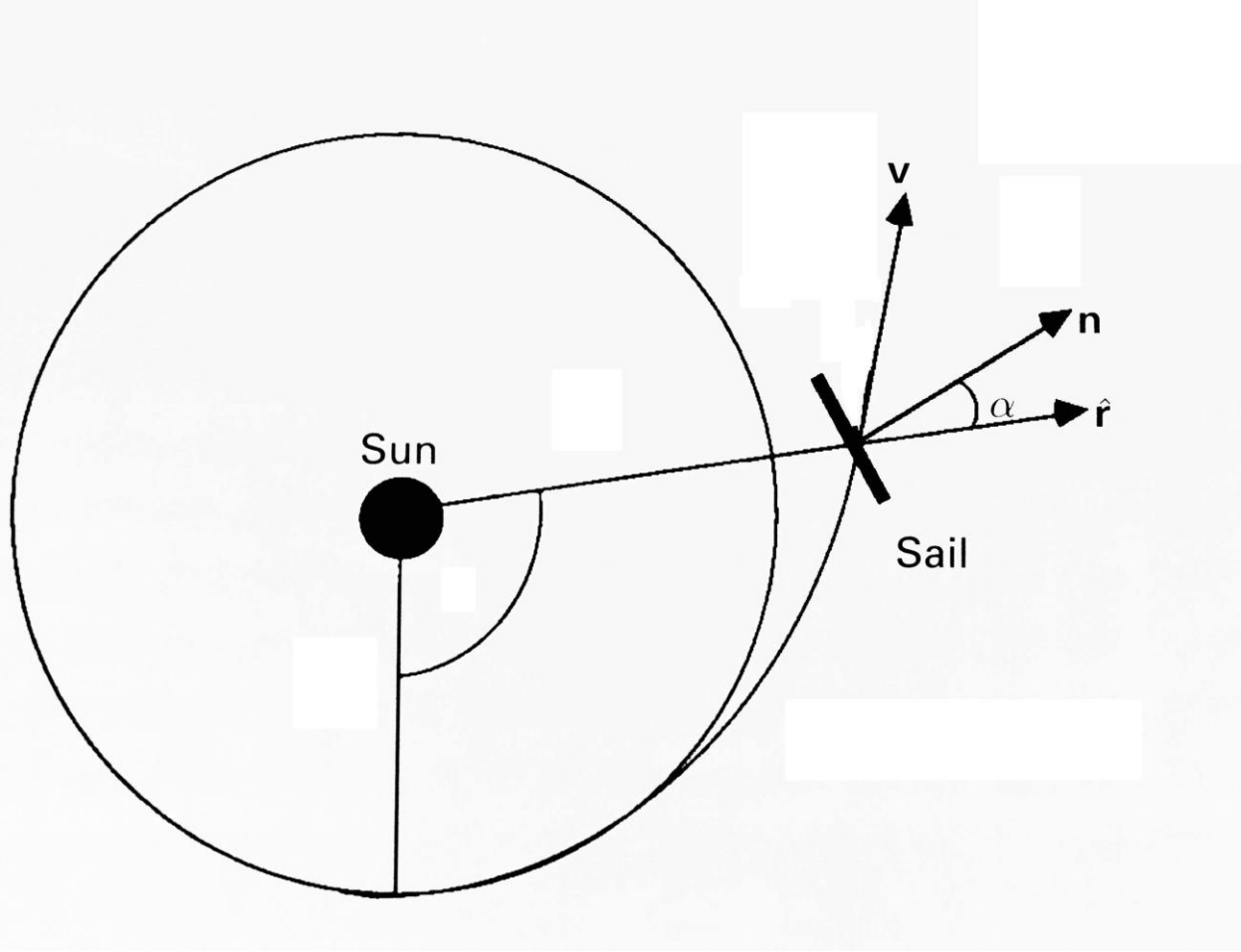

Figure 5.1 Definition of Sailcraft Azimuth Angle

5.1 Objective function

The objective function is presented below:

$$\alpha - \alpha_{\text{opt}} - \left(\frac{\alpha_{\text{i}} - \alpha_{\text{opt}}}{1 + \text{t}^5}\right) = 0 \tag{5.1}$$

This objective function optimizes thrust by taking the sailcraft from the current azimuth angle, α_i, to an azimuth angle that will maximize thrust from SRP in a specific direction, α_{opt}. The objective function is solved simultaneously with the sailcraft EOM system. When the solution is reached, the output of the LSFEM is the optimized trajectory and azimuth angles. Due to the high order global differentiability and high order polynomial approximations, the angular rates and angular accelerations associated with the optimization are also output.

5.2 Attitude Adjustment Torques

Due to the high order global differentiability and high order polynomial approximations, the angular rates and angular accelerations associated with the optimization are included in the output of the simulation. The angular rates and angular accelerations are input into the attitude dynamics equations [31] to determine the torque required to perform the maneuver. The only additional data needed to determine the torques are the sailcraft moments of inertia, which are a property of sailcraft mass and geometry.

6. Optimal Control Results

The LSFEM is used to optimize a trajectory. Results are obtained for the optimized trajectory, attitude dynamics, and control torque.

6.1 Thrust Optimization

A thrust maximization is performed that maneuvers the sailcraft from an initial orientation to a final orientation that provides maximum thrust in a specific direction. The following lists the initial conditions and the angle for maximized thrust:

$x = 1.0\ AU$

$\dot{x} =$ 0.0 AU/yr

$y =$ 0.0 AU

$\dot{y} =$ 1.0 AU/yr

$\alpha_i =$ 60 deg

$\alpha_{opt} =$ 30 deg

The two azimuth angles in the above list produce the objective function in Figure 6.1.

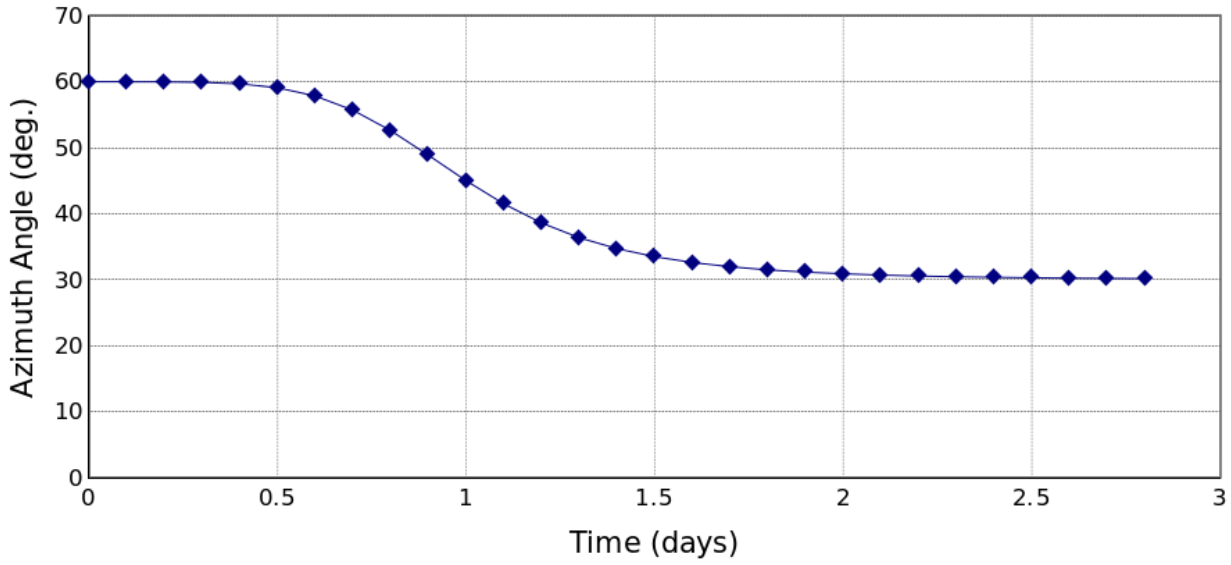

Figure 6.1 Objective Function for Thrust Maximization at 30° Azimuth

The sailcraft loadings are defined as:

$\sigma = 0.1$

$\sigma_{cr} = 0.5$

The following list provides the characteristics of the sailcraft (from [12] unless otherwise specified):

$\Re_s = 0.819$

$\Re_d = 0.062$

$A_f = 0.119$

$\tilde{\beta} = \pi/2 + 0.675\alpha$ [9]

$\vec{n} = [cos(-\alpha)\ \ sin(-\alpha)]^T$[9]

$\vec{u} = [1\ \ 0]^T$[9]

$\overrightarrow{x_s} = [sin(\alpha)\ \ cos(\alpha)]^T$[9]

$\varepsilon_f = 0.05$

$\varepsilon_b = 0.55$

$\chi_f = 0.79$

$\chi_b = 0.55$

Figure 6.2 shows the azimuth angle resulting from the thrust maximization.

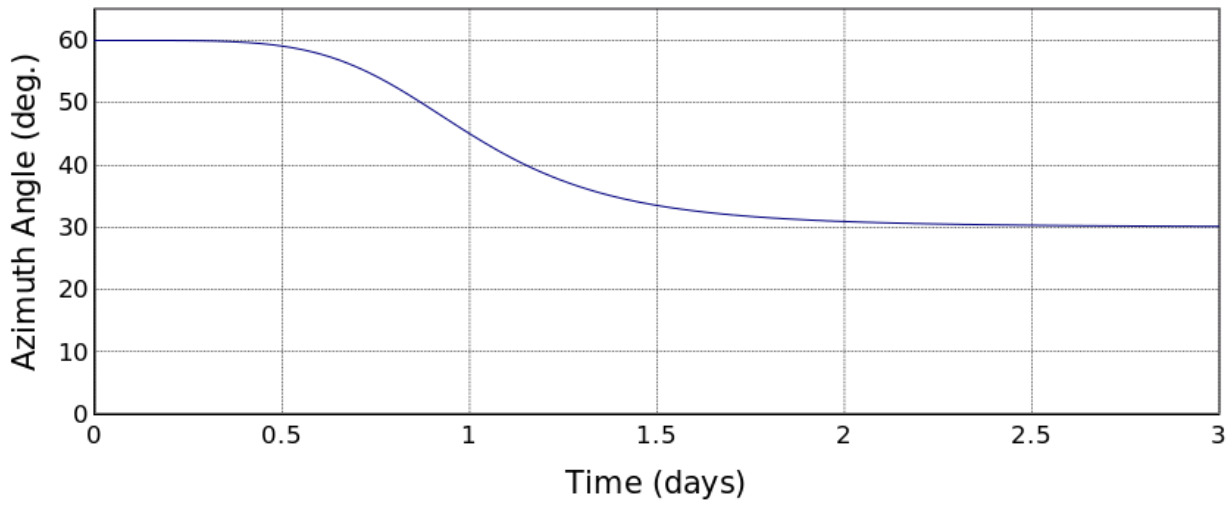

Figure 6.2 Azimuth Angle of Sailcraft for Thrust Maximization

Figure 6.3 shows the angular velocity resulting from the thrust maximization.

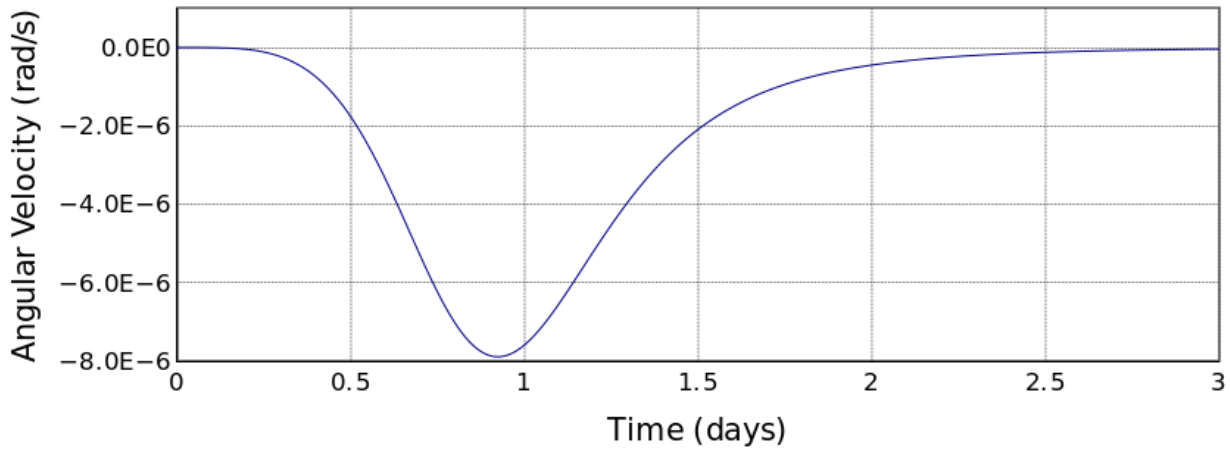

Figure 6.3 Azimuth Angular Rate of Sailcraft for Thrust Maximization

Figure 6.4 shows the angular acceleration resulting from the thrust maximization.

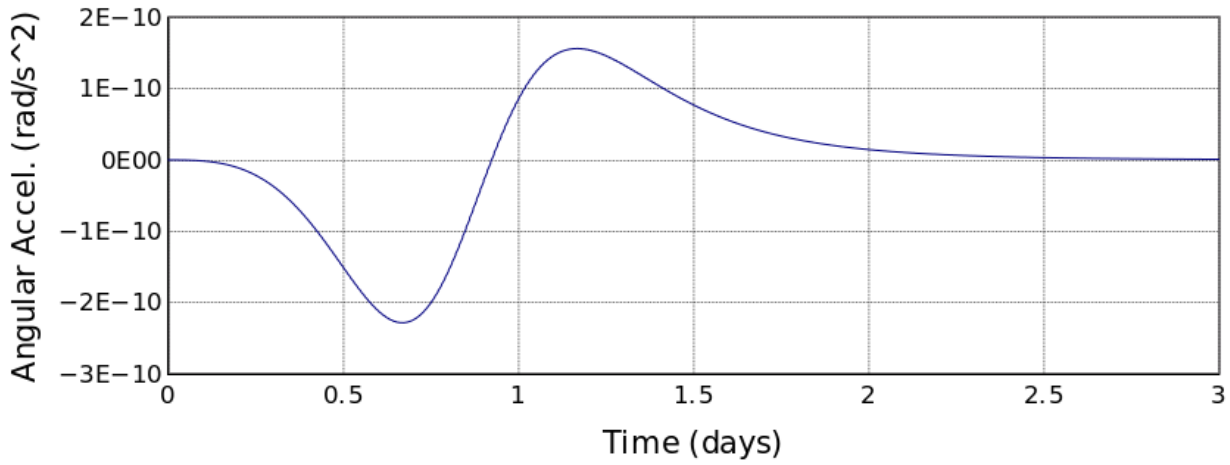

Figure 6.4 Azimuth Angular Acceleration of Sailcraft for Thrust Maximization

Figure 6.5 shows the trajectory resulting from the thrust maximization compared to the non-maximized trajectory.

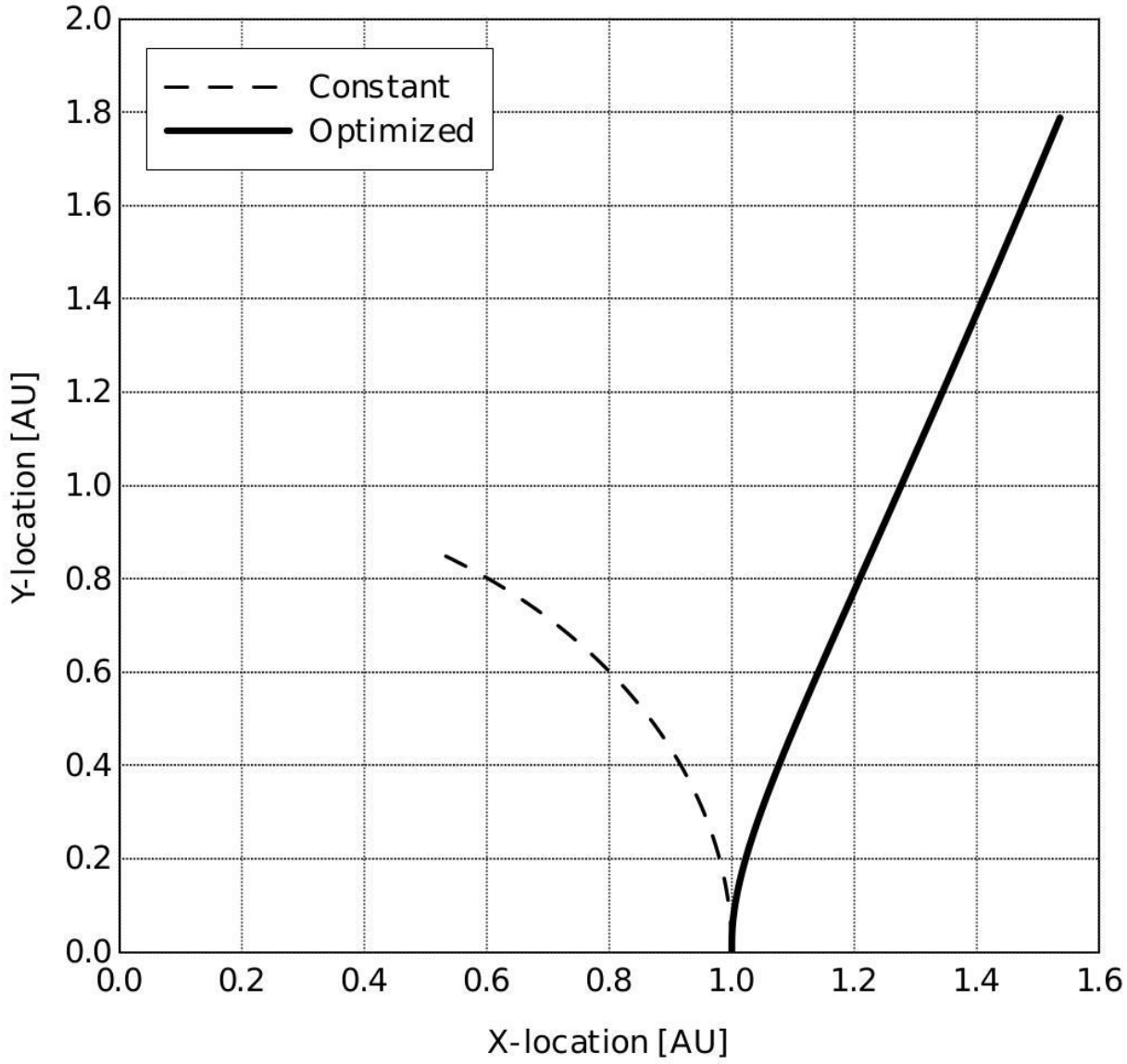

Figure 6.5 Trajectory for Thrust Optimization

The plot clearly shows that the sailcraft maneuvers to receive thrust in the maximized direction.

6.2 Torque

The angular acceleration from the optimization results is used with the attitude dynamics equations to calculate the torque required to achieve the azimuth angles required for maximizing

thrust.

For the two-dimensional case, the azimuth angle, which represents the rotation about the z-axis in HOF, is the only angle considered. Therefore, the attitude dynamics equations are reduce to:

$$I_z \dot{\omega}_z = T_z \tag{6.1}$$

A value of 66.38 slug-in^2 is used for the moment of inertia about the z-axis in HOF.

Figure 6.6 shows the required torque for performing the thrust optimization maneuver.

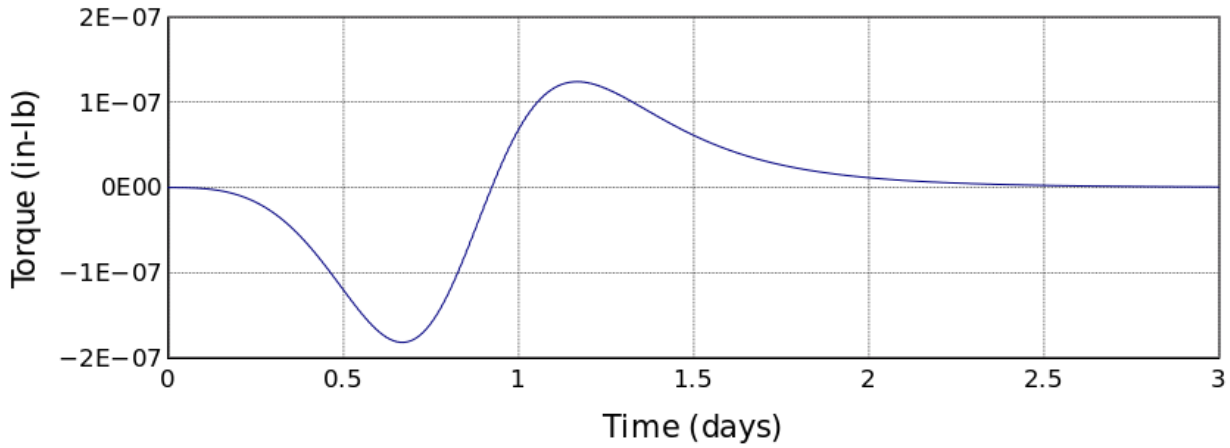

Figure 6.6 Torque for Thrust Optimization Maneuver

The magnitude of the torque applied is similar to what would be expected from a large, low-thrust spacecraft like a sailcraft.

7. Conclusion

A new method has been developed that provides unconditionally stable numerical solutions to sailcraft trajectories. It is able to handle a greater input of data compared to other propagation methods, which means a more detailed physical description of the trajectory is both input and output from the new method. It has the ability to incorporate basic optimal control and handles larger amounts of variables, which increases its accuracy over similar methods. The descriptions provided in this document have outlined the different aspects of the new approach for propagating sailcraft trajectories. Comparison of the IKAROS velocity data with the SRP acceleration model showed extremely close values. The AKATSUKI simulation results also matched the flight data and produced less error than the commonly used Adams-Bashforth-Moulton method. The closeness of the LSFEM results and the flight data verifies the accuracy of the LSFEM trajectory propagation and proves the new approach is worthy of continued research.

The LSFEM framework allows for more inputs, which results in more accurate output of data. The additional data and degrees of freedom in the model increase the detail of the mathematical description of the physics of sailcraft motion. The solution also benefits from the increase in degrees of freedom because more data can be output from a simulation. The proof of the increased accuracy is evidenced by the 0.072% more accurate solution compared to the ABM.

7.1 Impacts and accomplishments

The impacts and accomplishments of this research are summarized in the list below:

- Unconditionally stable trajectory propagation technique
- Thrust optimization incorporate into the trajectory propagation routine
- Improved physical description of the sailcraft trajectory through an increase of input and output variables
- Numerical solution is always unique
- 2^{nd} order and higher ODE system are solvable
- Data between times steps is always provided
- High order differentiability and polynomial approximations make simulation more true to physics
- Accuracy increase of 0.072% over the ABM.

Additional capabilities of the new method are:

- Initial conditions or initial and final conditions can be used
- Capable of simulating attitude changes and planetary perturbations

- The author developed the computer program for running trajectory simulations and optimizations

- Research on trajectory propagation presented at AIAA SciTech conference on January 5th

- Research on trajectory propagation and optimization will be submitted to AAS/AIAA Astrodynamics Specialist Conference (abstract in progress)

- Manuscript for research on trajectory propagation and optimization will be submitted to the Acta Astronautica journal (manuscript in progress)

7.2 Future Research

The following topics can expand the current research to include more spacecraft types and optimization techniques:

- Use the new method to propagate trajectories for spacecraft with chemical rocket and ion propulsion systems using the following equations:

$$\ddot{\boldsymbol{R}} + \mu \frac{\boldsymbol{R}}{|R|^3} = \frac{\boldsymbol{T}}{M}$$

$$\dot{M} = -\frac{|T|}{U_e}$$

- Include additional terms into the EOM to handle interplanetary perturbations and disturbances. Apply the current numerical framework to more optimal control techniques

- Study the numerical details of the current simulation, which may include numerical dissipation and runtime, and compare them to other trajectory propagation techniques

Future research can be assisted by using the material in the Appendices. Appendix A presents the input file for the one-dimensional SRP simulation, which was performed using [32]. Appendix B provides the full MATLAB source code for the two-dimensional EOM with planetary perturbations. Appendix C provides the inputs and output for using the HORIZONS code from [26]. With this material and a background in the numerical methods used to solve the EOM, this research can be continue to include the recommendations mentioned in this document and any possibilities from future researchers.

8. References

[1] The Planetary Society. (2015, February 26). *LightSail A Solar Sailing Spacecraft from the Planetary Society* [Online]. Available: http://sail.planetary.org/

[2] Japan Aerospace Exploration Agency. (2015, February 26). *Small Solar Power Sail Demonstrator "IKAROS" Topics* [Online]. Available: http://global.jaxa.jp/projects/sat/ikaros/topics.html#topics2522

[3] National Aeronautics and Space Administration. (2015, February 26). *Small Satellite Missions Nanosail-D Latest News* [Online]. Available: http://www.nasa.gov/mission_pages/smallsats/nanosaild.html

[4] B. Betts. (2005, June 21). *The Launch of Cosmos 1: Live Reports* [Online}. Available: http://www.planetary.org/blogs/bruce-betts/ss_update_20050622.html

[5] J. Davis. (2015, January 26). *It's Official: LightSail Test Flight Scheduled for May 2015* [Online]. Available: http://www.planetary.org/blogs/jason-davis/2015/20150112-lightsail-test-flight.html

[6] National Aeronautics and Space Administration. (2011, July 12). *Dawn Journey to the Asteroid Belt* [Online]. Available: http://www.nasa.gov/mission_pages/dawn/spacecraft/index.html

[7] T. Yamaguchi et. al., "Trajectory Analysis of Solar Sail Spacecraft Considering the Large Uncertainty of Solar Radiation Pressure," JAXA, Sagamihara, Japan, 2009.

[8] R. M. Georgevic, "Mathematical Model of the Solar Radiation Force and Torques Acting on the Components of a Spacecraft," NASA JPL, Pasadena, CA, TM 33-494, 1971.

[9] G. Vulpetti, *Fast Solar Sailing: Astrodynamics of Special Sailcraft Trajectories*. Springer, 2013.

[10] Y. Tsuda et al., "Flight status of IKAROS deep space solar sail demonstrator," Acta Astronautica, vol. 69, issue 9-10, pp. 833-840, Nov 2011.

[11] Y. Tsuda, et. al. "Achievement of IKAROS – Japanese deep space solar sail demonstration mission," Acta Astronautica, vol. 82, issue 2, pp. 183-188, Feb 2013.

[12] C. R. McInnes, "Solar Radiation Pressure," in *Solar Sailing: Technology, Dynamics and Mission Applications*, Chichester, UK, Praxis, 1999, ch. 2, pp. 43-49.

[13] L. Rios-Reyes and D. J. Scheeres, "Generalized Model for Solar Sails," *J. Spacecraft and Rockets*, vol. 42, no. 1, pp. 182-185, Jan. 2005.

[14] G. Vulpetti, "Sailcraft Trajectory Options for the Interstellar Probe: Mathematical Theory and Numerical Results," in *The Interstellar Probe (ISP): Pre-Perihelion Trajectories and Application of Holography*, NASA Marshall Space Flight Center, Huntsville, AL, NASA/CR -2002-211730, June 2002, ch. 4, pp.IV-1-IV-38.

[15] J. Ellis *et al*., "A Solar Sail Integrated Simulation Toolkit," in *14th AAS/AIAA Space Flight Mechanics Conf.*, Maui, HI, 2004.

[16] S. Thomas *et al.*, "Design and Simulation of Sailcraft Attitude Control Systems Using the Solar Sail Control Toolbox," in *AIAA Guidance, Navigation, and Control Conf. And Exhibit*, Providence, RI, 2004.

[17] MathWorks. (2014, July 20). *ode113* [online] Available: http://www.mathworks.com/help/matlab/ref/ode113.html#bti6pdv-49

[18] E. B. Shanks, "Higher Order Approximations of Runge-Kutta Type," NASA Langley, Washington D.C.,Tech. Note D-2920, Sept. 1965.

[19] D. A. Vallado, *Fundamentals of Astrodynamics and Applications,* 2Nd ed. El Segundo, CA: Microcosm Press, 2001.

[20] K. S. Surana and J. N. Reddy, "Mathematics of Computations and the Finite Element Method for Boundary Value Problems," unpublished.

[21] K. S. Surana and J. N. Reddy, "Mathematics of Computations and the Finite Element Method for Initial Value Problems," unpublished.

[22] J. H. E. Cartwright and O. Piro, "The Dynamics of Runge-Kutta Methods," Int. J. Bifurcation and Chaos, no. 2, pp. 427-449, 1992.

[23] P. J. Olver, *Applied Mathematics*, University of Minnesota, 2012, ch. 20.

[24] G. Vulpetti and S. Scaglione, "The Aurora Project: Estimation of the Optical Sail Parameters," *Acta Astronautica*, vol. 44, nos. 2-4, pp. 123-132, 1999.

[25] O. Mori *et al*., "First Solar Power Sail Demonstration by IKAROS," JAXA, Sagamihara, Japan, Rep. 2009-o-4-07v, 2009.

[26] Solar System Dynamics Group. (2014, August 19). JPL Horizons, version 3.93 [online] Available Telnet: horizons.jpl.nasa.gov 6775

[27] S Subchan, R. Zbikowski, *Computational Optimal Control Tools and Practice*, West Sussex, UK, Wiley, 2009.

[28] G, Fasano, J. Pinter, *Modeling and Optimization in Space Engineering*, New York, Springer, 2013.

[29] T. L. Friesz, "Nonlinear Optimal Control and Discrete-Time Optimal Control," in *Dynamic Optimization and Differential Games*, Springer, 2010, ch. 2, pp. 33-78.

[30] F. L. Lewis, D. L. Vrabie, V. L. Syrmos, *Optimal Control*, 3rd ed., Wiley, Hoboken, NJ, 2012.

[31] A. H. J. De Ruiter, et al., "Introduction to Spacecraft Attitude Stabilization," in *Spacecraft Dynamics and Control*, Wiley, West Sussex, UK, 2013, ch. 11, pp. 219-225.

[32] FINESSE, Finite Element System, Software Package, Lawrence KS, 2014.

[33] MATLAB, The MathWorks, Inc., Software Package, R2008b.

APPENDIX A: FINESSE Input File

```
finesse ss08
*title
Solar Sail Performance Analysis
*solution
0,0,0, 0,0,1, 0,0,0
*element selection
1,11,15,3, 0,0,0,  5,0,0,0,  11,0,0,0,  0,  2,0,0,0, 0,0
*incidences
$$-4,1,2
1,2,3 $ 1,1,1,0, 1,1,2
*coordinates
1, 0.0000, 0.0000, 0.0000, 0
9, 0.0100, 0.0000, 0.0000, 0, 1
*real
1
********
** K   |
**     |
********
 4.50045
*material
pe, 1 ,0 , 100.0
k,  1 ,0 , 100.0
*constraints
1
**
1, 1, 2, 0.4, p
1, 1, 2, 0.0, p1
1, 1, 2, 28.1278, p2
*initial
1
**
1, 9, 2, 0.4, p
1, 9, 2, 28.1278, p2
**debug
**0,0,0,0,   0, 0, 0, 0, 0,    1
**0,0,0,0, -20
**
*finesse
0, 30, 0, 2, 1.0e-6, 1.0e-6
**************************************
0,0,0,1,0
*quit
```

APPENDIX B: Two-Dimensional Simulation with Planetary Gravity

```
clc
clear all
tic
%------------------- initialization -------------------%
% input function
[he,step,pts,rho,tau,uE,uV,x1,dx1,y1,dy1]=inputF();

% initial guess
delta1=[x1;dx1;y1;dy1];

% Jacobian
J=he/2;

% preallocation
xp=zeros(1,step); yp=xp; dxp=xp; dyp=xp;
xp(1)=delta1(1); dxp(1)=delta1(2);
yp(1)=delta1(3); dyp(1)=delta1(4);
const=[J;rho;tau;uE;uV];
%------------------------------------------------------%


%---------------------- time loop ----------------------%
for dt=1:step
fprintf('\n=== Time Step : %i ===\n',dt);

% populating delta vector
[X,Y,Xe,Ye,Xv,Yv]=dofF(delta1,dt);

    %--------------------- newton loop ---------------------%
    g=1; it=0;
    while g >= 1e-6 && it<20
    it=it+1; flag=0;
    fprintf('\n--- Iteration: %i ---\n',it);

    % updating dofs per iteration
    X(3:4)=[delta1(1);delta1(2)];
    Y(3:4)=[delta1(3);delta1(4)];

    % Gauss 7pt quadrature
    [I,K,G]=gaussF(const,X,Y,Xe,Ye,Xv,Yv);

    %Newtons method
    [delta1,g]=newtonF(delta1,K,G);

    %output
    outputF(delta1,I,g);
    if it==20; flag=1; end
    end
    %------------------------------------------------------%

% plotting dofs per step
xp(dt+1)=delta1(1); dxp(dt+1)=delta1(2);
```

```
yp(dt+1)=delta1(3); dyp(dt+1)=delta1(4);
end
%-------------------------------------------------------%


%------------------ post processing --------------------%
% tabulation of solution variables
[Re,Ve]=EarthF(); [Rv,Vv]=VenusF();

xpe=Re(:,1); dxpe=Ve(:,1); ype=Re(:,2); dype=Ve(:,2);
xpv=Rv(:,1); dxpv=Vv(:,1); ypv=Rv(:,2); dypv=Vv(:,2);

[I_plot]=plotF(pts,xp ,dxp ,yp ,dyp ,step,he);
[E_plot]=plotF(pts,xpe,dxpe,ype,dype,step,he);
[V_plot]=plotF(pts,xpv,dxpv,ypv,dypv,step,he);

plot(I_plot(:,2),I_plot(:,5),E_plot(:,2),E_plot(:,5),...
     V_plot(:,2),V_plot(:,5));
axis equal;xlim([-1,1]);ylim([-1,1]);
fprintf('\nError indicator = %i\n',flag);
%-------------------------------------------------------%

toc
% end of MAIN %

function [X,Y,Xe,Ye,Xv,Yv]=dofF(delta1,dt)

% updating dofs per step (intital guess)
X=[delta1(1);delta1(2);delta1(1);delta1(2)];
Y=[delta1(3);delta1(4);delta1(3);delta1(4)];

% planetary variables
[Re,Ve]=EarthF(); [Rv,Vv]=VenusF();
Xe=[Re(dt,1);Ve(dt,1);Re(dt+1,1);Ve(dt+1,1)];
Ye=[Re(dt,2);Ve(dt,2);Re(dt+1,2);Ve(dt+1,2)];
Xv=[Rv(dt,1);Vv(dt,1);Rv(dt+1,1);Vv(dt+1,1)];
Yv=[Rv(dt,2);Vv(dt,2);Rv(dt+1,2);Vv(dt+1,2)];

%%

function [he,step,pts,rho,tau,uE,uV,x1,dx1,y1,dy1]=inputF()


step= 130;
 he = (3/365.25)*2*pi;
pts = 5;
rho = 0.534810;
tau =-0.248777;
 uE = 3.003486606393789e-06;
 uV = 2.454178594336319e-06;
 x1 = 0.9825873;
dx1 =-1.1851558/(2*pi);
```

```
 y1 = 0.1898193;
dy1 = 6.1665726/(2*pi);


%{
step= 30;
 he = (5/365.25)*2*pi;
pts = 5;
rho = 0;%0.000807505;
tau = 0;
 x1 =-1.504699915740330E-01;
dx1 = 1.479451861635297E-02*365/(2*pi);
 y1 =-9.526684223647366E-01;
dy1 =-2.688268126973769E-03*365/(2*pi);
%}
function [I,K,G]=gaussF(const,X,Y,Xe,Ye,Xv,Yv)
J=const(1);rho=const(2);tau=const(3); uE=const(4);uV=const(5);

% 7 point Gauss Quadrature
c=[ 0.1294849661688697   0.2797053914892766  0.3818300505051189...
    0.4179591836734694  0.3818300505051189  0.2797053914892766...
    0.1294849661688697];
x=[-0.9491079123427585 -0.7415311855993945 -0.4058451513773972...
    0.000000000000      0.4058451513773972  0.7415311855993945...
    0.9491079123427585];

I=0; K=0; G=0;
for i=1:7
    [I0,K0,G0]=funcIKG(x(i),const,X,Y,Xe,Ye,Xv,Yv);
    I=I+c(i).*I0.*J;
    K=K+c(i).*K0.*J;
    G=G+c(i).*G0.*J;
end

function [I,K,G]=funcIKG(ep,const,X,Y,Xe,Ye,Xv,Yv)
J=const(1);rho=const(2);tau=const(3);uE=const(4);uV=const(5);

% calling residuals and variations
[E1,E2,dE1,dE2]=funcE(ep,const,X,Y,Xe,Ye,Xv,Yv);

% I K G
I=(E1.^2+E2.^2);
K=(dE1*dE1.'+dE2*dE2.');
G=(E1.*dE1+E2.*dE2);

% truncating K and G down to dofs
BC=[1,2,5,6,[9:24]];
sBC=size(BC,2);
for i=sBC:-1:1
    K(BC(i),:)=[]; K(:,BC(i))=[];
    G(BC(i),:)=[];
end
```

```
%%

function [E1,E2,dE1,dE2]=funcE(ep,const,X,Y,Xe,Ye,Xv,Yv)
J=const(1);rho=const(2);tau=const(3);uE=const(4);uV=const(5);

% function call for polynomial approximation functions
[N,dN,d2N] = funcC1p3(ep,J);

% variable approximations
x=N*X; d2x=d2N*X;
y=N*Y; d2y=d2N*Y;
xe=N*Xe; xv=N*Xv;
ye=N*Ye; yv=N*Yv;

N=N.'; d2N=d2N.';

% Residual Equations {{x} {y} {xE} {yE} {xV} {yV}}
R=sqrt(x.^2+y.^2);
Re=sqrt((x-xe)^2+(y-ye)^2);
Rv=sqrt((x-xv)^2+(y-yv)^2);
Le=R/Re; Lv=R/Rv;

px=uE*(Le)^3*(x-xe)+uV*(Lv)^3*(x-xv);
py=uE*(Le)^3*(y-ye)+uV*(Lv)^3*(y-yv);

E1=R.^3.*d2x-(rho.*x-tau.*y-x)+px;
E2=R.^3.*d2y-(rho.*y+tau.*x-y)+py;

% variations of planet terms
pxX =uE*(3*Le^2*(x/(R*Re)-R*Re^-3*(x-xe))*(x-xe)+Le^3).*N + ...
     uV*(3*Lv^2*(x/(R*Rv)-R*Rv^-3*(x-xv))*(x-xv)+Lv^3).*N;
pyX =uE*(3*Le^2*(x/(R*Re)-R*Re^-3*(x-xe))*(y-ye)).*N + ...
     uV*(3*Lv^2*(x/(R*Rv)-R*Rv^-3*(x-xv))*(y-yv)).*N;
pxY =uE*(3*Le^2*(y/(R*Re)-R*Re^-3*(y-ye))*(x-xe)).*N + ...
     uV*(3*Lv^2*(y/(R*Rv)-R*Rv^-3*(y-yv))*(x-xv)).*N;
pyY =uE*(3*Le^2*(y/(R*Re)-R*Re^-3*(y-ye))*(y-ye)+Le^3).*N + ...
     uV*(3*Lv^2*(y/(R*Rv)-R*Rv^-3*(y-yv))*(y-yv)+Lv^3).*N;
pxXe=uE*(3*Le^2*R*Re^-3*(x-xe)*(x-xe)-Le^3).*N;
pyXe=uE*(3*Le^2*R*Re^-3*(x-xe)*(y-ye)).*N;
pxYe=uE*(3*Le^2*R*Re^-3*(y-ye)*(x-xe)).*N;
pyYe=uE*(3*Le^2*R*Re^-3*(y-ye)*(y-ye)-Le^3).*N;
pxXv=uV*(3*Lv^2*R*Rv^-3*(x-xv)*(x-xv)-Lv^3).*N;
pyXv=uV*(3*Lv^2*R*Rv^-3*(x-xv)*(y-yv)).*N;
pxYv=uV*(3*Lv^2*R*Rv^-3*(y-yv)*(x-xv)).*N;
pyYv=uV*(3*Lv^2*R*Rv^-3*(y-yv)*(y-yv)-Lv^3).*N;

%{{x} {y} {xE} {yE} {xV} {yV}}
dE1=[3.*R.*x.*d2x.*N + R.^3.*d2N - rho.*N+N + pxX;
      3.*R.*y.*d2x.*N + tau.*N + pxY;
     pxXe;
     pxYe;
```

```
     pxXv;
     pxYv];
dE2=[3.*R.*x.*d2y.*N - tau.*N + pyX;
      3.*R.*y.*d2y.*N + R.^3.*d2N - rho.*N+N + pyY;
     pyXe;
     pyYe;
     pyXv;
     pyYv];

%%

function [N,dN,d2N] = funcC1p3(ep,J)

N =[((1-ep)./2+(ep.^3-ep)./4);
    ((ep.^3-ep)./4-(ep.^2-1)./4).*J;
    ((1+ep)./2-(ep.^3-ep)./4);
    ((ep.^3-ep)./4+(ep.^2-1)./4).*J].';

dN=[(((3.*ep.^2)./4-3/4)./J);
    ((3.*ep.^2)./4-ep./2-1/4);
    (-((3.*ep.^2)./4-3/4)./J);
    ((3.*ep.^2)./4+ep./2-1/4)].';

d2N=[(3*ep)/(2*J^2);
      ((3*ep)/2 - 1/2)/J;
     -(3*ep)/(2*J^2);
      ((3*ep)/2 + 1/2)/J].';

function [delta1,g]=newtonF(delta0,K,G)

a=1;
deltaS=-inv(K)*G;
delta1=delta0+a*deltaS;
delta0=delta1;
g=max(abs(G));

function []=outputF(delta1,I,g)

fprintf(' x2 = %12.10e\n',delta1(1,1));
fprintf('dx2 = %12.10e\n',delta1(2,1));
fprintf(' y2 = %12.10e\n',delta1(3,1));
fprintf('dy2 = %12.10e\n',delta1(4,1));
fprintf('\nI = %8.6e\n',I);
fprintf('g = %8.6e\n',g);

function [v_plot]=plotF(pt,xp,dxp,yp,dyp,step,he)
% expands raw data into data points
st=-1:(2/(pt-1)):1;
tt=he/(pt-1);
J=he/2;
i=0;
t_time=0;
```

```
for dt=1:step
    X=[xp(dt);dxp(dt);xp(dt+1);dxp(dt+1)];
    Y=[yp(dt);dyp(dt);yp(dt+1);dyp(dt+1)];
for ar=1:pt
    i=i+1;
    ep=st(ar);
     [N,dN,d2N] = funcC1p3(ep,J);
    v_plot(i,1)=(t_time/(2*pi))*365.25;
    v_plot(i,2)=N*X;
     v_plot(i,3)=dN*X;
     v_plot(i,4)=d2N*X;
    v_plot(i,5)=N*Y;
     v_plot(i,6)=dN*Y;
     v_plot(i,7)=d2N*Y;
    t_time=t_time+tt;
end
t_time=he*dt;
end

function [R,V]=EarthF()

R=[-9.446539984473329E-02 -9.279854415182310E-01 -4.023030891522794E-
01;
  -9.973520644355244E-03 -9.323119633198301E-01 -4.041775691999610E-
01;
   7.455358562169211E-02 -9.300814474852619E-01 -4.032131876430253E-
01;
   1.585546242217790E-01 -9.213352621216739E-01 -3.994249656702445E-
01;
   2.414696015032418E-01 -9.061226419162007E-01 -3.928308030215096E-
01;
   3.227162853642873E-01 -8.845188807924735E-01 -3.834624975777912E-
01;
   4.016857161675280E-01 -8.566553471858608E-01 -3.713802500722312E-
01;
   4.777879423456552E-01 -8.227527036804405E-01 -3.566836120230795E-
01;
   5.505037168320409E-01 -7.830790742901678E-01 -3.394876218794931E-
01;
   6.193525362165220E-01 -7.379062673169930E-01 -3.199064018275714E-
01;
   6.838577639176538E-01 -6.875173906984221E-01 -2.980604706414564E-
01;
   7.435350530772362E-01 -6.322291368004207E-01 -2.740883806412449E-
01;
   7.979060170262137E-01 -5.724275871550708E-01 -2.481619590311347E-
01;
   8.465653712583271E-01 -5.085684704281598E-01 -2.204801334664474E-
01;
   8.891860909365293E-01 -4.411126199282144E-01 -1.912394465515568E-
01;
```

```
   9.254726320883451E-01 -3.705135070572933E-01 -1.606333584618669E-
01;
   9.551411022610802E-01 -2.972356712257044E-01 -1.288628822299108E-
01;
   9.779180114535151E-01 -2.217812157790199E-01 -9.614894499664325E-
02;
   9.935814497345946E-01 -1.447177506579229E-01 -6.274121370525497E-
02;
   1.002013776525697E+00 -6.663397900855210E-02 -2.889319850176821E-
02;
   1.003161190179927E+00  1.190966582522439E-02  5.155809778068748E-
03;
   9.969975789154286E-01  9.036913951437638E-02  3.917161842315768E-
02;
   9.835153227367447E-01  1.681949937943081E-01  7.291426906354910E-
02;
   9.627412946469501E-01  2.448030528254534E-01  1.061263889008820E-
01;
   9.347949737365887E-01  3.195777967651188E-01  1.385402867106921E-
01;
   8.998927558023139E-01  3.919393101212303E-01  1.699081758806857E-
01;
   8.582922377252042E-01  4.613574252566048E-01  2.000030235649783E-
01;
   8.102713784353023E-01  5.273308369285346E-01  2.286072005898223E-
01;
   7.561287651281177E-01  5.893606209345263E-01  2.555008461485627E-
01;
   6.962227953705078E-01  6.469314360122129E-01  2.804575820603324E-
01;
   6.310121749320247E-01  6.995545272932105E-01  3.032677293521060E-
01;
   5.610130584249298E-01  7.468178740595252E-01  3.237564823129853E-
01;
   4.867549012053213E-01  7.883725486040408E-01  3.417737927205386E-
01;
   4.087686155610895E-01  8.239084027708460E-01  3.571827890112296E-
01;
   3.276043696765851E-01  8.531238581557908E-01  3.698486765424744E-
01;
   2.438810707854747E-01  8.757376059117298E-01  3.796493176395928E-
01;
   1.582798194846803E-01  8.915469538450939E-01  3.865007264122930E-
01];

V=[1.685551453742792E-02 -1.523080074540962E-03 -6.597049547703459E-
04;
   1.692107967431582E-02 -2.083206410175591E-04 -9.049405687444465E-
05;
   1.687123880980941E-02  1.099104109028617E-03  4.757455973204354E-
04;
```

```
   1.671057200482215E-02  2.397812060174145E-03  1.038991916394572E-
03;
   1.643604534035033E-02  3.684797902521943E-03  1.597650538421812E-
03;
   1.604218450149661E-02  4.952537354784956E-03  2.147747319165797E-
03;
   1.552564659188579E-02  6.185283402385519E-03  2.681698794096107E-
03;
   1.489812933684606E-02  7.366685157942335E-03  3.193073344756471E-
03;
   1.417228050703764E-02  8.493756297908104E-03  3.681554302440104E-
03;
   1.335138407632479E-02  9.566000531013393E-03  4.146952344295335E-
03;
   1.243457141986153E-02  1.057911599464001E-02  4.586859228057449E-
03;
   1.142005423399952E-02  1.152340210490546E-02  4.996255445917846E-
03;
   1.031485908141034E-02  1.238166833669366E-02  5.367524226418572E-
03;
   9.138168997169349E-03  1.314663295529431E-02  5.698681399547937E-
03;
   7.900321863492040E-03  1.382065587623216E-02  5.991180344951620E-
03;
   6.604842819283895E-03  1.440358239652608E-02  6.244591586407432E-
03;
   5.253324430155441E-03  1.489097221359574E-02  6.456296014802340E-
03;
   3.849708927034955E-03  1.527168449366723E-02  6.620832632666454E-
03;
   2.412025335776387E-03  1.553388497782531E-02  6.733750568440768E-
03;
   9.592022268202616E-04  1.568102099188880E-02  6.797524184663511E-
03;
  -5.010726424900543E-04  1.571836574912277E-02  6.814305256420911E-
03;
  -1.964657436283823E-03  1.564721618119654E-02  6.784064816945554E-
03;
  -3.427601536597929E-03  1.546371344110105E-02  6.704418928954655E-
03;
  -4.878057651850695E-03  1.515861954614671E-02  6.571336721621155E-
03;
  -6.292995782616394E-03  1.473197408149846E-02  6.386000262967384E-
03;
  -7.659269341382400E-03  1.419502369993974E-02  6.153620070064548E-
03;
  -8.971648798763939E-03  1.355560290553280E-02  5.877106987566477E-
03;
  -1.022688038850195E-02  1.281723294491129E-02  5.557266003293843E-
03;
  -1.141844916721125E-02  1.197734008348718E-02  5.192550930718418E-
03;
```

```
  -1.252839865978329E-02  1.103445282227056E-02  4.783071360509651E-
03;
  -1.353851301480502E-02  1.000116287449982E-02  4.335222795875634E-
03;
  -1.444344726922960E-02  8.892598999122281E-03  3.855303395036973E-
03;
  -1.524215539798986E-02  7.719074221515482E-03  3.347115635236810E-
03;
  -1.593425289556969E-02  6.485187343467738E-03  2.811952666111317E-
03;
  -1.651079989386864E-02  5.191344359188702E-03  2.250210720018685E-
03;
  -1.695554122646210E-02  3.847385859820759E-03  1.667266594824369E-
03;
  -1.726207734912696E-02  2.472721722400982E-03  1.071816097959259E-
03];

V = V*365/(2*pi);

function [R,V]=VenusF()

R=[-7.188579050555668E-01 -2.097895968152247E-02  3.604902175164499E-
02;
  -7.116594258360722E-01 -1.131072109053967E-01 -5.856797782621908E-
03;
  -6.904152406621795E-01 -2.030038256418288E-01 -4.764734844820582E-
02;
  -6.555784539158444E-01 -2.889045726614958E-01 -8.850019653651305E-
02;
  -6.078690860964548E-01 -3.691334120448522E-01 -1.276156969486050E-
01;
  -5.482568747367821E-01 -4.421351085978560E-01 -1.642327549398743E-
01;
  -4.779393481781363E-01 -5.065046980512286E-01 -1.976434712077828E-
01;
  -3.983158340243400E-01 -5.610133100316741E-01 -2.272064050251582E-
01;
  -3.109581087644696E-01 -6.046299791222794E-01 -2.523582447924449E-
01;
  -2.175784097842352E-01 -6.365391953536870E-01 -2.726237285535598E-
01;
  -1.199955229632879E-01 -6.561540545227702E-01 -2.876237065539060E-
01;
  -2.009963301044854E-02 -6.631249646872635E-01 -2.970812826531075E-
01;
   8.018341532869437E-02 -6.573439460924430E-01 -3.008260102065277E-
01;
   1.789278438415507E-01 -6.389446266182234E-01 -2.987961503148014E-
01;
   2.742431044040076E-01 -6.082980844467669E-01 -2.910390262500681E-
01;
```

```
   3.643079791803892E-01 -5.660047277086627E-01 -2.777095280331349E-
01;
   4.474031623929194E-01 -5.128824296750653E-01 -2.590668363318709E-
01;
   5.219419068614982E-01 -4.499511578021708E-01 -2.354694461965387E-
01;
   5.864983506890959E-01 -3.784143494126568E-01 -2.073685800844180E-
01;
   6.398331649178645E-01 -2.996373005176173E-01 -1.753000874446342E-
01;
   6.809161810267058E-01 -2.151228500726547E-01 -1.398749362174337E-
01;
   7.089456701151200E-01 -1.264846638057014E-01 -1.017684122827223E-
01;
   7.233639609856763E-01 -3.541845024495488E-02 -6.170815702631523E-
02;
   7.238691026739160E-01  5.632852885337992E-02 -2.046118763009069E-
02;
   7.104222927354608E-01  1.469892559226558E-01  2.117993867539250E-
02;
   6.832508157057254E-01  2.348096179967366E-01  6.241163241835560E-
02;
   6.428462748679594E-01  3.180814342271445E-01  1.024342422212959E-
01;
   5.899579542316320E-01  3.951753045373129E-01  1.404672524987563E-
01;
   5.255812183155780E-01  4.645726857250759E-01  1.757644479990244E-
01;
   4.509409466477139E-01  5.248965587532648E-01  2.076287600737566E-
01;
   3.674701054731255E-01  5.749400184564312E-01  2.354264874767055E-
01;
   2.767836774569049E-01  6.136921016334339E-01  2.586005690301241E-
01;
   1.806482997293681E-01  6.403601777977679E-01  2.766825808264833E-
01;
   8.094809914697756E-02  6.543882613236935E-01  2.893031380713674E-
01;
  -2.035264569608203E-02  6.554706650655991E-01  2.962004010155150E-
01;
  -1.212492527215793E-01  6.435605047831449E-01  2.972264162966366E-
01;
  -2.197379146131870E-01  6.188726811166366E-01  2.923510703164449E-
01];

V=[1.877748581851345E-05 -1.852818106097147E-02 -8.337381279810280E-
03;
   2.854783731675988E-03 -1.826241985703917E-02 -8.397267675215441E-
03;
   5.627746998161154E-03 -1.763730084455460E-02 -8.291482753983642E-
03;
```

```
   8.282909407511431E-03 -1.666702095816037E-02 -8.022948954434575E-
03;
   1.076843973010194E-02 -1.537257516493980E-02 -7.597832441937728E-
03;
   1.303644022516558E-02 -1.378118506255340E-02 -7.025349800616863E-
03;
   1.504382796503850E-02 -1.192561555193120E-02 -6.317516372437838E-
03;
   1.675307817914986E-02 -9.843405159280670E-03 -5.488846981797454E-
03;
   1.813282397568159E-02 -7.576034957342081E-03 -4.556019955111907E-
03;
   1.915831194564747E-02 -5.168059059168799E-03 -3.537514741721067E-
03;
   1.981171720982302E-02 -2.666217260521794E-03 -2.453232605076073E-
03;
   2.008232459555903E-02 -1.185475684269200E-04 -1.324108768838386E-
03;
   1.996658468339423E-02  2.426486794909485E-03 -1.717231338997645E-
04;
   1.946805456751975E-02  4.920844549266865E-03  9.820846301915737E-
04;
   1.859723359232521E-02  7.317719051720348E-03  2.115591036142919E-
03;
   1.737130378789472E-02  9.572309844246530E-03  3.207552264803388E-
03;
   1.581378333173811E-02  1.164254824613966E-02  4.237552577790719E-
03;
   1.395410007170277E-02  1.348977375439825E-02  5.186335676412623E-
03;
   1.182709091254672E-02  1.507935853784401E-02  6.036117370291410E-
03;
   9.472431414793359E-03  1.638127717578382E-02  6.770878023678103E-
03;
   6.933998532352966E-03  1.737061802598504E-02  7.376632994322153E-
03;
   4.259169054506308E-03  1.802803104318881E-02  7.841678524940323E-
03;
   1.498057377495437E-03  1.834010611946235E-02  8.156810131598066E-
03;
  -1.297304016226367E-03  1.829967583004299E-02  8.315510593382943E-
03;
  -4.073837992892607E-03  1.790603421359774E-02  8.314103599967258E-
03;
  -6.778343961719093E-03  1.716506147580922E-02  8.151868068203318E-
03;
  -9.358457575131497E-03  1.608924445639898E-02  7.831107982399879E-
03;
  -1.176363659591342E-02  1.469758301678004E-02  7.357172652488820E-
03;
  -1.394615692103932E-02  1.301537319706069E-02  6.738422368780209E-
03;
```

```
  -1.586209913758628E-02  1.107385942451154E-02  5.986134687158183E-
03;
  -1.747230313763544E-02  8.909750740075889E-03  5.114347424176015E-
03;
  -1.874326598167340E-02  6.564600195637416E-03  4.139636250019376E-
03;
  -1.964795605621766E-02  4.084051667914209E-03  3.080827159909052E-
03;
  -2.016651530828227E-02  1.516963643007247E-03  1.958646501151266E-
03;
  -2.028682183295397E-02 -1.085575005339092E-03  7.953136404251189E-
04;
  -2.000488745380217E-02 -3.671316550742700E-03 -3.859160290492494E-
04;
  -1.932506902743487E-02 -6.187987063994455E-03 -1.561247322654512E-
03];
V = V*365/(2*pi);
%%

function [JD]=julianF(yr,mo,d,h,min,s)

JD=367*yr-7*(yr+(mo+9)/12)/4+275*mo/9+d+1721013.5+...
    ((s/60+min)/60+h)/24;
```

APPENDIX C: Horizons Input and Output

```
telnet horizons.jpl.nasa.gov 6775 <<eod
399
E
v
@sun
frame
AD 2010-May-17 1:00
AD 2010-Dec-13 1:00
5d
n
J2000
1
2
NO
NO
2
N

*******************************************************************************
*********

    /_ /|  /____/ \  /_ /|       Horizons On-line Ephemeris System
v3.97c
    | | | |  __ \ /| | | |       Solar System Dynamics Group
 ___| | | | |__) |/  | | |__     Jet Propulsion Laboratory
/___| | | |  ___/    | |/__ /|   Pasadena, CA, USA
|_____|/  |_|/       |_____|/


*******************************************************************************
*********
Ephemeris / PORT_LOGIN Thu Feb 26 21:38:38 2015 Pasadena, USA    /
Horizons
*******************************************************************************
*********
Target body name: Earth (399)                     {source: DE-0431LE-
0431}
Center body name: Sun (10)                        {source: DE-0431LE-
0431}
Center-site name: BODY CENTER
*******************************************************************************
*********
Start time      : A.D. 2010-May-17 01:00:00.0000 CT
Stop  time      : A.D. 2010-Dec-13 01:00:00.0000 CT
Step-size       : 7200 minutes
*******************************************************************************
*********
Center geodetic : 0.00000000,0.00000000,0.0000000 {E-
lon(deg),Lat(deg),Alt(km)}
Center cylindric: 0.00000000,0.00000000,0.0000000 {E-
lon(deg),Dxy(km),Dz(km)}
```

```
Center radii    : 696000.0 x 696000.0 x 696000.0 k{Equator, meridian,
pole}
Output units    : AU-D
Output format   : 02
Reference frame : ICRF/J2000.0
Output type     : GEOMETRIC cartesian states
Coordinate systm: Earth Mean Equator and Equinox of Reference Epoch
*******************************************************************
*********
JDCT
   X     Y     Z
   VX    VY    VZ
*******************************************************************
*********
$$SOE
2455333.541666667 = A.D. 2010-May-17 01:00:00.0000 (CT)
  -5.669344392669921E-01 -7.682750616079908E-01 -3.330649205062708E-01
   1.397360174170675E-02 -8.908906918253317E-03 -3.861566232181605E-03
2455338.541666667 = A.D. 2010-May-22 01:00:00.0000 (CT)
  -4.951346782777921E-01 -8.100052645164916E-01 -3.511532138314734E-01
   1.472746969744663E-02 -7.774736193387962E-03 -3.370248709301256E-03
2455343.541666667 = A.D. 2010-May-27 01:00:00.0000 (CT)
  -4.198422236597134E-01 -8.459499652764551E-01 -3.667367496738201E-01
   1.537197818655461E-02 -6.596579701884285E-03 -2.860291797909422E-03
2455348.541666667 = A.D. 2010-Jun-01 01:00:00.0000 (CT)
  -3.415869304744387E-01 -8.759060251361560E-01 -3.797268774545585E-01
   1.591281989418112E-02 -5.379281177116986E-03 -2.332773148809358E-03
2455353.541666667 = A.D. 2010-Jun-06 01:00:00.0000 (CT)
  -2.608928984346685E-01 -8.996784938946887E-01 -3.900353799235513E-01
   1.634623899441358E-02 -4.123598822469913E-03 -1.787891125236140E-03
2455358.541666667 = A.D. 2010-Jun-11 01:00:00.0000 (CT)
  -1.783175179129673E-01 -9.170860445039298E-01 -3.975811400681003E-01
   1.666376967925708E-02 -2.834482144483316E-03 -1.228299807109011E-03
2455363.541666667 = A.D. 2010-Jun-16 01:00:00.0000 (CT)
  -9.446539984473329E-02 -9.279854415182310E-01 -4.023030891522794E-01
   1.685551453742792E-02 -1.523080074540962E-03 -6.597049547703459E-04
2455368.541666667 = A.D. 2010-Jun-21 01:00:00.0000 (CT)
  -9.973520644355244E-03 -9.323119633198301E-01 -4.041775691999610E-01
   1.692107967431582E-02 -2.083206410175591E-04 -9.049405687444465E-05
2455373.541666667 = A.D. 2010-Jun-26 01:00:00.0000 (CT)
   7.455358562169211E-02 -9.300814474852619E-01 -4.032131876430253E-01
   1.687123880980941E-02  1.099104109028617E-03  4.757455973204354E-04
2455378.541666667 = A.D. 2010-Jul-01 01:00:00.0000 (CT)
   1.585546242217790E-01 -9.213352621216739E-01 -3.994249656702445E-01
   1.671057200482215E-02  2.397812060174145E-03  1.038991916394572E-03
2455383.541666667 = A.D. 2010-Jul-06 01:00:00.0000 (CT)
   2.414696015032418E-01 -9.061226419162007E-01 -3.928308030215096E-01
   1.643604534035033E-02  3.684797902521943E-03  1.597650538421812E-03
2455388.541666667 = A.D. 2010-Jul-11 01:00:00.0000 (CT)
   3.227162853642873E-01 -8.845188807924735E-01 -3.834624975777912E-01
   1.604218450149661E-02  4.952537354784956E-03  2.147747319165797E-03
2455393.541666667 = A.D. 2010-Jul-16 01:00:00.0000 (CT)
```

```
   4.016857161675280E-01 -8.566553471858608E-01 -3.713802500722312E-01
   1.552564659188579E-02  6.185283402385519E-03  2.681698794096107E-03
2455398.541666667 = A.D. 2010-Jul-21 01:00:00.0000 (CT)
   4.777879423456552E-01 -8.227527036804405E-01 -3.566836120230795E-01
   1.489812933684606E-02  7.366685157942335E-03  3.193073344756471E-03
2455403.541666667 = A.D. 2010-Jul-26 01:00:00.0000 (CT)
   5.505037168320409E-01 -7.830790742901678E-01 -3.394876218794931E-01
   1.417228050703764E-02  8.493756297908104E-03  3.681554302440104E-03
2455408.541666667 = A.D. 2010-Jul-31 01:00:00.0000 (CT)
   6.193525362165220E-01 -7.379062673169930E-01 -3.199064018275714E-01
   1.335138407632479E-02  9.566000531013393E-03  4.146952344295335E-03
2455413.541666667 = A.D. 2010-Aug-05 01:00:00.0000 (CT)
   6.838577639176538E-01 -6.875173906984221E-01 -2.980604706414564E-01
   1.243457141986153E-02  1.057911599464001E-02  4.586859228057449E-03
2455418.541666667 = A.D. 2010-Aug-10 01:00:00.0000 (CT)
   7.435350530772362E-01 -6.322291368004207E-01 -2.740883806412449E-01
   1.142005423399952E-02  1.152340210490546E-02  4.996255445917846E-03
2455423.541666667 = A.D. 2010-Aug-15 01:00:00.0000 (CT)
   7.979060170262137E-01 -5.724275871550708E-01 -2.481619590311347E-01
   1.031485908141034E-02  1.238166833669366E-02  5.367524226418572E-03
2455428.541666667 = A.D. 2010-Aug-20 01:00:00.0000 (CT)
   8.465653712583271E-01 -5.085684704281598E-01 -2.204801334664474E-01
   9.138168997169349E-03  1.314663295529431E-02  5.698681399547937E-03
2455433.541666667 = A.D. 2010-Aug-25 01:00:00.0000 (CT)
   8.891860909365293E-01 -4.411126199282144E-01 -1.912394465515568E-01
   7.900321863492040E-03  1.382065587623216E-02  5.991180344951620E-03
2455438.541666667 = A.D. 2010-Aug-30 01:00:00.0000 (CT)
   9.254726320883451E-01 -3.705135070572933E-01 -1.606333584618669E-01
   6.604842819283895E-03  1.440358239652608E-02  6.244591586407432E-03
2455443.541666667 = A.D. 2010-Sep-04 01:00:00.0000 (CT)
   9.551411022610802E-01 -2.972356712257044E-01 -1.288628822299108E-01
   5.253324430155441E-03  1.489097221359574E-02  6.456296014802340E-03
2455448.541666667 = A.D. 2010-Sep-09 01:00:00.0000 (CT)
   9.779180114535151E-01 -2.217812157790199E-01 -9.614894499664325E-02
   3.849708927034955E-03  1.527168449366723E-02  6.620832632666454E-03
2455453.541666667 = A.D. 2010-Sep-14 01:00:00.0000 (CT)
   9.935814497345946E-01 -1.447177506579229E-01 -6.274121370525497E-02
   2.412025335776387E-03  1.553388497782531E-02  6.733750568440768E-03
2455458.541666667 = A.D. 2010-Sep-19 01:00:00.0000 (CT)
   1.002013776525697E+00 -6.663397900855210E-02 -2.889319850176821E-02
   9.592022268202616E-04  1.568102099188880E-02  6.797524184663511E-03
2455463.541666667 = A.D. 2010-Sep-24 01:00:00.0000 (CT)
   1.003161190179927E+00  1.190966582522439E-02  5.155809778068748E-03
  -5.010726424900543E-04  1.571836574912277E-02  6.814305256420911E-03
2455468.541666667 = A.D. 2010-Sep-29 01:00:00.0000 (CT)
   9.969975789154286E-01  9.036913951437638E-02  3.917161842315768E-02
  -1.964657436283823E-03  1.564721618119654E-02  6.784064816945554E-03
2455473.541666667 = A.D. 2010-Oct-04 01:00:00.0000 (CT)
   9.835153227367447E-01  1.681949937943081E-01  7.291426906354910E-02
  -3.427601536597929E-03  1.546371344110105E-02  6.704418928954655E-03
2455478.541666667 = A.D. 2010-Oct-09 01:00:00.0000 (CT)
   9.627412946469501E-01  2.448030528254534E-01  1.061263889008820E-01
```

```
  -4.878057651850695E-03  1.515861954614671E-02  6.571336721621155E-03
2455483.541666667 = A.D. 2010-Oct-14 01:00:00.0000 (CT)
   9.347949737365887E-01  3.195777967651188E-01  1.385402867106921E-01
  -6.292995782616394E-03  1.473197408149846E-02  6.386000262967384E-03
2455488.541666667 = A.D. 2010-Oct-19 01:00:00.0000 (CT)
   8.998927558023139E-01  3.919393101212303E-01  1.699081758806857E-01
  -7.659269341382400E-03  1.419502369993974E-02  6.153620070064548E-03
2455493.541666667 = A.D. 2010-Oct-24 01:00:00.0000 (CT)
   8.582922377252042E-01  4.613574252566048E-01  2.000030235649783E-01
  -8.971648798763939E-03  1.355560290553280E-02  5.877106987566477E-03
2455498.541666667 = A.D. 2010-Oct-29 01:00:00.0000 (CT)
   8.102713784353023E-01  5.273308369285346E-01  2.286072005898223E-01
  -1.022688038850195E-02  1.281723294491129E-02  5.557266003293843E-03
2455503.541666667 = A.D. 2010-Nov-03 01:00:00.0000 (CT)
   7.561287651281177E-01  5.893606209345263E-01  2.555008461485627E-01
  -1.141844916721125E-02  1.197734008348718E-02  5.192550930718418E-03
2455508.541666667 = A.D. 2010-Nov-08 01:00:00.0000 (CT)
   6.962227953705078E-01  6.469314360122129E-01  2.804575820603324E-01
  -1.252839865978329E-02  1.103445282227056E-02  4.783071360509651E-03
2455513.541666667 = A.D. 2010-Nov-13 01:00:00.0000 (CT)
   6.310121749320247E-01  6.995545272932105E-01  3.032677293521060E-01
  -1.353851301480502E-02  1.000116287449982E-02  4.335222795875634E-03
2455518.541666667 = A.D. 2010-Nov-18 01:00:00.0000 (CT)
   5.610130584249298E-01  7.468178740595252E-01  3.237564823129853E-01
  -1.444344726922960E-02  8.892598999122281E-03  3.855303395036973E-03
2455523.541666667 = A.D. 2010-Nov-23 01:00:00.0000 (CT)
   4.867549012053213E-01  7.883725486040408E-01  3.417737927205386E-01
  -1.524215539798986E-02  7.719074221515482E-03  3.347115635236810E-03
2455528.541666667 = A.D. 2010-Nov-28 01:00:00.0000 (CT)
   4.087686155610895E-01  8.239084027708460E-01  3.571827890112296E-01
  -1.593425289556969E-02  6.485187343467738E-03  2.811952666111317E-03
2455533.541666667 = A.D. 2010-Dec-03 01:00:00.0000 (CT)
   3.276043696765851E-01  8.531238581557908E-01  3.698486765424744E-01
  -1.651079989386864E-02  5.191344359188702E-03  2.250210720018685E-03
2455538.541666667 = A.D. 2010-Dec-08 01:00:00.0000 (CT)
   2.438810707854747E-01  8.757376059117298E-01  3.796493176395928E-01
  -1.695554122646210E-02  3.847385859820759E-03  1.667266594824369E-03
2455543.541666667 = A.D. 2010-Dec-13 01:00:00.0000 (CT)
   1.582798194846803E-01  8.915469538450939E-01  3.865007264122930E-01
  -1.726207734912696E-02  2.472721722400982E-03  1.071816097959259E-03
$$EOE
*******************************************************************
*********
Coordinate system description:

  Earth Mean Equator and Equinox of Reference Epoch

    Reference epoch: J2000.0
    xy-plane: plane of the Earth's mean equator at the reference epoch
    x-axis  : out along ascending node of instantaneous plane of the
Earth's
```

```
              orbit and the Earth's mean equator at the reference
epoch
    z-axis  : along the Earth mean north pole at the reference epoch

Symbol meaning [1 au=149597870.700 km, 1 day=86400.0 s]:

    JDCT     Epoch Julian Date, Coordinate Time
      X      x-component of position vector (AU)
      Y      y-component of position vector (AU)
      Z      z-component of position vector (AU)
      VX     x-component of velocity vector (AU/day)
      VY     y-component of velocity vector (AU/day)
      VZ     z-component of velocity vector (AU/day)

Geometric states/elements have no aberration corrections applied.

 Computations by ...
     Solar System Dynamics Group, Horizons On-Line Ephemeris System
     4800 Oak Grove Drive, Jet Propulsion Laboratory
     Pasadena, CA  91109   USA
     Information: http://ssd.jpl.nasa.gov/
     Connect    : telnet://ssd.jpl.nasa.gov:6775  (via browser)
                  telnet ssd.jpl.nasa.gov 6775    (via command-line)
     Author     : Jon.Giorgini@jpl.nasa.gov
*******************************************************************************
*********
```